INVESTIGATION OF ULTRAVIOLET PHOTOIONIZATION SUSTAINED DISCHARGE FOR GAS LASERS

R. C. Lind

Hughes Research Laboratories

Prepared for:

Office of Naval Research

March 1976

INVESTIGATION OF ULTRAVIOLET PHOTOIONIZATION SUSTAINED DISCHARGE FOR GAS LASERS

R.C. LIND

HUGHES RESEARCH LABORATORIES
3011 Malibu Canyon Road
Malibu, CA 90265

MARCH 1976

SEMIANNUAL TECHNICAL REPORT 6

for Period 1 July 1975 through 31 December 1975

Sponsored by

DEFENSE ADVANCED RESEARCH PROJECTS AGENCY
DARPA Order No. 1807

Semiannual Technical Report
Contract N00014-73-C-0287
Reporting Period: 1 July 1975 through 31 December 1975

DARPA Order No. 1807
Program Code No. 5E20

Effective Data of Contract:	2 January 1973
Contract Expiration Date:	31 August 1975
Amount of Contract:	$446,170.00
Principal Investigator:	R. C. Lind (213) 456-6411
Scientific Officer:	Director, Physics Program Physical Sciences Division Office of Naval Research Department of the Navy 800 North Quincy Street Arlington, VA 22217

Letter on file

This research was supported by the Defense Advanced Research Projects Agency of the Department of Defense and was monitored by ONR under Contract N00014-73-C-0287.

UNCLASSIFIED

SECURITY CLASSIFICATION OF THIS PAGE (When Date Entered)

REPORT DOCUMENTATION PAGE		READ INSTRUCTIONS BEFORE COMPLETING FORM
1. REPORT NUMBER	2. GOVT ACCESSION NO.	3. RECIPIENT'S CATALOG NUMBER
4. TITLE (and Subtitle) Investigation of Ultraviolet Photoionization Sustained Discharge for Gas Lasers		5. TYPE OF REPORT & PERIOD COVERED Semiannual Tech. Rpt. 6 1 July 1975-31 Dec. 1975
		6. PERFORMING ORG. REPORT NUMBER
7. AUTHOR(s) R. C. Lind		8. CONTRACT OR GRANT NUMBER(s) N00014-73-C-0287
9. PERFORMING ORGANIZATION NAME AND ADDRESS Hughes Research Laboratories 3011 Malibu Canyon Road Malibu, CA 90265		10. PROGRAM ELEMENT, PROJECT, TASK AREA & WORK UNIT NUMBERS DARPA Order No. 1807 Program Code No. 5E20
11. CONTROLLING OFFICE NAME AND ADDRESS Defense Advanced Research Projects Agency 1400 Wilson Boulevard Arlington, VA 22209		12. REPORT DATE March 1976
		13. NUMBER OF PAGES 102
14. MONITORING AGENCY NAME & ADDRESS (if different from Controlling Office) Office of Naval Research Department of the Navy Arlington, VA 22217		15. SECURITY CLASS. (of this report) Unclassified
		15a. DECLASSIFICATION DOWNGRADING SCHEDULE

16. DISTRIBUTION STATEMENT (of this Report)

17. DISTRIBUTION STATEMENT (of the abstract entered in Block 20, if different from Report)

18. SUPPLEMENTARY NOTES

19. KEY WORDS (Continue on reverse side if necessary and identify by block number)

CO_2 Laser, Discharge, Ultraviolet Radiation, Photoionization, Seed Gas

20. ABSTRACT (Continue on reverse side if necessary and identify by block number)

The objectives of this program are to investigate and improve ultraviolet (uv) photoionization plasma conditioning techniques, to perform the demonstration of a uv sustained electrical discharge atmospheric pressure CO_2 laser, and to establish scalability limits.

Initially, fundamental experiments employing small scale (1 x 2 x 15 cm^3) discharge volumes established that in excess of 200 J/l-atm

DD FORM 1 JAN 73 1473 EDITION OF 1 NOV 65 IS OBSOLETE

UNCLASSIFIED

SECURITY CLASSIFICATION OF THIS PAGE (When Date Entered)

could be input to 1 atm CO_2 laser mixture by the uv photoionization of an added low ionization potential organic molecule. These and additional experiments led to conjectures for mixture mean-free paths for certain critical CO_2, N_2, He tri-n-propylamine mixture ratios on the order of 8 cm.

Power extraction and small signal gain measurements were undertaken next using a device with a larger discharge volume (2.5 x 15 x 50 cm^3) and an improved uv source configuration. Output energies in excess of 45 J/l-atm with pulse lengths to 37 μm have been achieved.

The limits of scalability of the uv sustained plasma conditioning technique are now being addressed. A large volume (20 x 20 x 100 cm^3) discharge device has been constructed, and testing is now in progress. With a reduced active volume, nearly 300 J has been extracted from the device in a 30 μsec pulse length. This extraction energy corresponds to an energy density of 25 J/l-atm. Spatially resolved gain measurements have been completed with good uniformity found in both the discharge height and width dimension. Medium homogeneity measurements have been completed with media quality better than $\lambda/8$ at 10.6 μm found.

A scaling model for the uv-sustained laser has been developed. Using the model, predictions of the characteristics of a high average power uv-sustained laser have been made. The principal result of the model is that the level of the uv source flux must increase if performance competitive with current E-beam sustained devices is to be achieved. Experiments to achieve such increased performance are in progress.

TABLE OF CONTENTS

SECTION		PAGE
	LIST OF ILLUSTRATIONS	5
I	INTRODUCTION	7
II	ULTRAVIOLET SOURCE STUDIES	11
	A. Electron Density	11
	B. Ultraviolet Source Circuit Discussion	12
	C. Experimental Results	17
	D. Spectral Match Considerations	18
	E. Summary	18
III	ARC SENSOR CIRCUIT	19
	A. Objective	19
	B. Fault-Detector Electronics	21
	C. Operation	22
IV	SUMMARY AND FUTURE PROGRAM PLAN	27
	A. Summary of Results	27
	B. Program Plan	27
	REFERENCES	31
APPENDIXES		
A	Summary of Previous Results—Small Scale Measurements	33
B	Summary of Previous Results—Large Scale Performance	57
C	Ultraviolet Sustained Laser Scalability	89
D	Scaling Model	107

LIST OF ILLUSTRATIONS

FIGURE		PAGE
1	Electrical layout	20
2	Timing diagram of fault detector signals	23
3	Fault detector block diagram	24
4	Arc sensor circuit.	26
5	Program schedule	28

I. INTRODUCTION

The objective of this program is to investigate and improve ultraviolet (uv) photoionization plasma conditioning techniques. The specific goal of the demonstration of a uv sustained electrical discharge atmospheric pressure CO_2 laser is within the scope of this objective. The dynamics of the plasma generation in this mode are similar to those of the electron beam controlled discharge; the voltage applied to the main discharge electrodes can be reduced below that required for a self-sustained avalanche mode. The principal advantage realized in this approach is complete control of the main discharge by the uv source at all times during operation.

The attractive feature of uv-sustained as opposed to e-beam-sustained operation is the simplicity of construction. Specifically, a foil is not required and the high voltages needed to give efficient electron penetration of the foil are not necessary.

The crucial questions that need to be answered through the research conducted during this program are (1) whether an electron density sufficient to sustain the discharge in a CO_2 laser mixture can be produced by a uv photoionization technique; specifically, plasma densities of 10^{12} electrons/cm^3 over pulse lengths of 20 μsec or longer must be attained, and (2) what the scalability parameters are for such a technique.

The first year program to investigate these questions consisted basically of the following three tasks:

1. Determination of the emission spectrum and power saturation characteristics of uv spark sources operated in CO_2 laser mixture, metal vapors, and other gas additives

2. Development of seeding techniques which will improve the photoionization efficiency of the laser medium

3. Evaluation of uv photoionization sustained CO_2 laser gas discharge characteristics and laser performance by means of small signal gain and laser power output measurements.

During the first reporting period[1] results were obtained on tasks one and two. The principal results were plasma densities required ($n_e = 10^{12}$ electrons/cm^3 for >20 μsec) have been demonstrated, emission spectra of spark discharges have been obtained, and a mixture mean-free path of 8 cm is conjectured for an appropriate mixture of CO_2, N_2, He and seed gas. Based on these results, baseline operating conditions for laser gas mixtures, seed gas concentrations, and uv intensities were established. These were then used as a guideline for laser measurements (Task 3) reported during the second reporting period.[2] The principal results obtained during the second reporting period were the demonstration of laser output energy up to 50 J/l-atm, in a 37 μsec (total) pulse length in a 2.5 x 15 x 50 cm^3 device in a completely uv-sustained mode of operation and the design of a large volume 20 x 20 x 100 cm^3 discharge device for scalability studies.

With the successful demonstration of extraction energies of 50 J/l-atm in a long pulse, the objective of the next phase of the program is directed toward an understanding and demonstration of the scalability limits of the uv-sustained scheme. This will be accomplished by the testing of the large-scale (20 x 20 x 100 cm^3) discharge device.

During the third[3] and fourth[4] reporting period measurements of input loading, spatially and temporally resolved small signal gain, the power extraction using a stable cavity were performed. An extraction energy of 200 J was obtained using a stable cavity in a configuration for which the electrode gap spacing was adjusted to 6 cm. Based on the measured mode volume, this represents an extraction energy density of 28 J/l-atm. Numerous comparisons of the experimental results with an established CO_2 kinetic code were made. Gain measurements taken in both the discharge width and electrode gap

spacing dimension indicate good uniformity and lead to expectations of continued scalability.

During the fifth[5] reporting period, measurements of media quality and power extraction using an unstable resonator were made. An extraction energy of nearly 300 J was obtained with the 6 cm gap spacing. The media quality, inferred from holograms taken, indicates better than $\lambda/30$ at 10.6 μm for regions unaffected by uv and cathode waves and $\lambda/8$ including such waves.

In addition, during this reporting period, a scaling model for the uv-sustained laser was developed. This model uses the results of the large-scale experiments as benchmarks for scaling. Using the model, we predicted the characteristics of a high average power uv-sustained laser. The principal result of the model is that the level of the uv source flux must increase if performance competitive with current E-beam sustained devices is to be achieved. Achieving such increases forms the basis of the work for the next period.

During the present reporting period the effort has been primarily directed toward achieving techniques for improving the uv source performance. To date, none of the techniques studied has provided significant increased performance. Further studies remain and these will be discussed.

In addition, the incorporation of an arc-sensing circuit into the operation of the large scale device (LSD) has been completed and will be described.

The remainder of this report is divided into three sections followed by four appendixes. Section II describes the uv source improvement studies, Section III describes the arc sensor circuit, and Section IV discusses the program plan for the remainder of the program. Appendixes A and B describe the previous experimental results obtained on a small-scale device and on the large-scale device. Appendix C presents the scalability model for the uv-sustained laser, and Appendix D presents the equations used in the model.

II. ULTRAVIOLET SOURCE STUDIES

Based on the conclusions of the scaling model presented in the last semiannual report (discussed in Appendix C for review), an improvement in the performance of the uv source must be achieved if a high power uv-sustained laser is to be achieved. In this section we present the studies directed toward obtaining such improvements that have been performed to date.

A. Electron Density

The objective of the improved performance of the uv source is to achieve higher electron densities in the main discharge region. To obtain higher electron densities requires that the useful uv radiation energy, i.e., the energy delivered by the uv source in the wavelength range which produces photoionization of the seed gas, be increased. This wavelength range has been determined from previous experiments to be 1200 to 1700 Å. The useful uv energy can be written as

$$E_{uv} = \epsilon_{uv} \cdot \epsilon_{el} \cdot E_{stored} \quad .$$

There are three avenues by which the useful uv energy can be increased. We will discuss some of the approaches attempted below. It is important to understand that improvements in the uv source do not result in a change in the spatial distribution of the radiative intensity. This is, of course, fixed by the mean free path. They affect only the efficiency of generation of the radiation or the absolute level of the radiation throughout the spatial extent.

1. Electrical Efficiency, ϵ_{el}

The efficiency, ϵ_{el}, which represents the conversion efficiency of total stored energy to total radiated energy, is basically determined by circuit parameters, e.g., by inductance and resistance in the wires and elements employed.

Because the uv arcs employed have a low characteristic impedance, the driving circuit must be of low impedance for maximum power transfer.

2. Ultraviolet Radiation Efficiency, ϵ_{uv}

This efficiency represents the conversion of total radiated power (into all wavelengths) to radiation in the 1200 to 1700 Å bandwidth useful for photoionization. Assuming the source arcs radiate as black bodies then in the range 1200 to 1700 Å, the maximum efficiency possible is 25%. This occurs for a black body temperature of 20,000°K and a total radiative flux of 700 kW/cm^2.

This efficiency is essentially a reflection of the wavelength match between the emitting gas of the uv source and the photoionization cross section of the seed gas.

3. Stored Energy

This quantity indicates what amount of energy must be stored in the capacitor discharge circuits to give a certain electron density. It also indicates what density of arcs is needed.

The work that has been completed to date deals with electrical efficiency and the stored energy. We will combine them into a single category of circuit design considerations.

B. Ultraviolet Source Circuit Discussion

The uv source configuration of a series of copper chips is essentially a low voltage, high current arc where the arc cascades the complete length of the chips. The uv source arcs may be represented to a first approximation by a constant voltage battery. The arcs are arranged in series to obtain a better voltage match to the pulser circuitry. The operating voltage of each arc is typically $V_{uv}^{1} \sim 100$ V

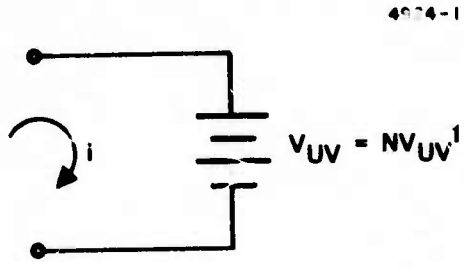

Thus in the LSD, where the number of chips (or arcs) for each row is N ~ 20, we have the voltage of the battery of about $V_{uv} = 20\ V_{uv}^1 = 2$ kV. The main design problem is matching this low battery voltage to the large voltage (approximately 20 kV) required to break the gaps down and cause the arc cascade to start. This can be seen from a simple analysis of the circuit of one row of arcs.

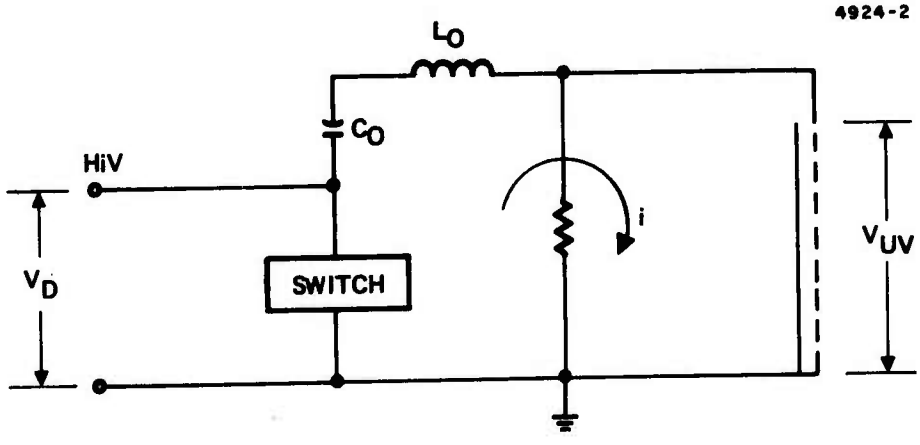

The expression for the current is

$$i = \omega_o C_o (V_o - V_{uv}) \sin \omega_o t \qquad (1)$$

where

$\omega_o = 1/\sqrt{L_o C_o}$

V_o = charging voltage

V_{uv} = voltage across uv row

and the charge on the capacitor C_o is given by

$$q_o = V_{uv} C_o + C_o (V_o - V_{uv}) \cos \omega_o t \quad . \qquad (2)$$

At the end of the first half-cycle the current has fallen to zero. This is the period over which you would like to deliver the stored energy to the arc boards. The optimum situation for delivering all the stored energy (e.g., $q_o = 0$ at some time) is when $V_o = 2\ V_{uv}$. That is, if $V_o = 2\ V_{uv}$, the final charge on the capacitor is zero and all the stored energy is delivered to the discharge.

Unfortunately, V_o in the present case is about 20 kV which, of course, is much larger than $2\ V_{uv} = 2(2\ \text{kV}) \sim 4$ kV. Thus a voltage mismatch occurs, charge is still left on the capacitor at the end of the pulse, and the circuit "rings." If the resistance of the arc discharge were higher, V_{uv} would be larger and a better match would result. It is known empirically that the resistivity, ρ, of an arc discharge varies inversely proportional to the square root of the field strength

$$\rho \propto \sqrt{\frac{L}{V_{uv}^1}} \quad ,$$

where L is the gap separation of the arc electrodes and V_{uv} is the voltage across the arc. It is also known that the radius r of the arc is proportional to the fourth root of the energy deposition per unit length,

$$r \propto (E/L)^{1/4}$$

where E is the total energy discharged. Thus the total arc resistance

$$R = \frac{\rho L}{\pi r^2} \propto L^2 \quad .$$

The arc resistance varies directly with the length of the arc (squared). Thus we see that to increase R we would like as long an arc as possible.

Now the energy deposited into the arc discharge can be found by multiplying eq. (1) by V_{uv} and integrating over the time interval (of one half sine wave). We find that

$$E_{arc} = 2 C_o (V_o - V_{uv}) V_{uv}$$

and that E_{arc} is maximum when $V_o = 2 V_{uv}$. The efficiency ϵ_{el} is then given by the ratio of E_{arc} to $E_{stored} = 1/2 \left(C_o V_o^2\right)$

$$\epsilon_{el} = 4 \frac{V_{uv}}{V_o} \left(1 - \frac{V_{uv}}{V_o}\right) \quad .$$

For our situation

$$V_{uv} \sim 2 \text{ kV} \quad ; \quad V_o \sim 20 \text{ kV} \quad ,$$

therefore,

$$\epsilon_{el} \cong 30\% \quad .$$

The energy delivered into the arc, E_{arc}, has been measured and was found to be ~25% of the stored energy, in agreement with this simple analysis.

To summarize the results of these expressions we see that to increase the energy delivered to the arc we want (1) to increase the operating voltage of the arc V_{uv}, (2) to increase the resistance of the arc by increasing the arc length, and (3) to lower the charge voltage V_o.

All of these effects give a better voltage match between V_o and V_{uv}. In addition to maximizing ϵ_{el}, we also want E_{stored} as large as necessary to give the electron densities needed. To see how this varies with the circuit parameters we examine the current that flows through the circuit. For the present time we assume that V_{uv} is a constant across the arcs; hence the light output will vary with the current. The maximum current given from eq. (1) is

$$i_{max} = \sqrt{\frac{C_o}{L_o}} (V_o - V_{uv}) \quad .$$

Since V_{uv} is $\ll V_o$

$$i_{max} \approx V_o \sqrt{\frac{C_o}{L_o}} \quad .$$

Thus we see that to maximize the current you want to decrease the inductance and increase the capacitance and the charge voltage. Note that i only varies as the square root of C_o but varies linearly with V_o.

C. Experimental Results

The experimental results to date have been confined to examining what effects changes in C_o and L_o have upon the electron density production. The small-scale device (2.5 x 15 x 50 cm^3) has been used for all the measurements. The capacitor size was doubled and the electron density achieved increased as expected. It is important to note that the electron density varies (see Appendix D) as

$$n_e \propto \sqrt{E_{uv}}$$

$$n_e \propto (C_o/L_o)^{1/4} \quad .$$

Therefore, doubling the capacitor size produced only about a 15% increase in n_e. (Larger size capacitors were not studied because of the prohibitive costs involved.)

Next, the circuit inductance was decreased. This was accomplished by using coaxial cables to feed the capacitor energy to each row together with making all connections from a low inductance copper sheet. It was found that the improvement in electron density production was again small. The basic result can be summarized by noting that although an increase in the peak electron density occurred, the loss rate (controlled by electron recombination) also increased. Hence the total energy into the gas discharge which is the integral of the current pulse remains about the same as in the higher inductance case. There is the benefit that the overall efficiency is slightly higher.

A further experiment that will be performed during the next reporting period is to alter the chip spacing and number to change V_{uv}. If the spacing can be made smaller and the number of chips increased, the total operating voltage will be larger (it is expected that the operating voltage of an individual arc will not depend greatly upon the spacing)

and hence a closer match to V_o might be possible. The opposite effect, that of increasing the spacing to increase the arc resistance, will also be tried.

D. Spectral Match Considerations

The remaining factor to consider is the efficiency of matching the uv source spectra to the seed gas photoionization cross section. In preliminary experiments described in the first semiannual report, it was found that removing the CO_2 from the source region and replacing it with N_2 resulted in a twofold increase in electron density production. Upon examination of the spectral characteristics of N_2 it was found that many lines appear in 1200 to 1700 Å window useful for photoionization of tri-n-propylamine. Based on these considerations a N_2 purge system is being constructed for operation on the small scale device (2.5 x 15 x 5 cm^3). This system will consist of several feed lines with small holes drilled in them. These feed lines will be located directly above the arc board and below the mesh screen electrode. Just before the arc board is fired, a valve will be actuated that will blow N_2 across the boards and purge the region of CO_2. It is not expected that this will affect the gas mixture in the discharge region to a great extent, but this will be investigated. The effect of this purge gas on the electron production will then be investigated.

E. Summary

Based on the experimental results discussed above negligible improvements in uv source performance have been achieved. However, it is expected that the remaining tests to be performed (described above) will lead to improvements, and these will be reported in the next reporting period.

III. ARC SENSOR CIRCUIT

In this section the arc sensor circuit required to discharge the large energy storage bank on the LSD will be described. The design, construction, and testing of this unit (included in Task 1) is complete.

A. Objective

Three arc regimes for the uv sustained laser exist. First, the well known post-arc phenomenon common to e-beam sustained lasers exists. This arc regime is due to the heated gas in the discharge center expanding out and lowering the density. Since the energy storage bank is essentially operating as a large dc battery, the voltage is still applied to the electrodes and hence the local E/N is higher leading to a post-arc (arc after the laser pulse is over). This arc regime does not affect the laser performance but presents a system operational problem (see below). Second, if an operational failure occurs with switching of the uv sources, a premature arc can be caused. Finally, attempts to load too much energy into the discharge regime can cause a glow-to-arc transition (GAT). All three regimes lead to arcs which cause serious damage to the fragile mesh screens that are wrapped around the Bruce electrodes. It must be remembered that since the energy storage bank is designed to provide essentially constant voltage throughout the pulse length it is of very large capacity. Approximately, only a 10% decrease in the energy of the bank occurs during a normal run. However, when an arc occurs the entire bank dumps with sufficient energy to damage the screens each time. Therefore, it is important to incorporate an arc-sensing circuit into the firing sequence to dump the bank before it can discharge into the screens.

The basic block diagram of the electrical layout involved is shown in Figure 1. (The arc-sensing circuit will be described in detail later.) The crowbar is shown together with the CP50 Marx bank which fires the crowbar. The key problem of the arc-sensing

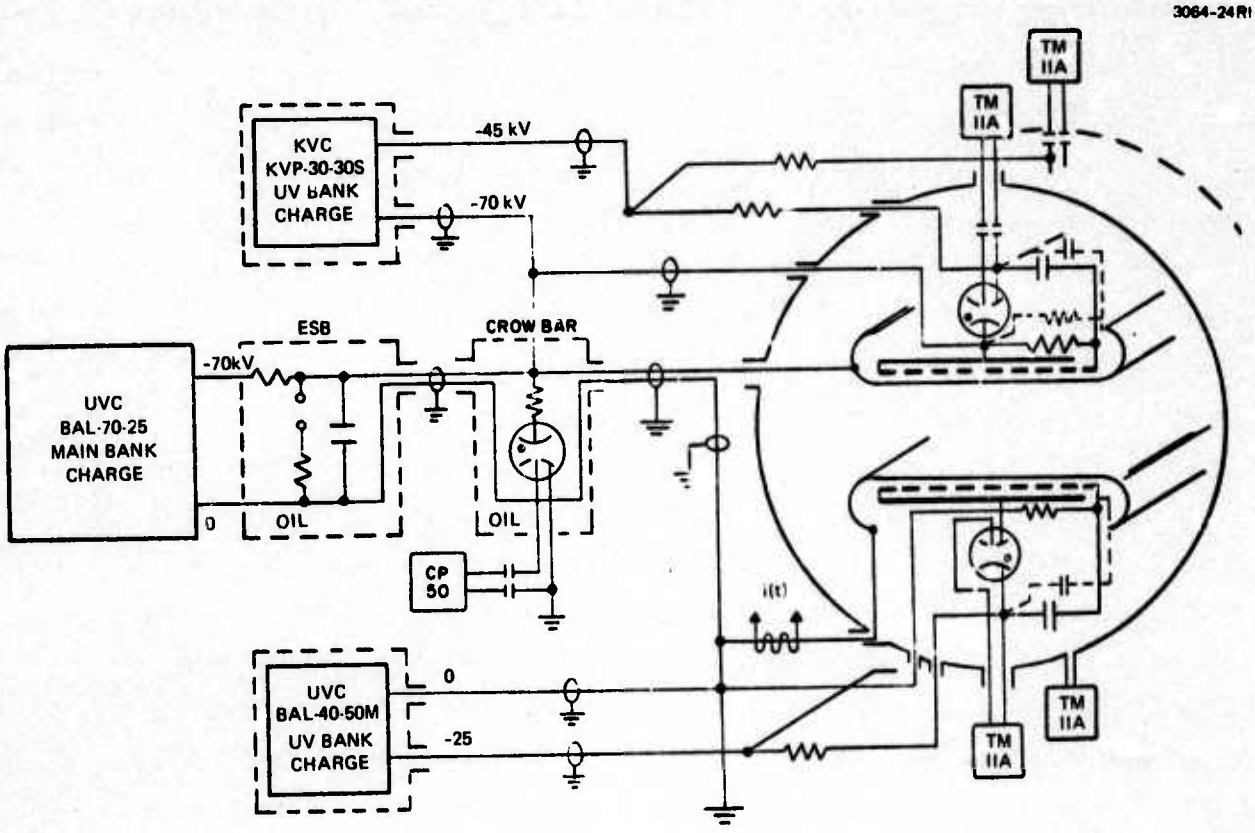

Figure 1. Electrical layout.

circuit is to provide a signal to the CP50. This signal is generated by sensing an arc in the device using a small capacitor connected to the high voltage electrode. This capacitor is charged when the bank is normally charged. If an arc occurs during a run, the voltage immediately drops on the electrode producing a small current through the capacitor proportional to dV/dt. This current is then sensed, processed to give the correct characteristics to fire the CP50 Marx bank, and then sent to the CP50 which fires the crowbar. This complete process takes about 500 nsec.

This is the basic arc sensing sequence. However, severe problems arise in this system because of the high EMI noise environment of the experiment. The primary problem is caused by the signals generated in the arc-sensing circuit by the uv circuits firing. This is a real signal, but represents an unwanted noise to the arc-sensing circuit. This type of problem required modular construction, light pipe connections, and blocking-out signals before successful operation was possible. A detailed description follows.

B. Fault-Detector Electronics

Two objectives of the fault-detection electronics are (1) it must detect current faults in the laser, and (2) it must provide a high voltage pulse to the laser supply crowbar circuitry to shut down the experiment and prevent mechanical damage to the laser. Because of the high noise environment associated with the experiment and the large currents flowing in the laser, the following guidelines were established for the electrical and mechanical construction of the electronics package:

- Unit must be battery operated
- All input signals must be optically coupled
- Mechanical construction must use standard EMI-RFI restraints. (The mechanical aspects will not be discussed in this report.)

C. Operation

The fault-detection electronics is comprised of a number of different independent sections. By following the signal timing diagram (Figure 2) and referring to the system block diagram (Figure 3) the unit can be explained as follows.

There are two signal inputs to the unit. One is from the laser control console and is designated "Arm Signal;" the other is from the laser fault sampling line (see Figure 3) and is designated "Fault Signal." When the laser is fired an arm signal, coincident with the fire signal, is sent through an optical light coupler to the fault detector. Because the speed of operation of the fault detector is critical, this coupler uses a very fast SCR and an LED (typically 10 nsec) for the transmitter and a silicon photodetector coupled to an FET input wide band amplifier for the receiver. This configuration yields a fast signal response time and very high electrical noise isolation between the experiment and the fault detector.

As seen in Figure 2, at the same time the arm pulse is sent, signals are appearing on the fault-detection sampling line. These signals are identical, in both shape and amplitude, with a real fault signal. These, however, are not fault signals but are signals generated when the uv sources are fired.

With this in mind, the arm signal out of the wide band amplifier is fed to the variable delay section. Here the arm signal can be delayed for 1 to 10 μsec, and the amount of delay is controlled by the laser operator. The proper delay setting is just after the noise generated by the uv sources has decayed (~3 to 5 μsec).

Once delayed, the arm signal is fed to the arm window section. Here the pulse is used to generate a time window that is controllable by the operator. Once this window is generated the fault detector will not only detect faults in the laser but will react to them as well. When the arm window is generated, a panel-mounted LED is lit to indicate to the operator that the unit is armed.

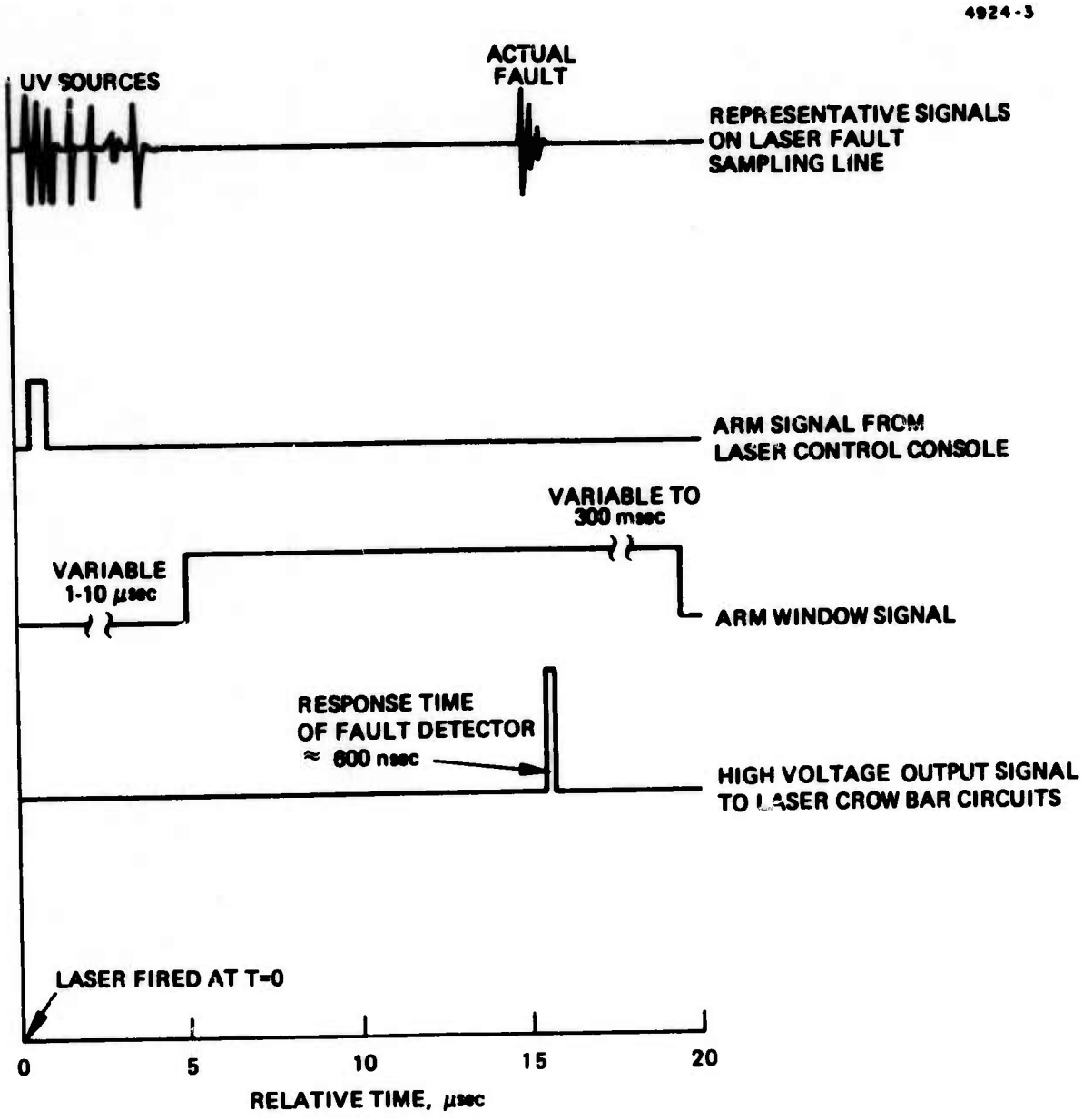

Figure 2. Timing diagram of fault detector signals.

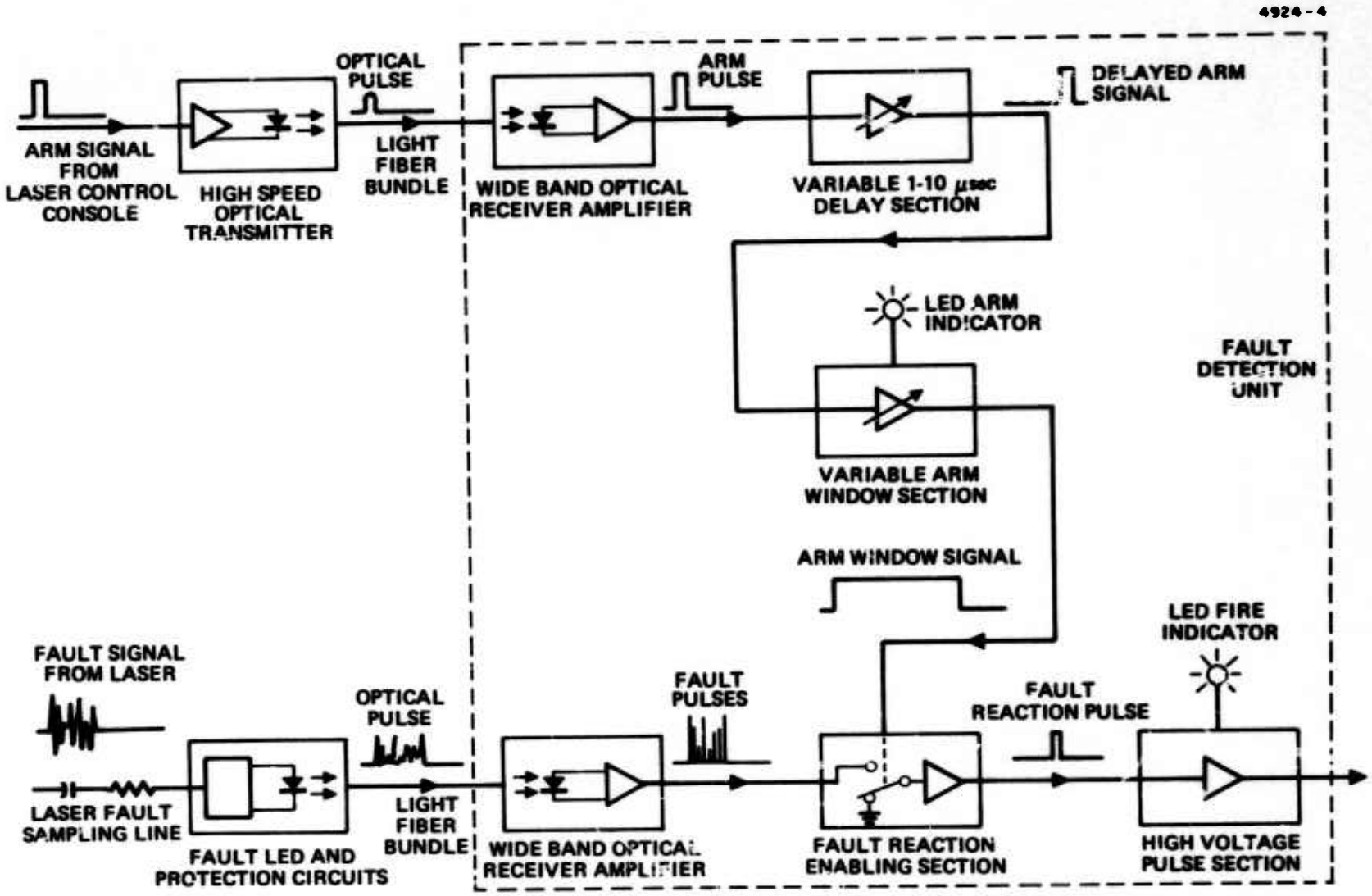

Figure 3. Fault detector block diagram.

The fault signals to be detected originate in the fault detection sampling line, where the key component of the fault detector is. It is simply a high speed, high current LED with some associated protection circuitry. By using an LED as the signal source we again have high electrical noise isolation plus fast response time and good signal sensitivity. The optical fault signal is fed through 30 ft of low-loss optical fiber to the fault detector where it is received and amplified by an amplifier identical to the arm pulse receiver.

When the arm window is present and a fault signal is received it is amplified and fed to the high voltage pulse section. It is used to ignite a gas filled discharge tube connected to a high voltage supply. This generates a high voltage pulse which is transformer coupled to the laser supply crowbar circuitry thus ending the laser current. A panel-mounted LED is provided to inform the operator that a fault was detected and a crowbar output signal was sent.

The response time of the fault detection unit is ~500 nsec. Although this figure could be reduced by 50%, the noise immunity of the electronics would be greatly reduced and unreliable operation would result.

A detailed circuit diagram is shown in Figure 4.

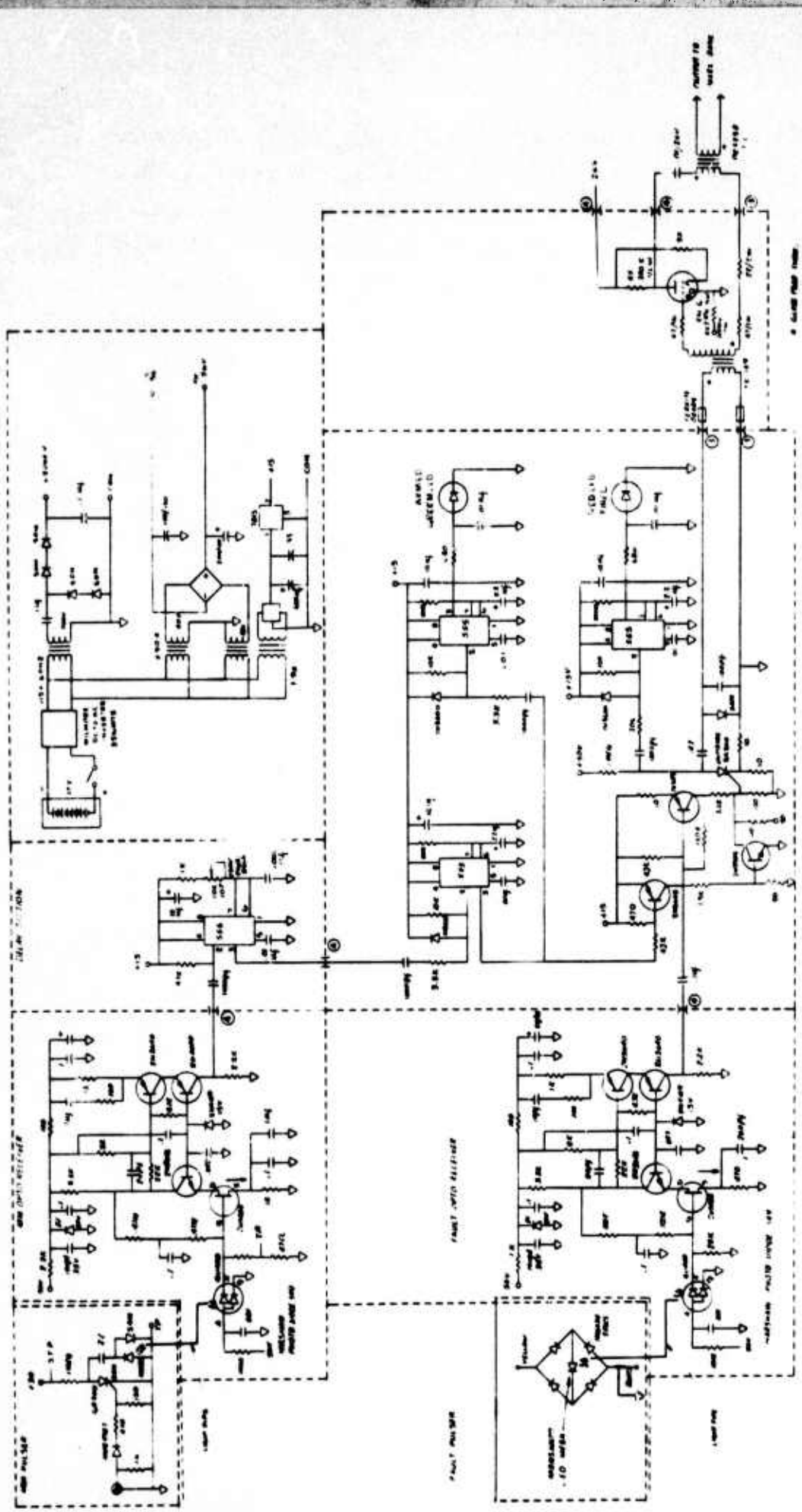

Figure 4. Arc sensor circuit.

IV. SUMMARY AND FUTURE PROGRAM PLAN

A. Summary of Results

Significant results obtained on the contract to date on the large scale device are as follows:

- Near 300 J extraction energy in a reduced discharge geometry using an unstable resonator
- Characterization of small signal gain, spatial variation of <5% in electrode gap dimension and 25% in discharge width dimension
- Gain magnitude of ~0.85%/cm typical
- Medium quality better than $\lambda/30$ for region unaffected by uv and cathode wave and $\lambda/8$ including such waves.

B. Program Plan

The objective of the proposed program is to determine the scalability of the uv-sustained laser on a single pulse basis. To achieve this objective the program will establish

- Demonstrated energy extraction with the largest electrode gap possible in the large scale device
- Consistency with scaling model to give uv flux requirements and design criteria for high power uv-sustained laser.

The tasks proposed to achieve the above objective are discussed below. The program plan is shown in Figure 5.

Task 1

Under this task, the uv source flux required for scalability to larger gap spacings on the LSD will be determined. Energy extraction measurements at a gap height of 10 cm will be performed using the

4181 – 2RI

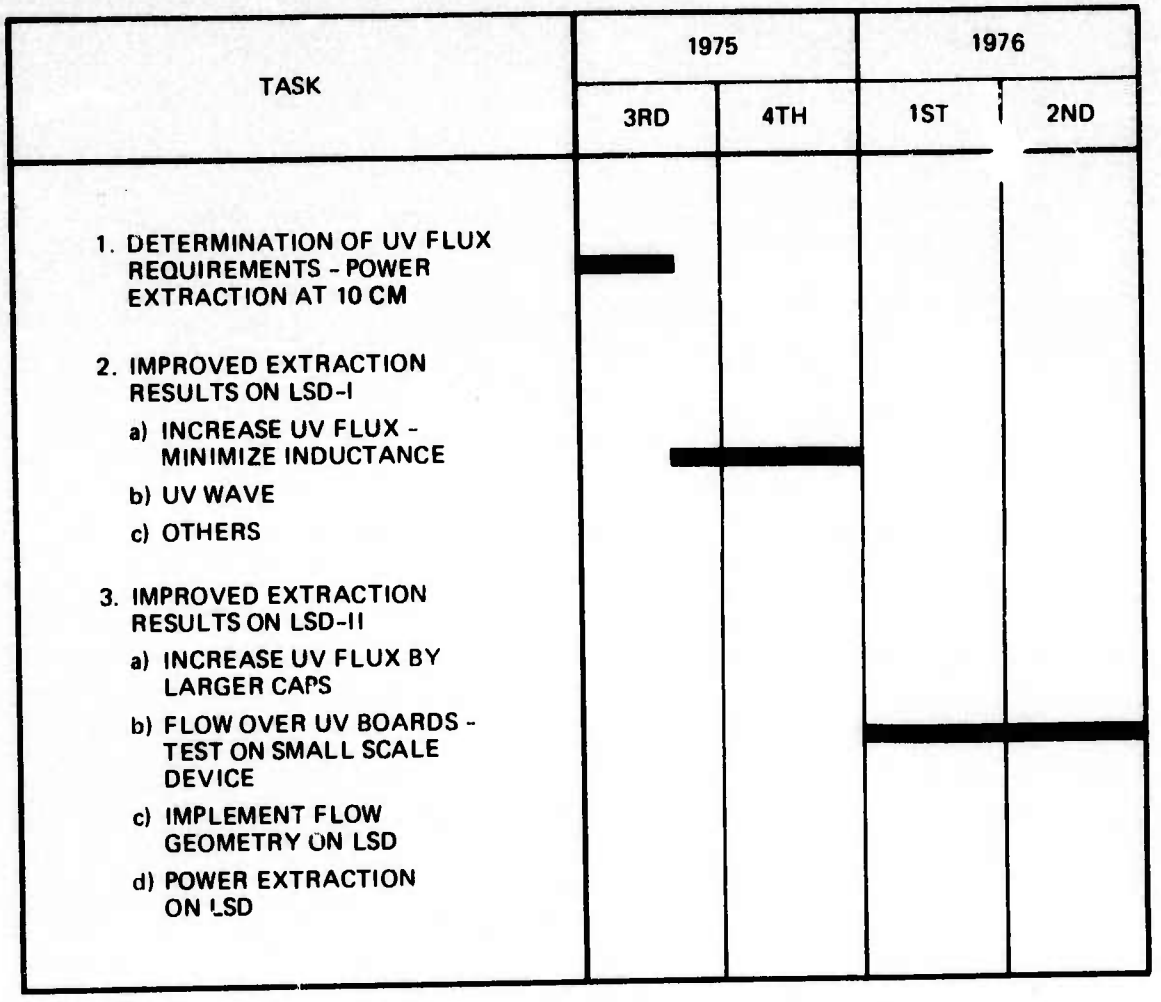

Figure 5. Program schedule.

existing uv source. These measurements, together with the extraction results obtained at 6 cm, will be compared with the scalability model predictions. (See Figure C-9 curve labeled "uv source not scaled.") The results of the comparison will indicate the uv source strength required to maintain a linear output energy with gap height (curve labeled "uv source scaled"). Achieving this flux level will occupy a major portion of the remaining tasks. In addition, an operational improvement to the LSD will be made. This will consist of incorporating an arc sensing circuit into the firing sequence. This unit will discharge the large energy storage bank if an arc occurs in the system, thus preventing the bank from discharging into the electrode screen and causing permanent damage.

Task 2

Work under this task represents the first step toward obtaining an increase in the extraction energy at 10 and 12 cm gap heights over that achieved under Task 1. This was to be accomplished by increasing the uv flux levels through a minimization of circuit inductance. In particular, multiple spark gaps would be employed to switch the uv arc rows. However, in view of the experimental results with decreased circuit inductance, it has been decided not to employ multiple spark gaps. Techniques developed under Task 3 will be used instead.

Task 3

Under this task the uv source will be improved. The objective of this task is to demonstrate a linear scalability of the LSD consistent with achieving a 1 kJ output.

The uv source flux will be improved in two steps. First, an increase in the size of the capacitors feeding the arc array will be implemented. Second, a detailed investigation of the effect of purging the arc array region with some other gas such as He or N_2 will be made. These flow tests will be performed on an existing small-scale device in order to establish the proper geometry. Upon completion of these small scale tests, the chosen geometry will be implemented on the LSD. Power extraction will follow.

REFERENCES

1. R. C. Lind and J. Y. Wada, "Investigation of Ultraviolet Photoionization Sustained Discharge for Gas Lasers," First Semiannual Technical Report, Contract N00014-73-C-0287, Hughes Research Laboratories, Malibu, California (1973).

2. R. C. Lind, W. M. Clark, and J. Y. Wada, "Investigation of Ultraviolet Photoionization Sustained Discharge for Gas Lasers," Second Semiannual Technical Report, Contract N00014-73-C-0287, Hughes Research Laboratories, Malibu, California, March 1974.

3. R. C. Lind, "Investigation of Ultraviolet Photoionization Sustained Discharge for Gas Lasers," Third Semiannual Technical Report, Contract N00014-73-C-0287, Hughes Research Laboratories, Malibu, California, August 1974.

4. R. C. Lind, "Investigation of Ultraviolet Photoionization Sustained Discharge for Gas Lasers," Fourth Semiannual Technical Report, January 1975.

5. R. C. Lind, "Investigation of Ultraviolet Photoionization Sustained Discharge for Gas Lasers," Fifth Semiannual Technical Report, January 1975.

6. H. J. J. Sequin et al., Appl. Phys. Lett. 23, No. 9, 527, November 1973.

APPENDIX A

SUMMARY OF PREVIOUS RESULTS – SMALL-SCALE MEASUREMENTS

During the first year of the program, extensive measurements have been undertaken on two crucial phases of the uv sustained plasma conditioning scheme. The first was a parametric investigation to determine achievable levels of discharge input energy. Second, as a direct result of the demonstration of the capability to obtain input discharge energy densities that would efficiently excite CO_2 laser mixtures, small signal gain distribution and power extraction measurements were performed. The results of these tests will be discussed below.

1. Input Energy and Mean Free Path Determination

The input energy measurements were performed on a small device which employed uv arc discharges located adjacent to the main discharge electrodes (see Fig. A-1). Both the uv source and main discharge electrodes were mounted in a high vacuum glass enclosure to permit accurate control of the discharge environment. All internal supporting components were selected from those materials with low vapor pressure and outgassing properties and with high resistance to seed gas additives. Various mixture ratios of CO_2, N_2, He, seed gas concentrations, total pressures, and uv spark energies were studied to allow a complete mapping of obtainable sustainer energy densities.

Before presenting the results of these experiments and in order to provide a theoretical basis for the assessment of these data, we will first discuss a calculation of the uv produced electron number density expected for such a system. In Fig. A-2, the computed sustainer energy densities as a function of uv current are summarized for a wide

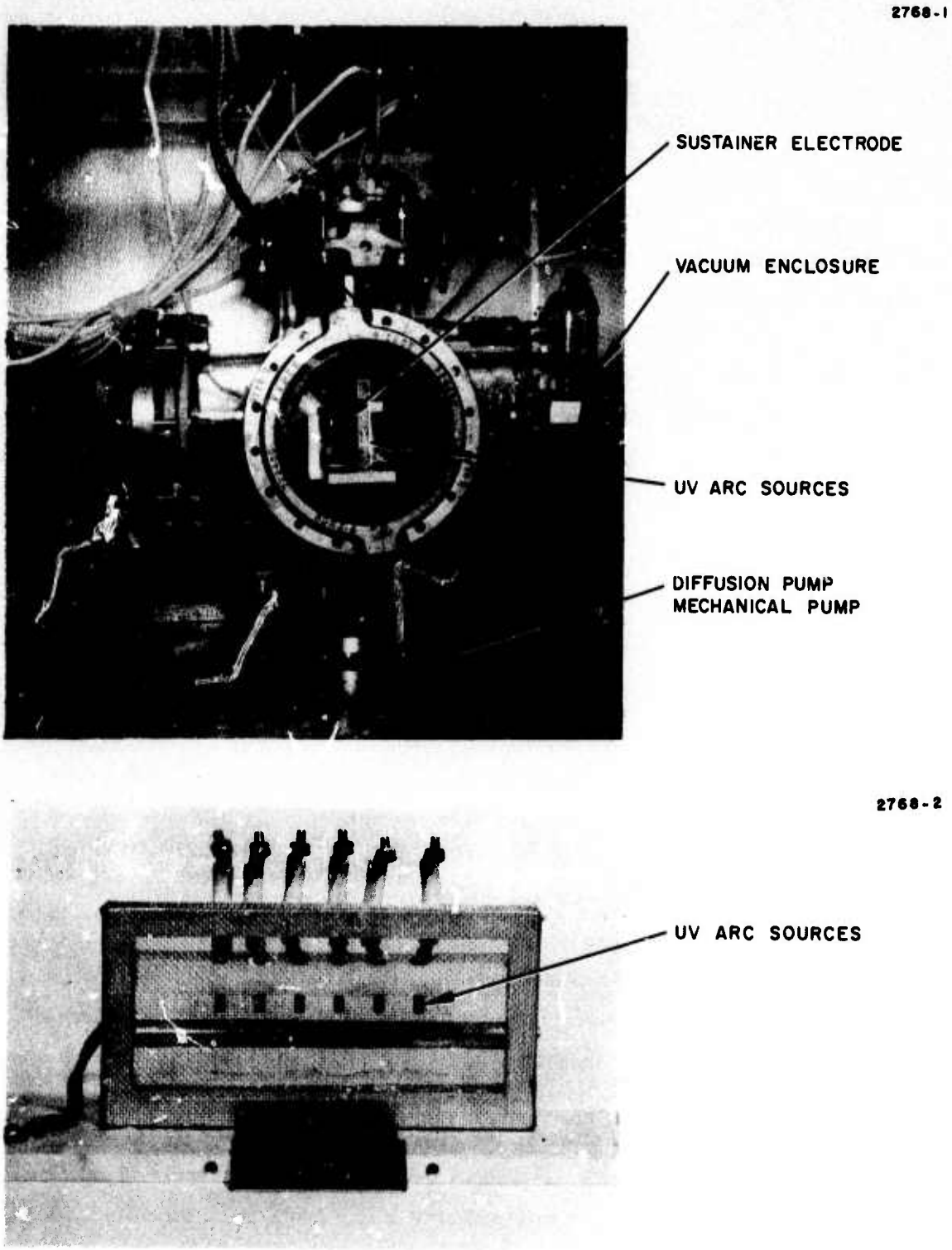

Fig. A-1. Experimental uv sustained discharge device.

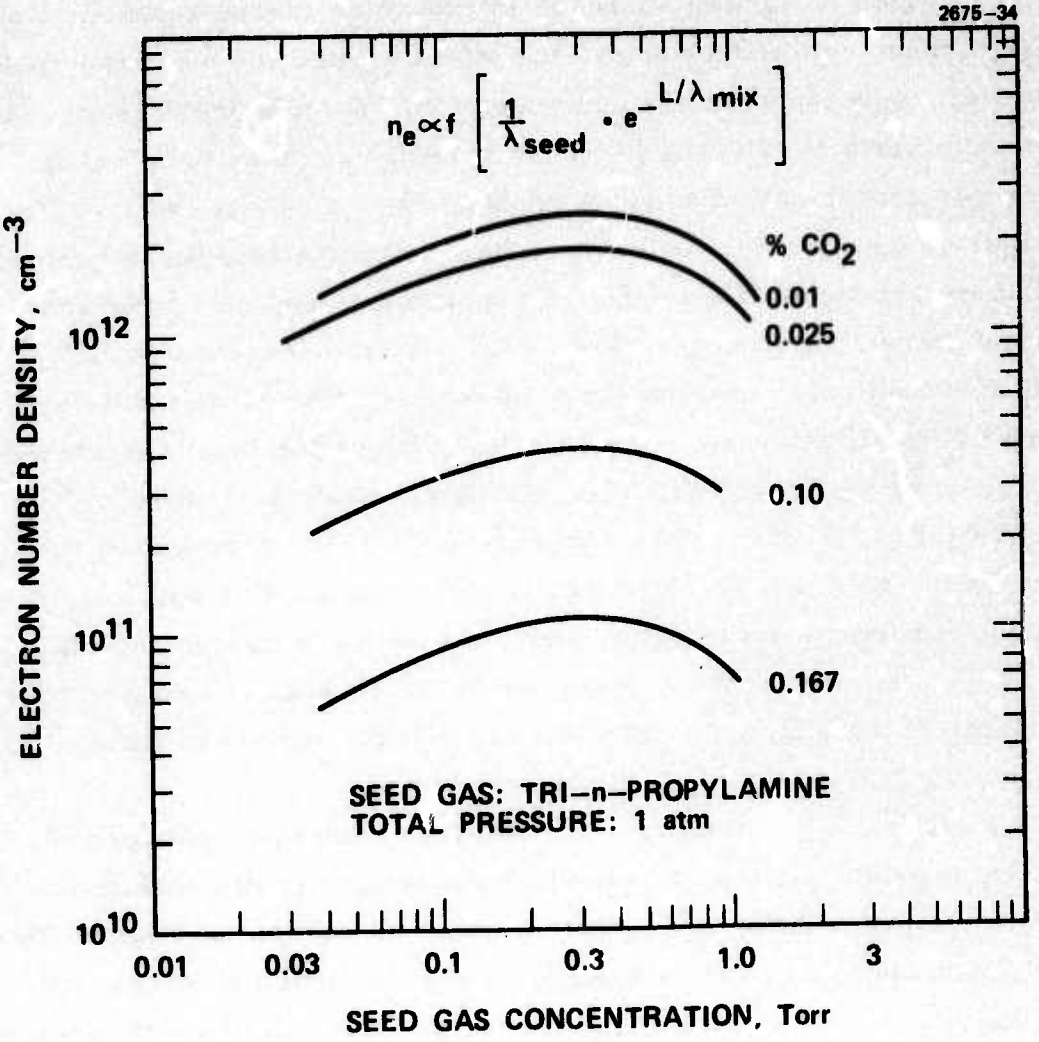

Fig. A-2. Calculated electron number density.

range of gas mixtures. This calculation assumes single-step photoionization of the added seed gas (in this example, tri-n-propylamine is used) and a recombination limited plasma. From this figure, we see two important effects. First, there is a minimum CO_2 concentration below which no further increase in sustainer energy results. As the CO_2 concentration decreases, the effective mixture mean free path is determined by the seed gas concentration. Second, there is a broad optimum in sustainer energy for a large (order of magnitude) change in seed gas concentration which produces only a small variation in the sustainer energy because at low seed gas concentrations the uv absorption characteristic is dictated by CO_2 molecules, and only when the seed gas concentration is increased does the seed gas absorption play a dominant role. Both of these effects are critical to the determination of the limiting mean free path and hence the limit of scalability.

Two of the results of the experimental study are shown in Figs. A-3(a) and A-3(b). First, in Fig. A-3(a), the normalized sustainer energy obtained as a function of the normalized uv spark current is plotted for four mixture ratios and fixed seed gas concentrations while in Fig. A-3(b), similar plots are for three seed gas concentrations with a fixed mixture ratio. We see that the results of these experiments follow the trends predicted above.

Figure A-4 gives the absolute sustainer energies obtained for the mixture producing the largest relative energy density results shown in the previous figures. With a uv spark current of 3 kA a value of 300 J/liter-atm has been obtained. The pulse lengths corresponding to these energies depend solely on the pulse length of the uv source; for the present case, this corresponds to an underdamped ringing arc circuit of approximately 50 μs in duration. Although 300 J/liter-atm is the input energy requirement for efficient CO_2 excitation, a considerable amount of radiated energy is expended to achieve this level. Estimates of this energy based on the 3 kA spark current indicate that approximately equal amounts of energy are deposited in the sparks and the sustainer discharge. Further experimental measurements directed toward alleviating this undesirable situation have demonstrated

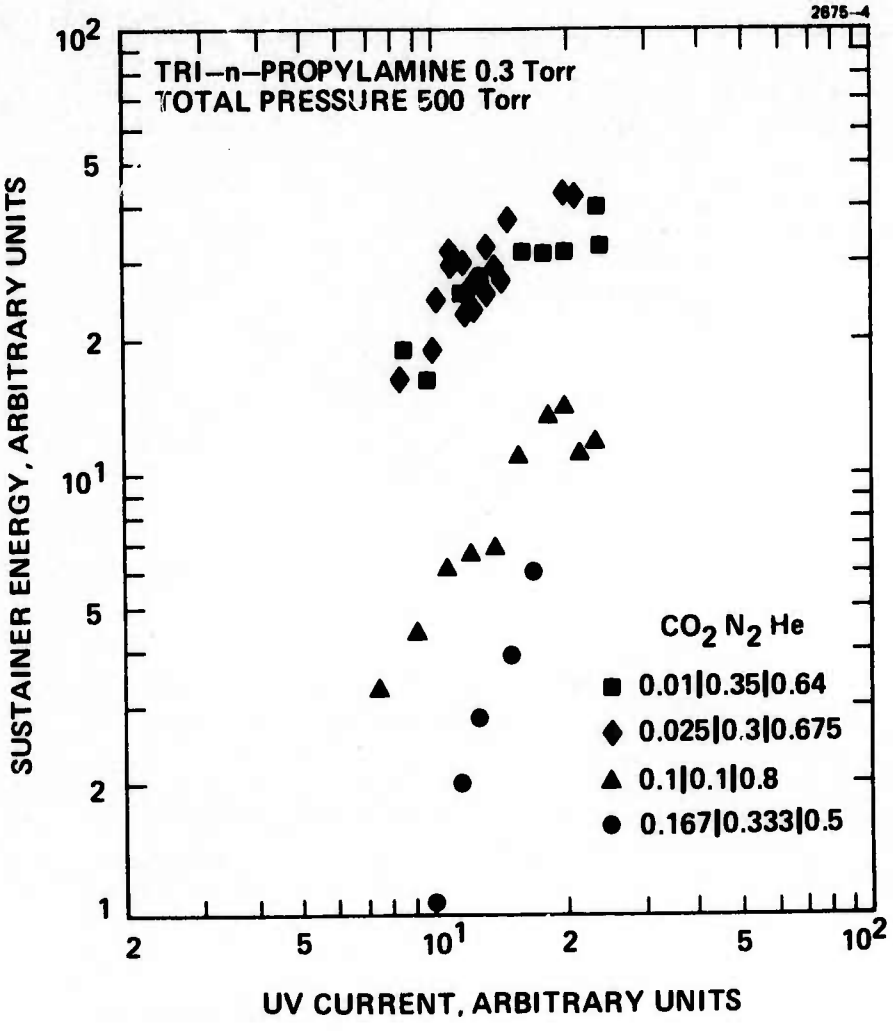

a. For various laser mixtures.

Fig. A-3. Sustainer energy as a function of uv current.

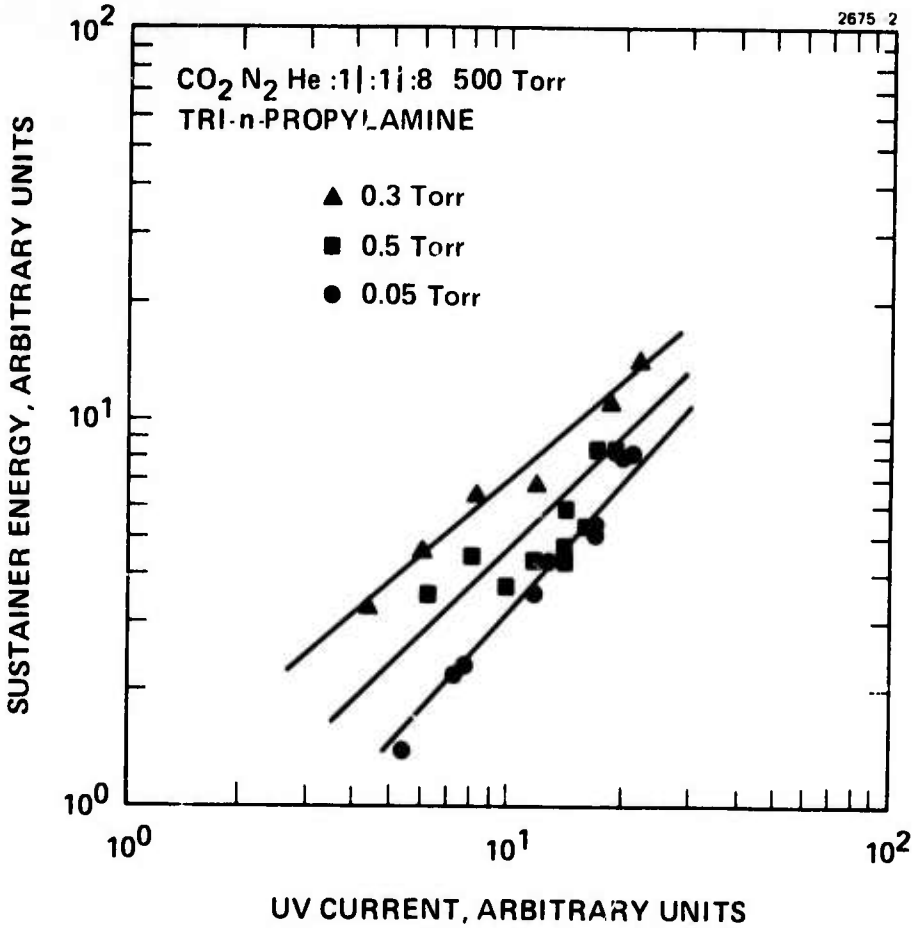

b. For various concentrations of tri-n-propylamine.

Fig. 3. (Continued)

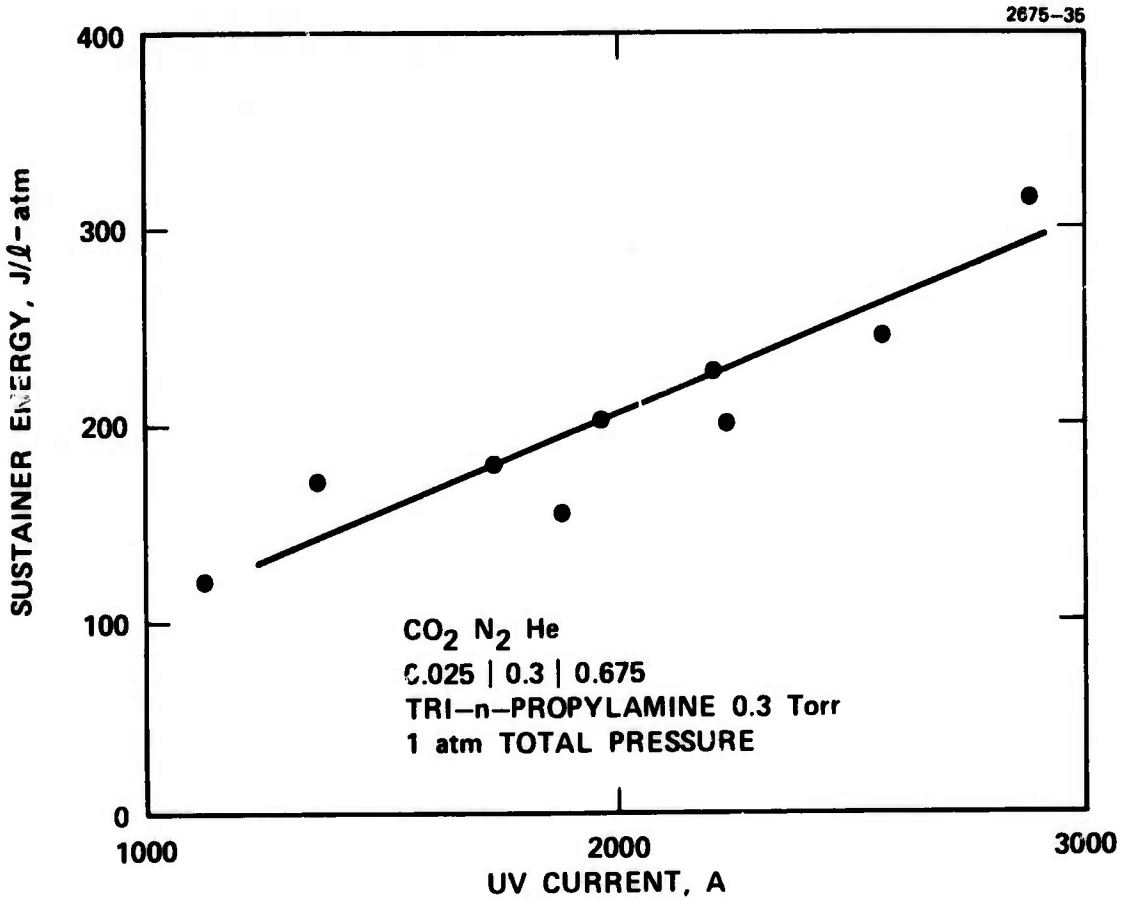

Fig. A-4. Maximum input sustainer energy in J/ℓ-atm as a function of uv current in amps.

that a substantial decrease in the amount of radiated energy required can be obtained by the use of a type of "vacuum sliding spark" system (discussed below).

The effective mean free paths of the CO_2 and seed gas molecules have been evaluated from such data and summarized in Table A-1. For a typical CO_2 mixture of 0.015 atm of CO_2 and 0.3 Torr of seed gas, the effective mean free paths are 11 cm and 20 cm, respectively, whereas the corresponding overall mixture mean free path is approximately 8 cm. As further conformation for this projected mean free path a characterization of the wavelengths responsible for the production of the observed photoionization of the added seed gases was undertaken. The results of such tests indicated that the observed dense plasma was produced by radiation with wavelengths between approximately 1200 and 1700 Å with more than 60% between 1500 to 1700 Å. Such a result can be explained by examination of the mean free path through CO_2 shown in Fig. A-5. Because the ionization potential of tri-n-propylamine is 1720 Å, we conclude that single step photoionization is the production mechanism for the plasma. It is clear from the mean free path shown that below 1200 Å no radiation is transmitted through any reasonable size device that uses CO_2; thus we arrive at the limiting wavelengths obtained experimentally.

Table A-1. Measured Effective Mean Free Paths of CO_2 and Seed (tri-n-propylamine) Gas

Molecules	Effective Mean Free Path[a] cm-Atm
CO_2	0.16
Tri-n-propylamine	8×10^{-3}

[a]Typical mixture of 1 atm: CO_2:N_2:He:seed gas 0.02:0.3:0.7:0.004.

T1195

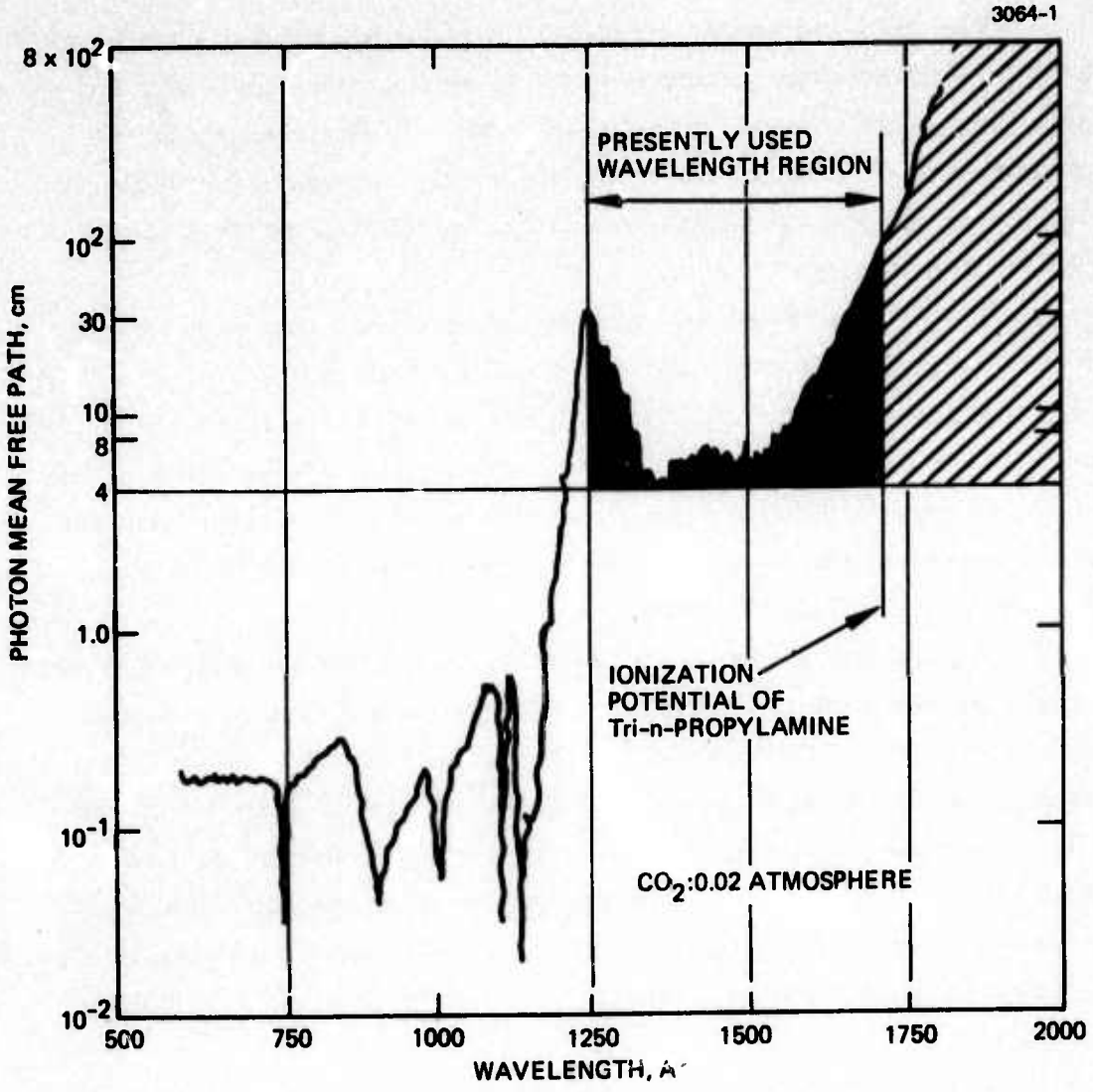

Fig. A-5. Ultraviolet photon mean free path through CO_2 at 0.02 atm.

2. Small Signal Gain and Power Extraction

The gain and power extraction measurements were performed on a larger discharge device employing an improved source for the UV radiation. This source consisted of a two-dimensional array of cascaded arc discharges across a dielectric substrate (as shown in Fig. A-6). (See second Semiannual Technical Report for a more detailed description.)

To test the feasibility of this cascaded arc discharge source to uv sustained plasma conditioning, a medium volume ($2.5 \times 15 \times 50$ cm^3) test device was constructed from an existing laser testbed. This device had a Bruce profiled cathode located 2.5 cm from a flat mesh anode. Brewster angle windows were employed for use with external laser optics which consisted of a 4.5 m total reflector and a 20% transmitting dielectric coated output mirror.

Figure A-7 gives typical current traces for the cascaded arc circuit and the sustainer plasma discharge obtained in a uv sustained mode. Figure A-7(a) was obtained at an $E/N = 1.7 \times 10^{-16}$ V-cm^2 and Fig. A-7(b) at an $E/N = 1.85 \times 10^{-16}$ V-cm^2. For the higher E/N the discharge is terminated by an arc occurring at approximately 22 μs into the pulse. Also, for the arc circuit, ringing occurs indicating that even though this uv source is more efficient there is a certain degree of impedance mismatch because of unavoidable circuit inductance.

The energy input to the discharge was calculated by integrating the area under sustainer current curves such as these and then multiplying by the dc bias voltage. For the results of Fig. A-7 this corresponds to about 350 J input which was the maximum value obtained for all cases run. By operating at higher bias voltages arcing occurred much earlier in the pulse and hence led to the attainment of smaller input energies. The calculation of energy density depends on the discharge volume (which at this time has not been determined with a high degree of accuracy). However, taking the physical size of the electrode of 15 cm by 50 cm as the discharge area we find that

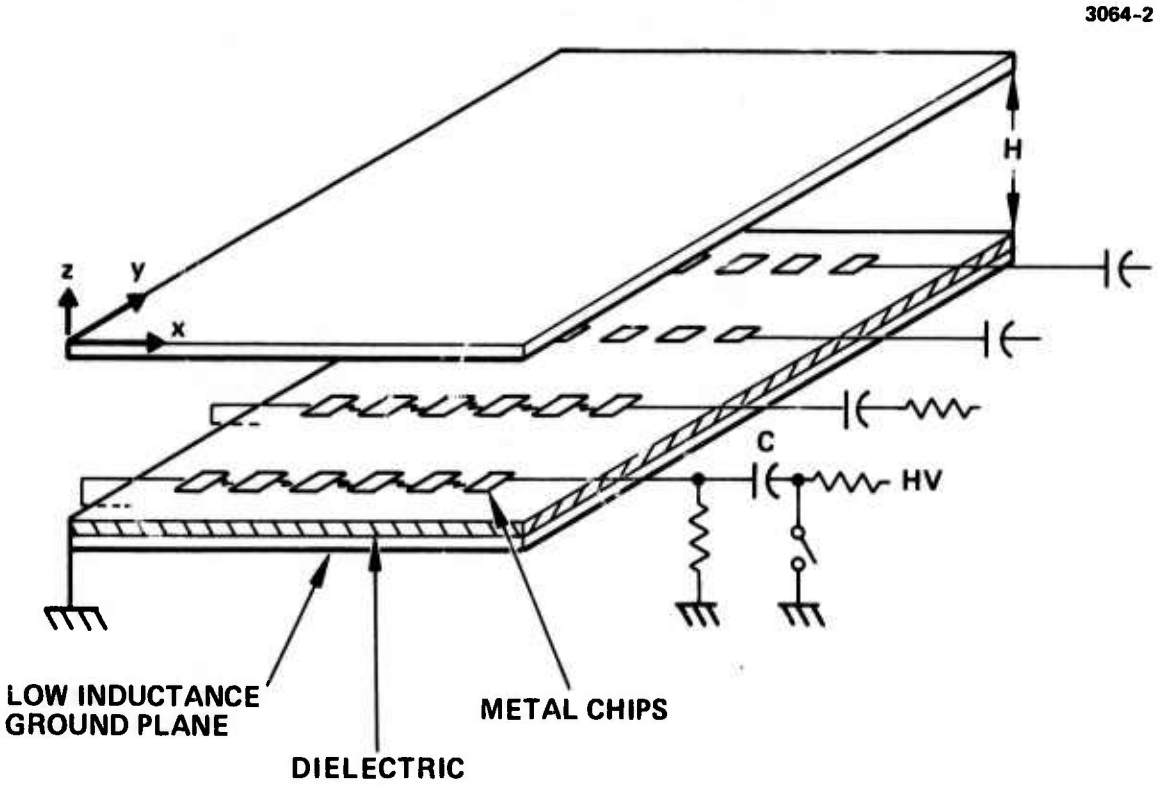

Fig. A-6. Cascaded arc discharge system.

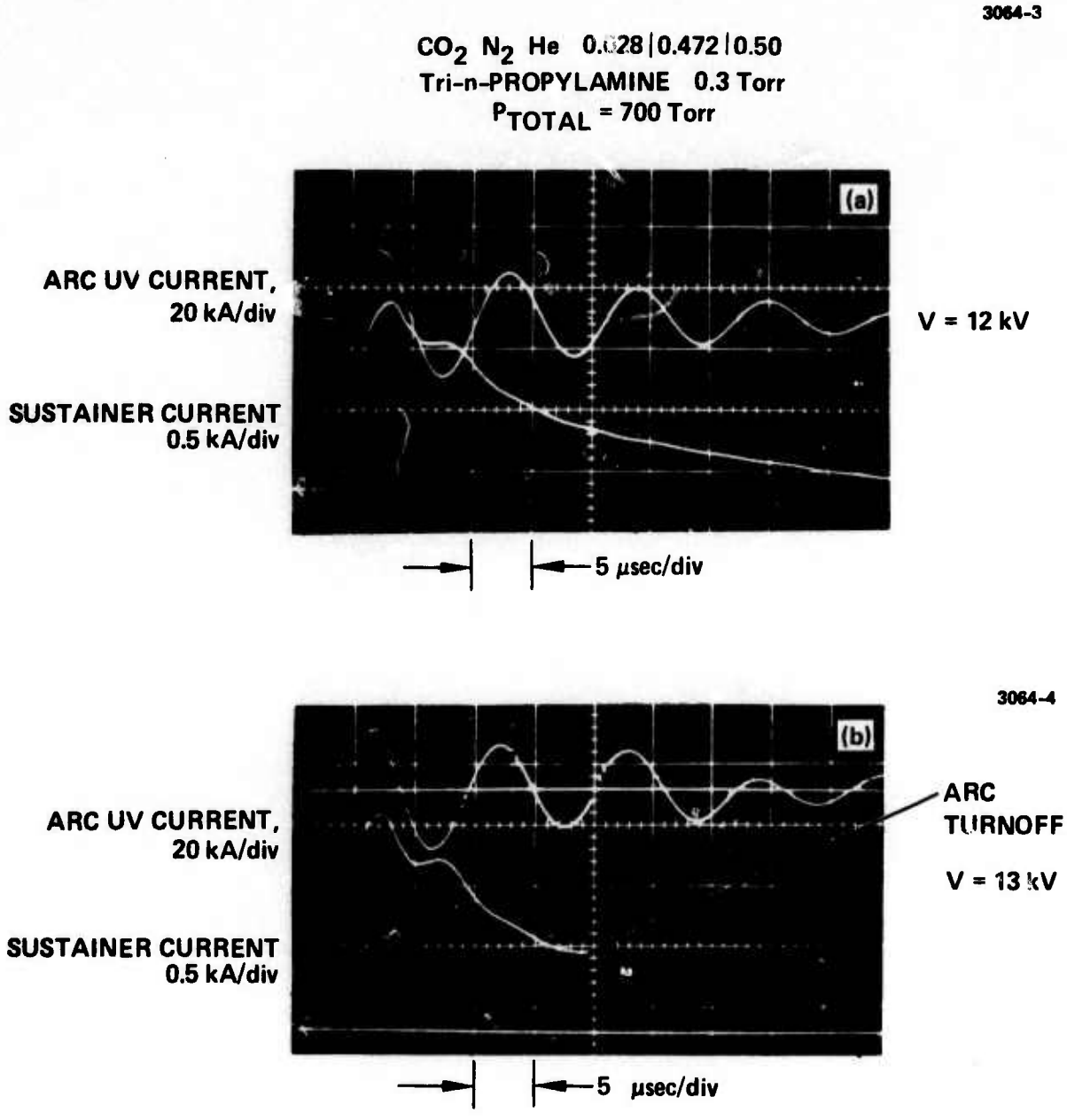

Fig. A-7. Sustainer current and cascaded arc discharge current waveforms.

an input energy density of 200 J/liter-atm has been obtained for the above case.

The small signal gain was also measured for various mixtures, bias voltages (E/N), and position. A typical gain waveform is shown in Fig. A-8. This trace was obtained at a point of 3.5 mm from the mesh anode, position 1 (see Fig. A-9 for orientation), which corresponds to a location approximately 2.5 cm from the cascaded arc discharge uv source. From this trace the arrival of the acoustic disturbance from the uv source to the point where the probe laser is located is evident. The gain is observed to rise continuously throughout the pulse.

The gain distribution across the gap spacing was measured for various bias voltages. The results for a CO_2, N_2, He 0.028/0.472/0.50, 0.3 Torr tri-n-propylamine mixture are shown in Figs. A-10 and A-11. In Fig. A-10 the gain as a function of bias voltage for the five probe positions is given. The gain varies in a nearly linear manner except for the position nearest the cathode where the gain begins to level off with increased voltage as observed in e-beam pumped systems.[A-1] In Fig. A-11 the gain as a function of position for three bias voltages is given. We see here that the gain increases, as opposed to decreasing, as the distance from the uv source increases. These results are indicative of the field strength increasing to maintain constant current, as n_e decreases moving away from the uv source, and thus rising to a value where possibly some local avalanching by the seed gas is occurring. In addition, the much higher gain near the cathode is a typical result seen for gain behavior in the cathode sheath region.[A-2] To indicate the very different nature of the gain waveforms near the cathode, the results obtained at position 5 are given in Fig. A-12. Figure A-12(a) is for 12 kV bias voltage and shows maximum pumping at the beginning of the pulse, because of the much higher n_e levels than obtained at position 1, and subsequent heating of the lower laser level during the remainder of the pulse (see Fig. A-8). Figure A-12(b) is for 8 kV bias voltage, and thus, much lower n_e levels, and shows pumping throughout the pulse duration but at a rate much lower than the case shown in Fig. A-8 which was for 12 kV bias voltage.

3084-5

CO_2 N_2 He 0.028 | 0.327 | 0.645
Tri-n-PROPYLAMINE 0.3 Torr
P_{TOTAL} = 700 Torr

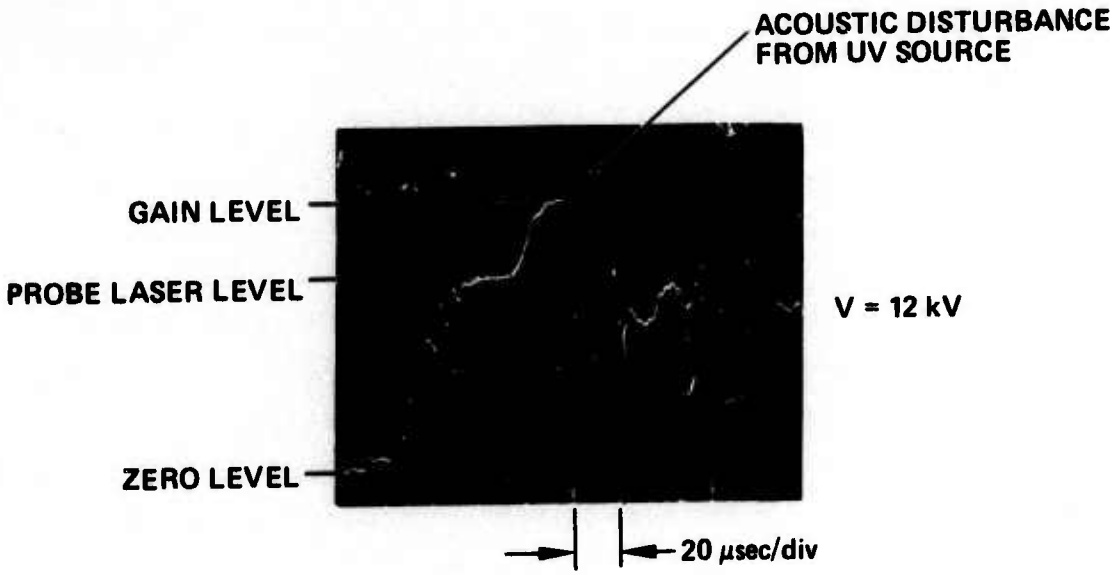

Fig. A-8. Small signal gain waveform at position 1.

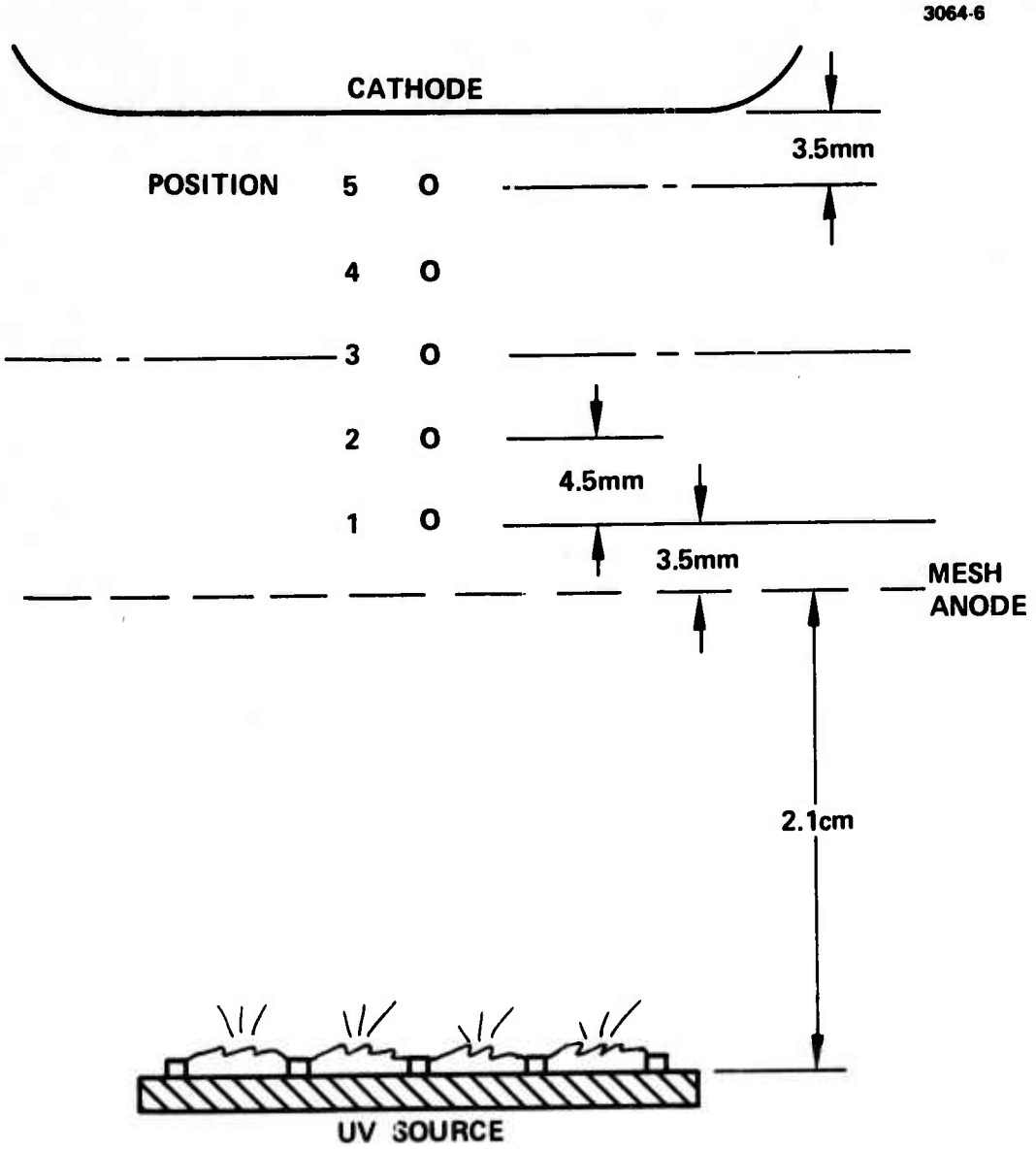

Fig. A-9. Continuous wave probe laser positions.

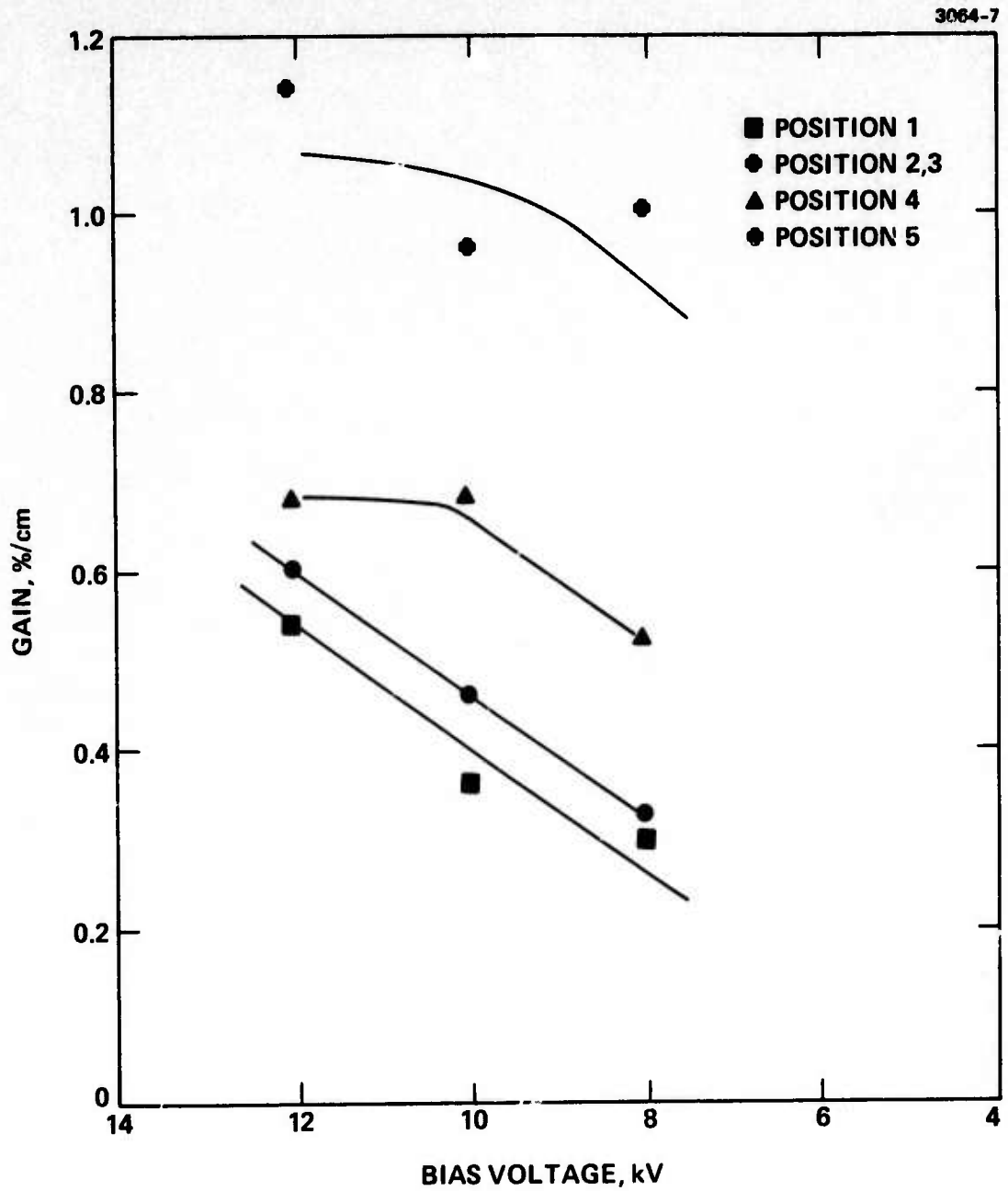

Fig. A-10. Small signal gain as a function of bias voltage for 5 positions.

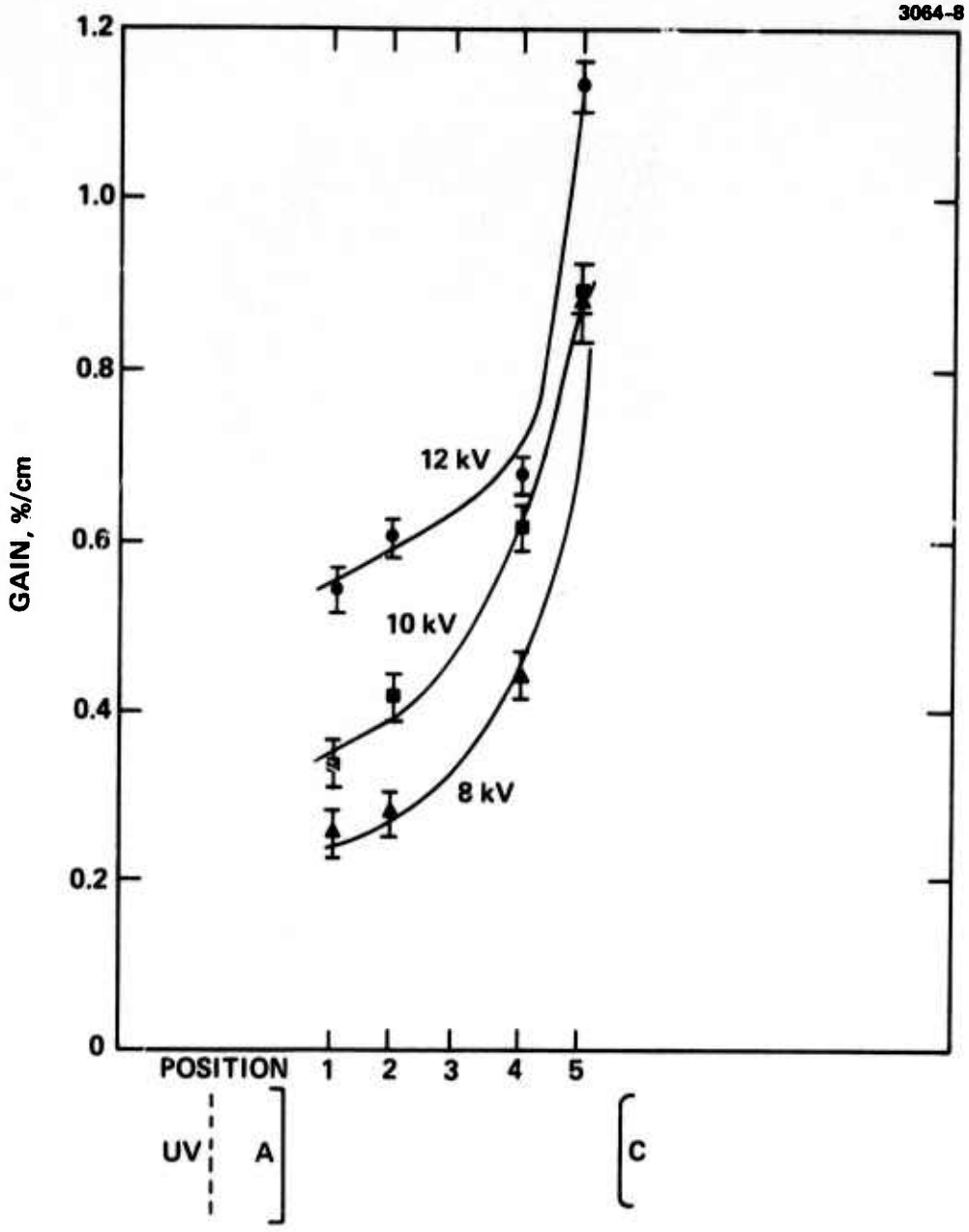

Fig. A-11. Small signal gain as a function of position for various bias voltages.

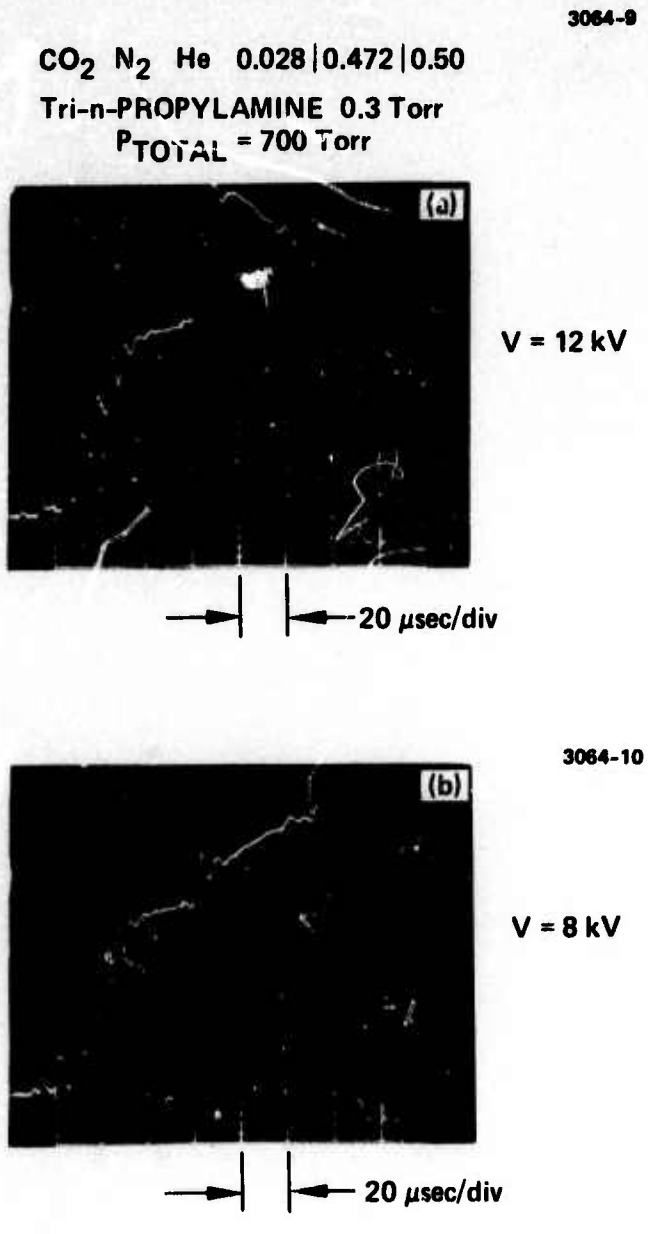

Fig. A-12. Small signal gain at position 5 for two bias voltages.

Extensive measurements of laser output were made using a stable cavity arrangement and a Hadron Model 117 calorimeter. The measurements consisted of keeping the uv source energy fixed and varying the bias voltage (E/N) of the discharge and varying the gas mixture. Typical laser pulse shapes are shown in Fig. A-13. The laser output shown in Fig. A-13(a) and 13(b) corresponds to the cases discussed previouslv and shown in Fig. A-7(a) and A-7(b), respectively. Figure A-13(a) gives a pulse with a multimode energy of 9.6 J and a pulse length of 37 μs. Figure A-13(b) gives a pulse with a multimode energy of 12 J with a pulse that is terminated by an arc which occurs 22 μs into the pulse.

The nearfield burn pattern for the laser output is shown in Fig. A-14. This pattern was obtained by using thermal chart recording paper. However, to determine the mode area more accurately, exposed photographic paper was used. This gave a slightly larger area than that shown. With the mode volume established in this manner the laser output energy density can be determined. For the 37 μs pulse of Fig. A-13(a), 47 J/liter-atm was obtained, and for the shorter pulse (≈29 μs) of Fig. A-13(b), 61 J/liter-atm was obtained.

To indicate a typical variation in output with E/N, Fig. A-15 gives such results for three CO_2-N_2-He, tri-n-propylamine mixtures. The fact that the output is lower at the largest E/N for the higher CO_2 concentration case results from an arc which occurred early in the pulse and lowered the obtainable input energy.

To calculate the electrical-to-optical conversion efficiency the input energy density is required. Using the estimated 200 J/liter-atm value discussed previously we find that an efficiency of about 20 to 25% is obtained.

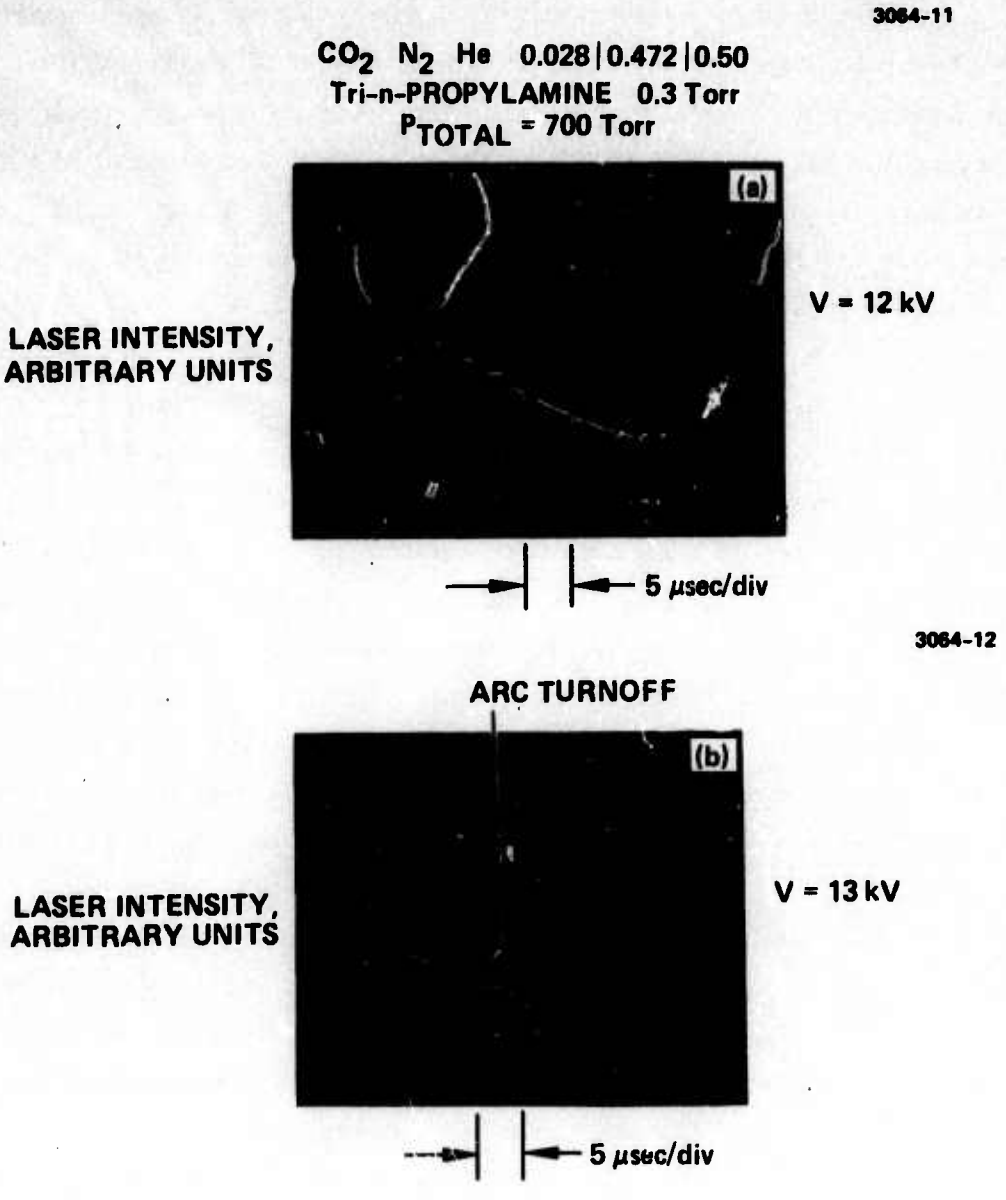

Fig. A-13. Laser pulse shape.

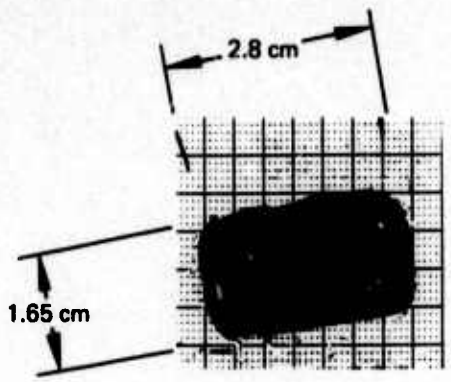

Fig. A-14.
Near-field burn pattern.

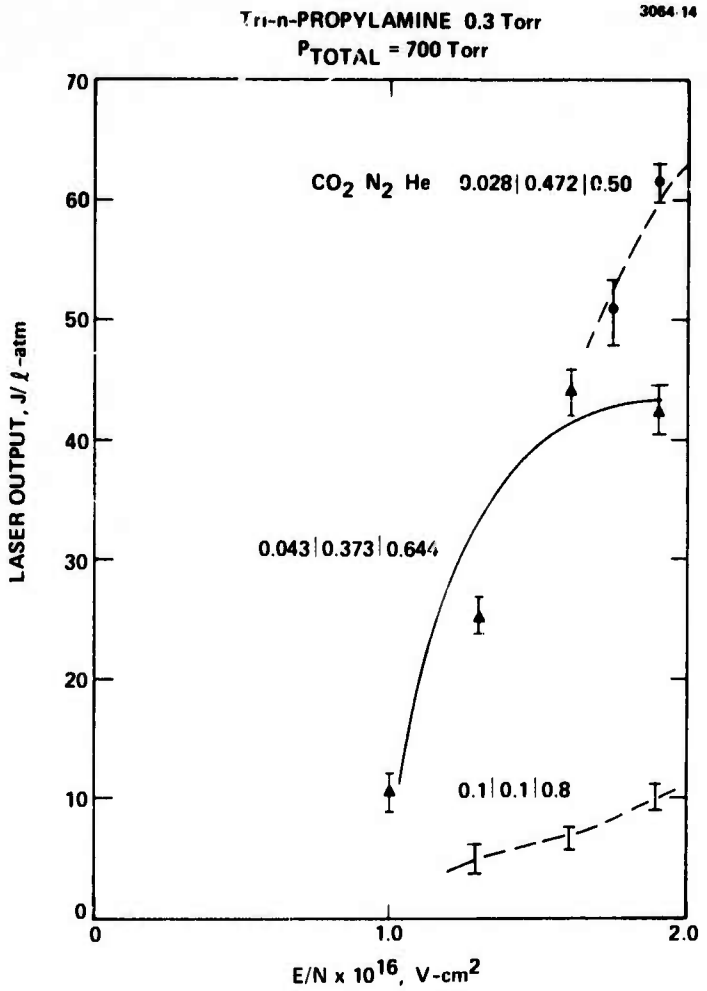

Fig. A-15. Laser output as a function of E/N.

REFERENCES

A-1. T. F. Stratton, et al., "Electron-Beam-Controlled CO_2 Laser Amplifiers," IEEE J. Quantum Electron. QE-9, No. 1, 157-163 (1973).

A-2. T. F. Deutsch and R. I. Rudko, "Spatial and Temporal Dependence of the Gain of a Transversely Excited Pulsed CO_2 Laser," Appl. Phys. Lett. 20, No. 11, 423-425 (1972).

APPENDIX B

SUMMARY OF PREVIOUS RESULTS – LARGE-SCALE DEVICE PERFORMANCE

During the second and third year of the program, a large scale UV sustained laser device was constructed and tested. Extensive performance data on the device has subsequently been obtained. In particular, input energy loading, spatially and temporally resolved small signal gain, and power extraction using a stable cavity have been investigated. The principal result obtained was that a maximum extraction energy of 200 J was demonstrated using a stable hole coupled cavity and 300 J using an unstable resonator. These results were obtained in a reduced volume configuration with the electrode gap adjusted to 6 cm height. In this appendix these results will be presented.

1. Input Energy Density

Input energy density measurements were made for several mixtures and the results are given in Fig. B-1. The energy input was calculated by integrating the area under the sustainer current waveform (see Fig. B-11(a) for a typical pulse shape) and then multiplying by an adjusted value of the dc bias voltage. The adjustment was made to account for the voltage droop on the capacitor bank that occurs during a shot. This adjustment was typically 10 to 15%. To determine the discharge volume, Teflon masks were inserted in the electrode gap region (see Fig. B-2). These masks confine the discharge in the width dimensions with some spillage of the discharge outside the end regions allowed. Thus the energy density calculated using this volume can be somewhat higher (5 to 15%) than achieved. We see from these results that energy densities up to 180 J/l-atm have been achieved. These results are comparable to those achieved on the medium size device (see Appendix A) although somewhat lower.

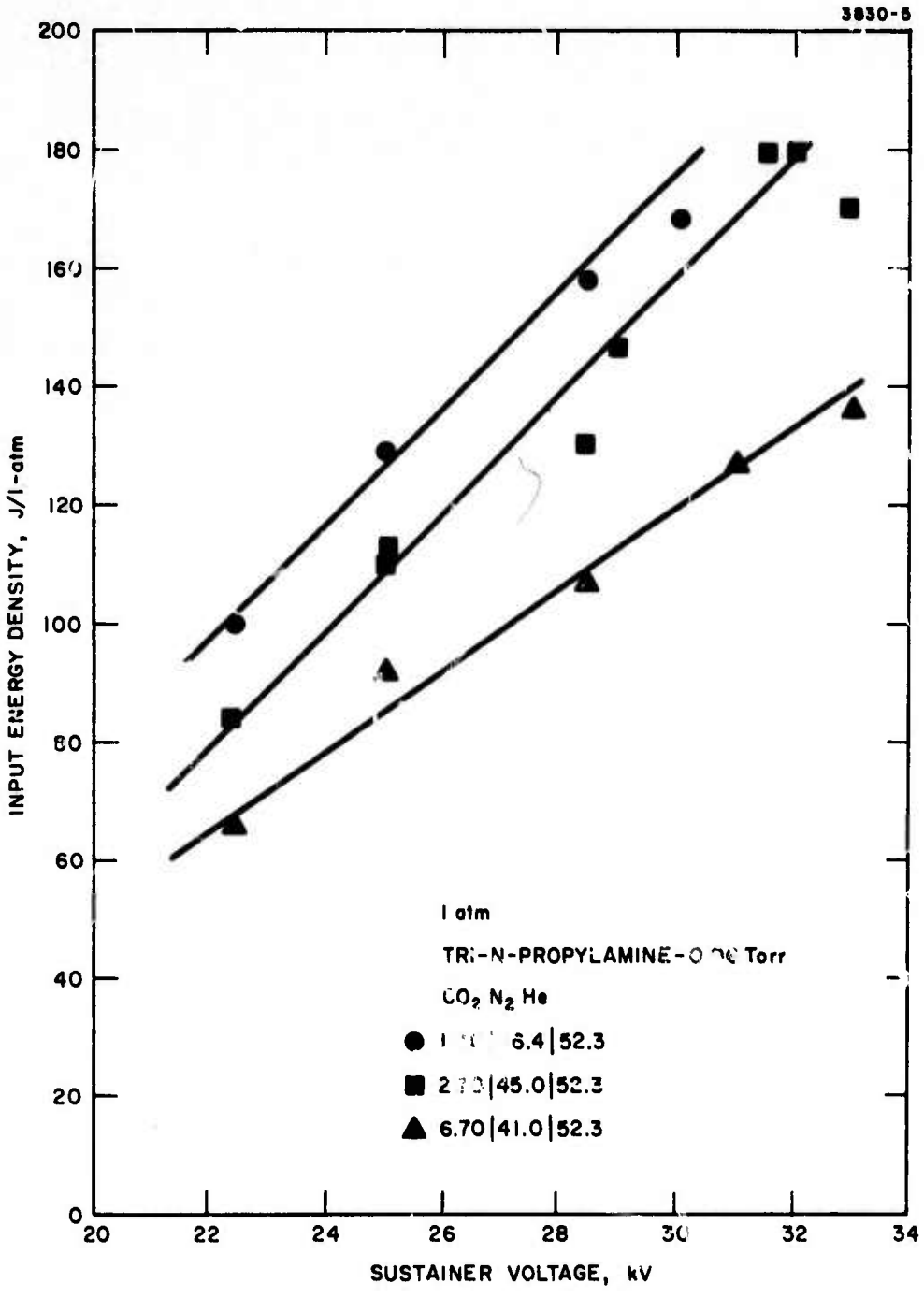

Fig. B-1. Input energy density as a function of sustainer voltage.

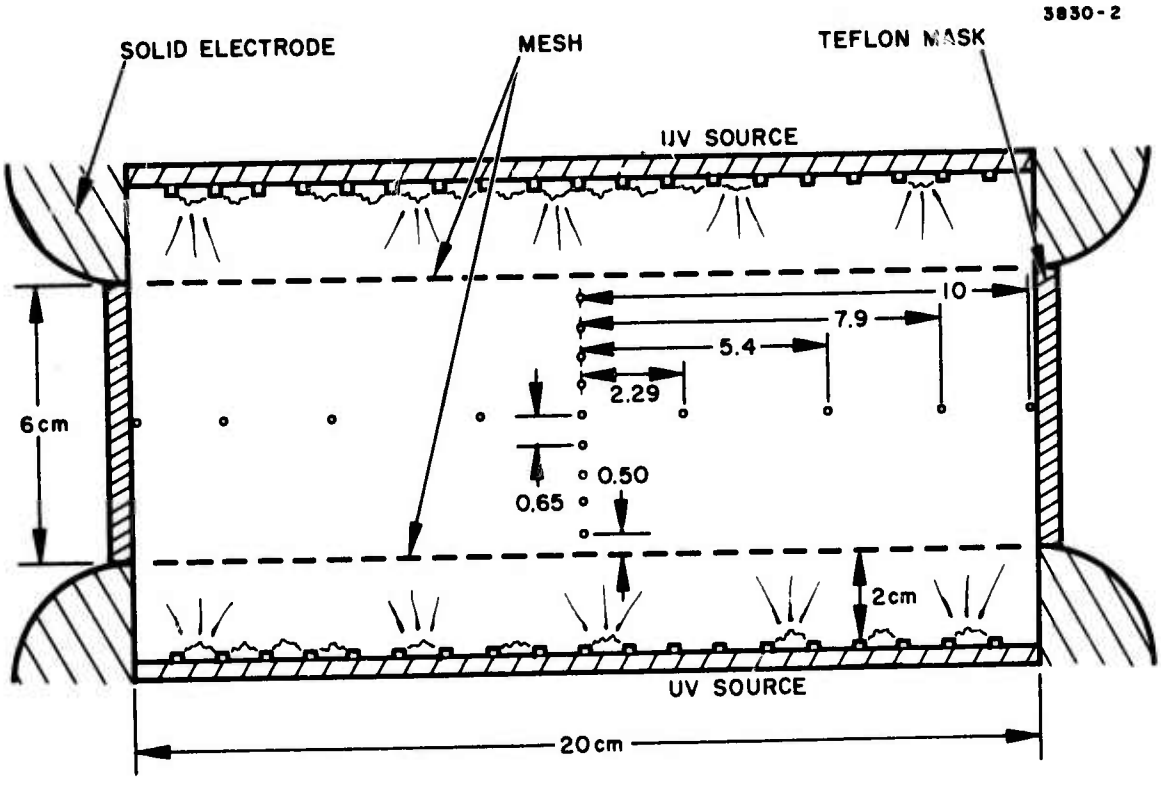

Fig. B-2. Continuous wave probe laser positions.

2. Small Signal Gain

The small signal gain was measured for various mixtures, sustainer voltages, and spatial position. Figure B-3 gives the magnitude of the gain as a function of sustainer voltage for the mixture shown to give maximum laser output (see Fig. B-9). We see that the maximum gain for the uv-sustained laser is about 0.85%/cm, which is consistent with that expected for the low CO_2 concentration mixtures employed. Also shown on this figure are calculated values for the gain. These values were determined using a four-temperature CO_2-N_2-He kinetic model with the crucial electron pumping rates determined from a solution of the electron Boltzmann equation. The purpose for making such comparisons is to establish that consistent predictions of the performance of the large-scale device can be made. The program can then be used as an aid in determining the expected performance of other such devices and in particular can determine the optimum output coupling for a uv sustained laser. This information was used to design the unstable resonator built for optimum full scale energy extraction studies.

Typical gain waveforms are shown in Fig. B-4. The trace shown in Fig. B-4(a) was obtained at the center of the discharge and Fig. B-4(b) was obtained at a point 5 mm from the cathode (see Fig. B-2 for orientation). Both traces indicate the arrival of the acoustic disturbance from the uv source. At the center of the discharge (Fig. B-4(a)) the disturbance appearing emanates from both uv sources and arrives at a time later than the disturbance emanating form the cathode alone, shown in Fig. B-4(b). An additional effect shown in Fig. B-4(b) is the large modulation of the gain near the cathode. This is similar to the result obtained previously and hence is not surprising (see explanation below). The predicted gain waveform was calculated for a specific experimental case (similar to that shown in Fig. B-4(a)) with the comparison given in Fig. B-5. We see that the agreement is excellent.

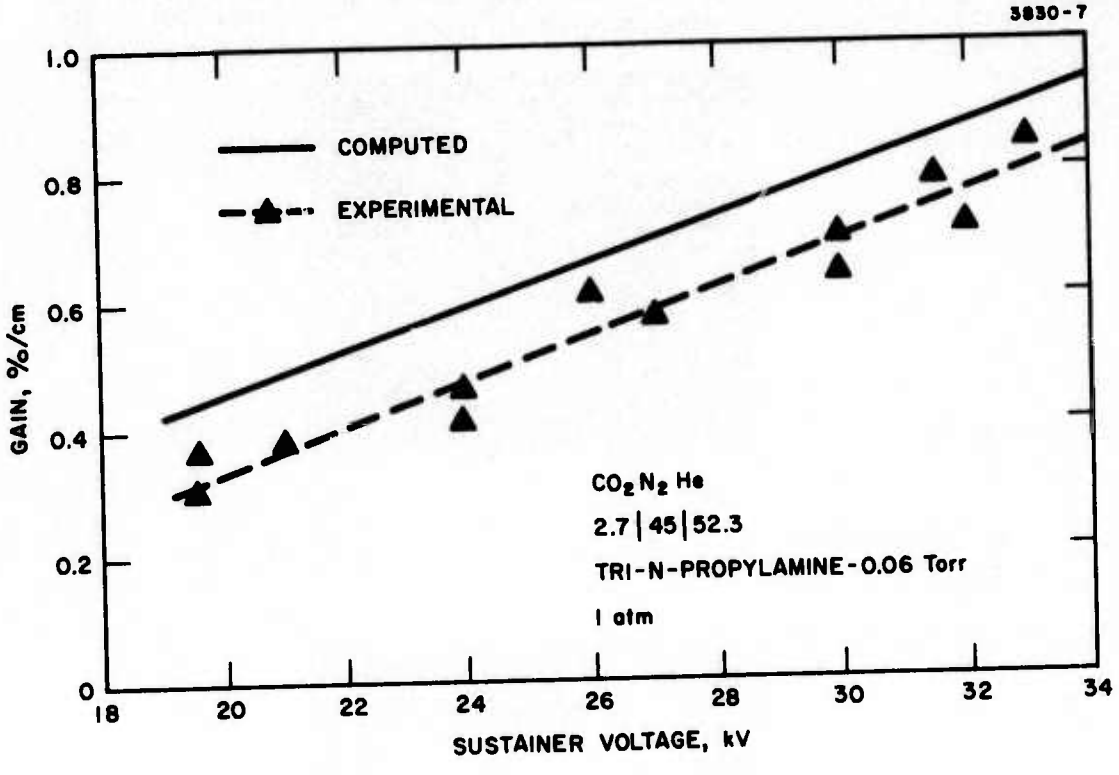

Fig. B-3. Small signal gain as a function of sustainer voltage.

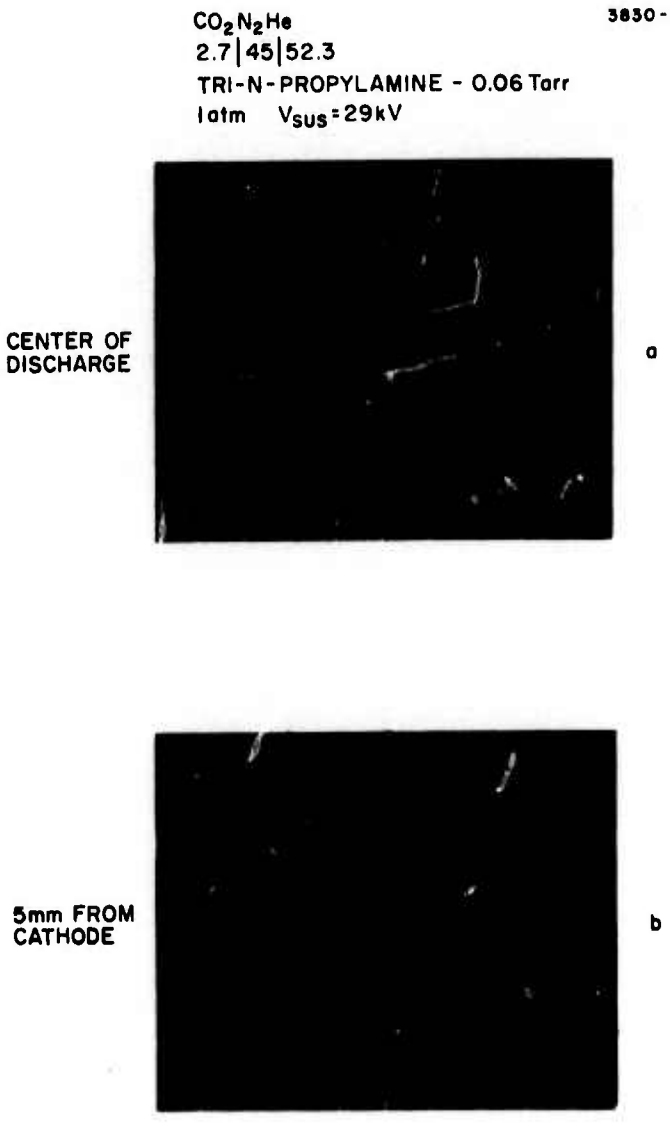

Fig. B-4. Small signal gain waveforms.

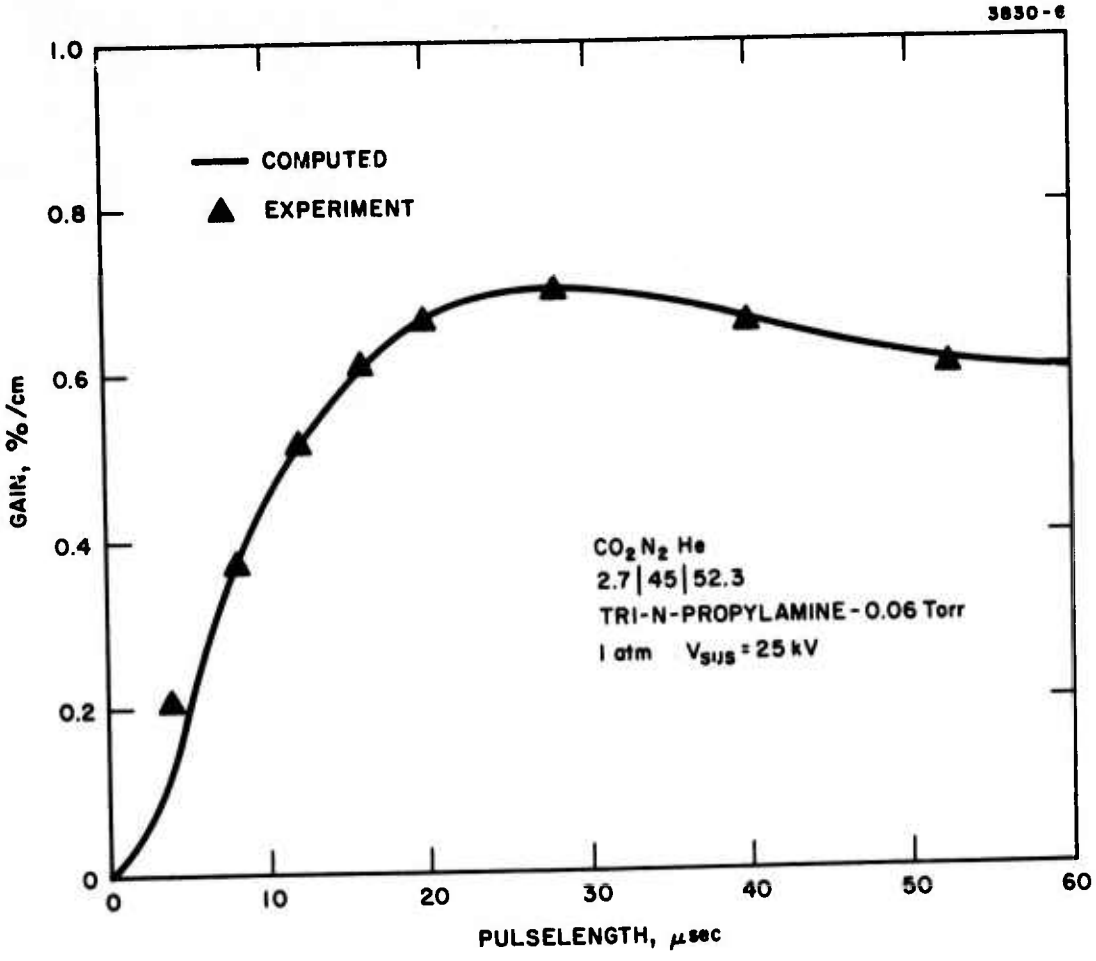

Fig. B-5. Small signal gain waveform, comparison of theory and experiment.

Spatially resolved gain measurements were next performed with both the electrode gap spacing and the discharge width traversed by the measurements. The cw probe laser positions used are given in Fig. B-2. The gain distribution across the 6 cm electrode gap dimension is shown in Fig. B-6. The magnitude of the gain is seen to be uniform to within ±10% across the entire gap. These data were taken with both sources operating which is the standard mode for obtaining data. The important aspect of these data is that contrary to the results obtained previously (see Fig. A-11) where only one source was employed, no large increase in gain was obtained as approach to the cathode is made. In the previous case it was speculated[6] that the large increase was due in part to uv-induced photoelectron emission from the solid cathode (the uv source was located behind a mesh anode). The additional electrons then causing localized avalanching near the cathode. An additional contributing factor as explained previously (see discussion following Fig. A-11) is the increased field strength in the region of low electron density near the cathode. The increased field strength then being sufficient to produce avalanching. In this case it is assumed that the electron density is established entirely by the uv source and subsequent photoionization of the seed gas (not by photoelectrons). The flux level, hence electron density, falls off when moving away from the anode toward the cathode. In order to maintain constant current across the gap, the field strength must then increase proportionally to this decrease in electron density. In the present situation this latter effect is absent entirely because there is a uv source located behind the cathode also contributing a large electron density in that region. Consequently, the field strength does not increase and no avalanching is expected. Furthermore, since a mesh is used for the cathode (50% transmitting) the photoemission is reduced by a factor of two and its effect is greatly reduced. In spite of this, however, some avalanching is apparently occurring as evidenced by the waveform shown in Fig. B-4(b) and by the large error bar shown in Fig. B-6 for the data taken near the cathode. The overall uniformity is good, however, and should present no limitation to beam quality.

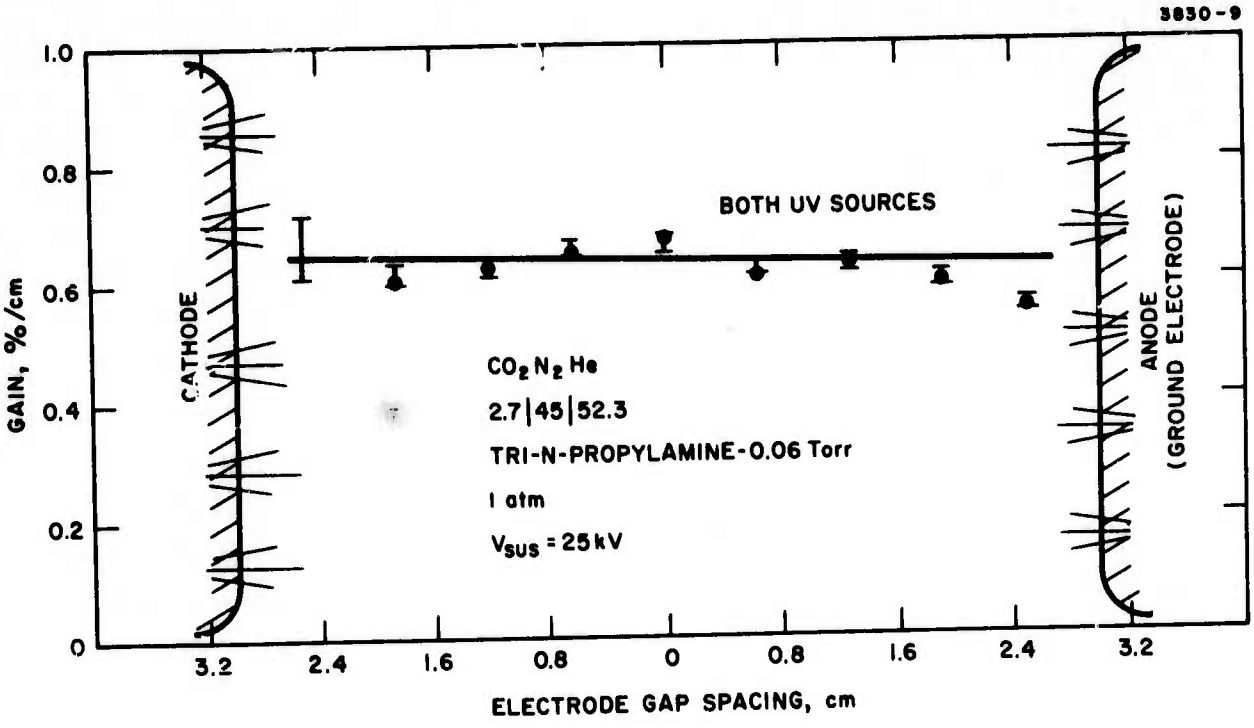

Fig. B-6. Small signal gain as a function of electrode gap spacing.

The gain distribution across the 20 cm discharge width dimension is shown in Fig. B-7. We find that the gain falls off uniformly toward either end with a maximum of 30% observed. The active uv source region spans the center 16 cm and hence the falloff obtained is to be expected.

3. Energy Extraction Results — Stable Cavity

Extensive energy extraction measurements have been obtained using a hole coupled stable cavity arrangement. The optical arrangement used for the stable cavity measurements is shown in Fig. B-8.

The output energy obtained with this optical arrangement for several gas mixtures as a function of sustainer voltage is shown in Fig. B-9. We find a maximum energy of 200 J for the particular mixture of 0.06 Torr tri-n-propylamine and a $CO_2/N_2/He$ mixture ratio of 2.7/45/52.3 (total pressure 1 atm). The near-field burn pattern for this case is shown in Fig. B-10. The burn pattern covers roughly a 6 x 13 cm^2 area. This represents the largest extraction area possible, taking into account the limiting apertures in the present optical arrangement, i.e., the right-hand side of the pattern is clipped by the external beam splitter required for energy measurements and the left-hand side by the 13 cm diameter hole coupled output mirror. The 6 cm dimension is apertured by the electrodes.

Returning to Fig. B-9 we find that increasing the CO_2 concentration by a factor of 2.5 times only resulted in a 20% falloff in output energy. A similar falloff was observed when the tri-n-propylamine concentration was increased as much as four times the optimum value. These results indicate (as stated in the third semiannual report) that scalability to at least twice the present size (i.e., 12 cm) should be expected.

A typical laser pulse shape together with a sustainer current and uv current pulse shape is shown in Fig. B-11. We see that the laser output has a pulse length of about 35 μsec and turns off simultaneously with the sustainer current pulse. It is also seen that the

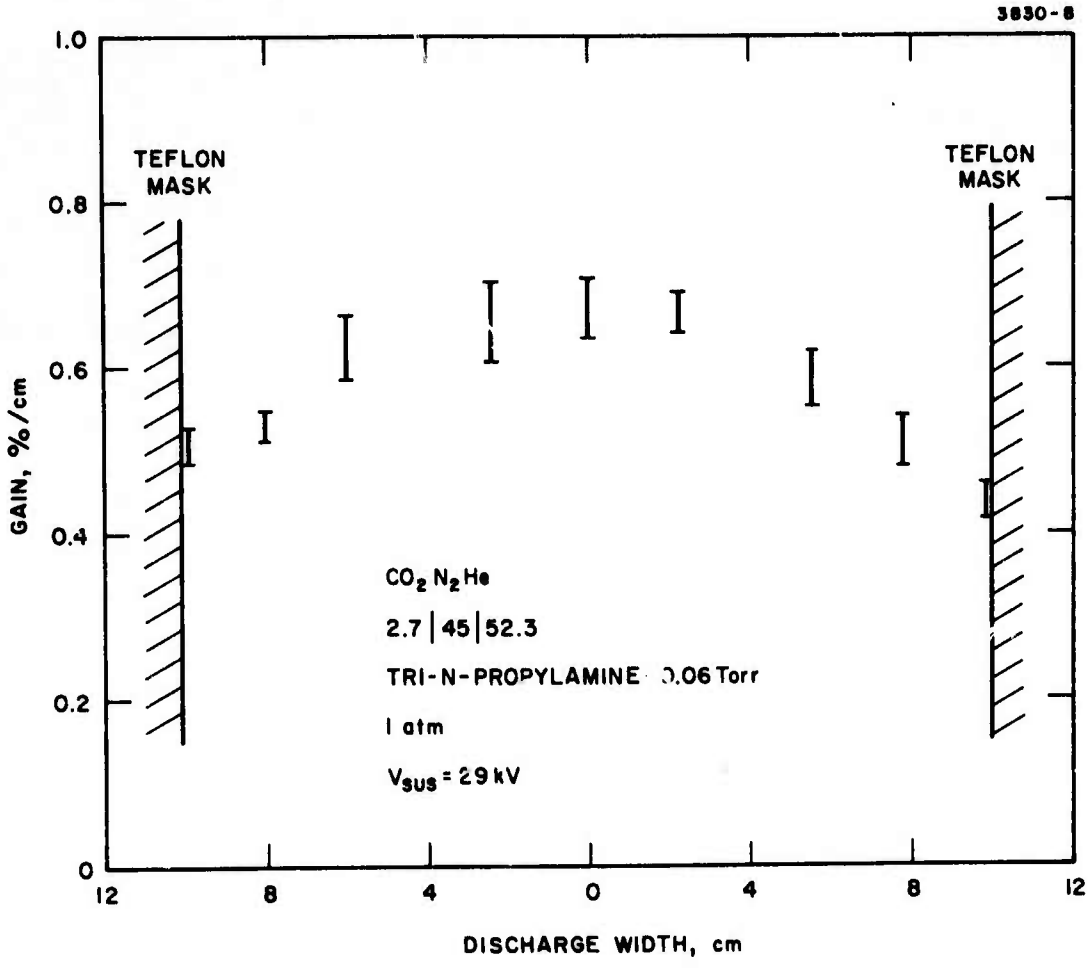

Fig. B-7. Small signal gain as a function of discharge width.

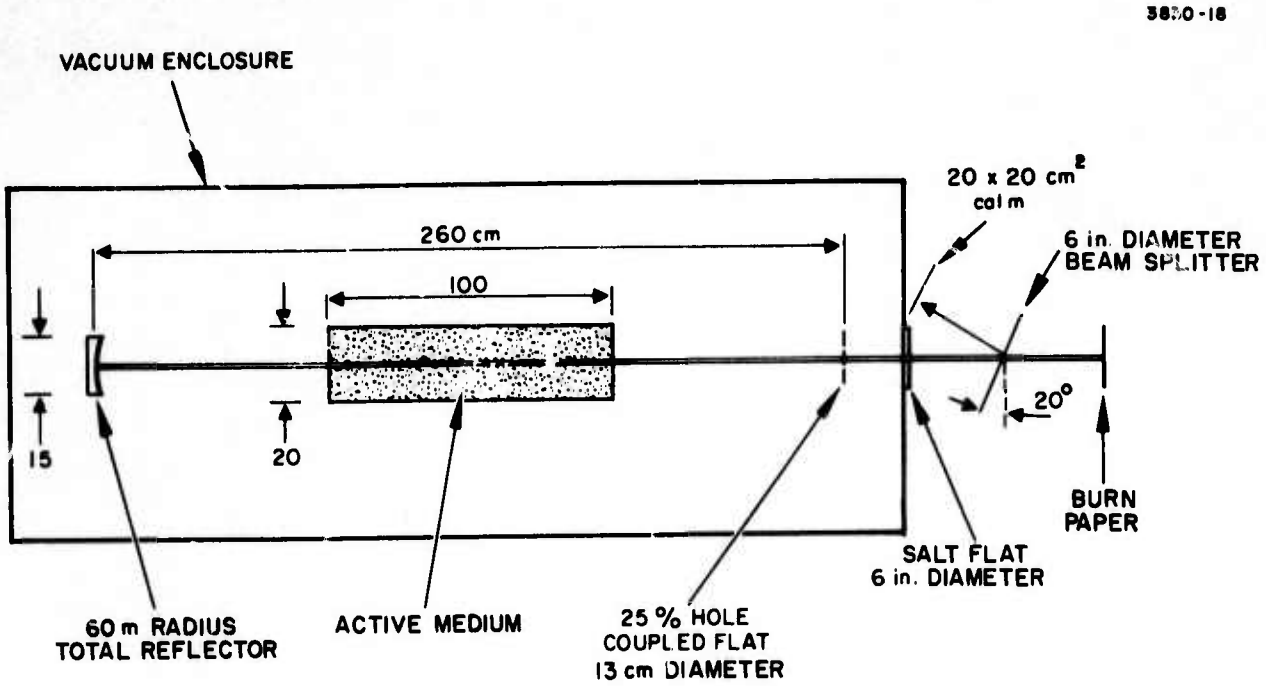

Fig. B-8. Optical arrangement for present energy extraction measurements.

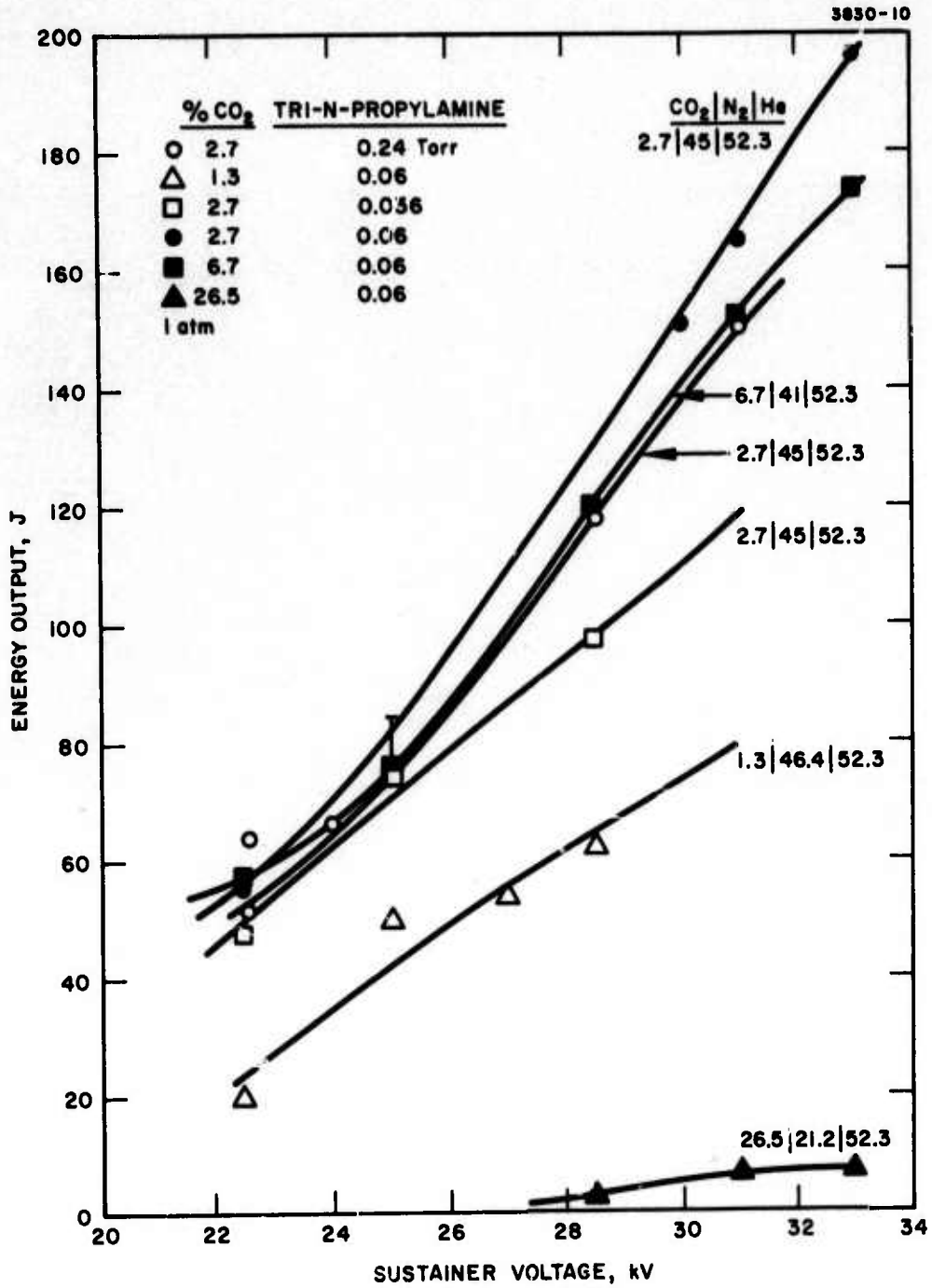

Fig. B-9. Laser output as a function of sustainer voltage.

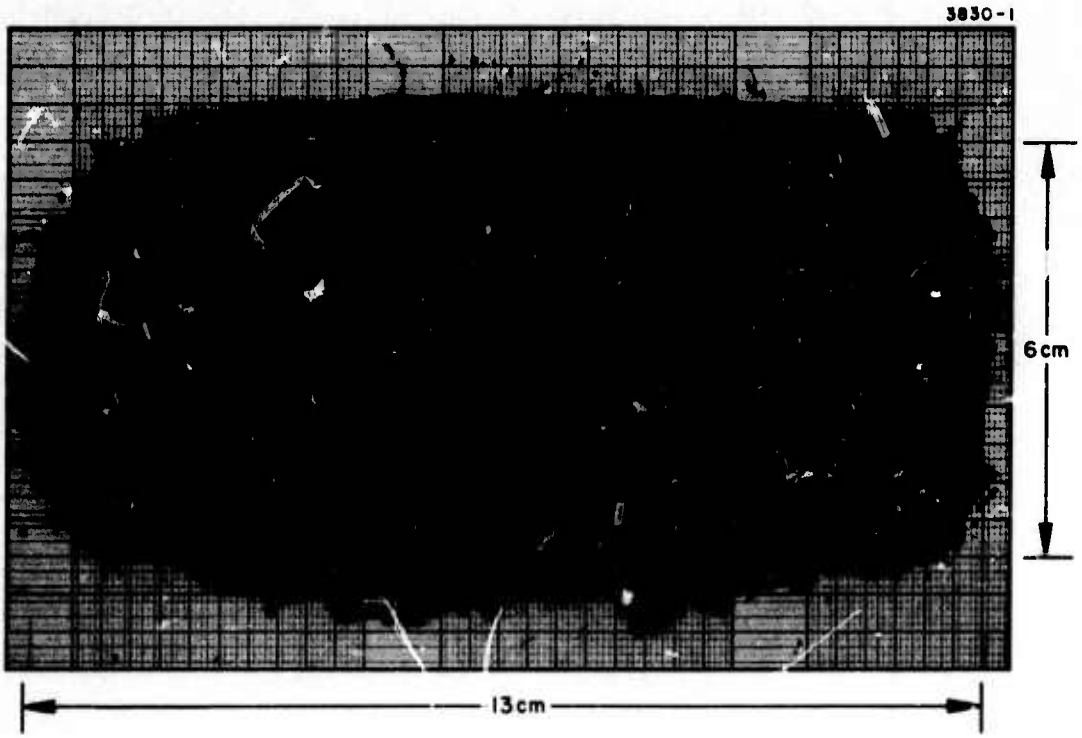

Fig. B-10. Near-field burn pattern.

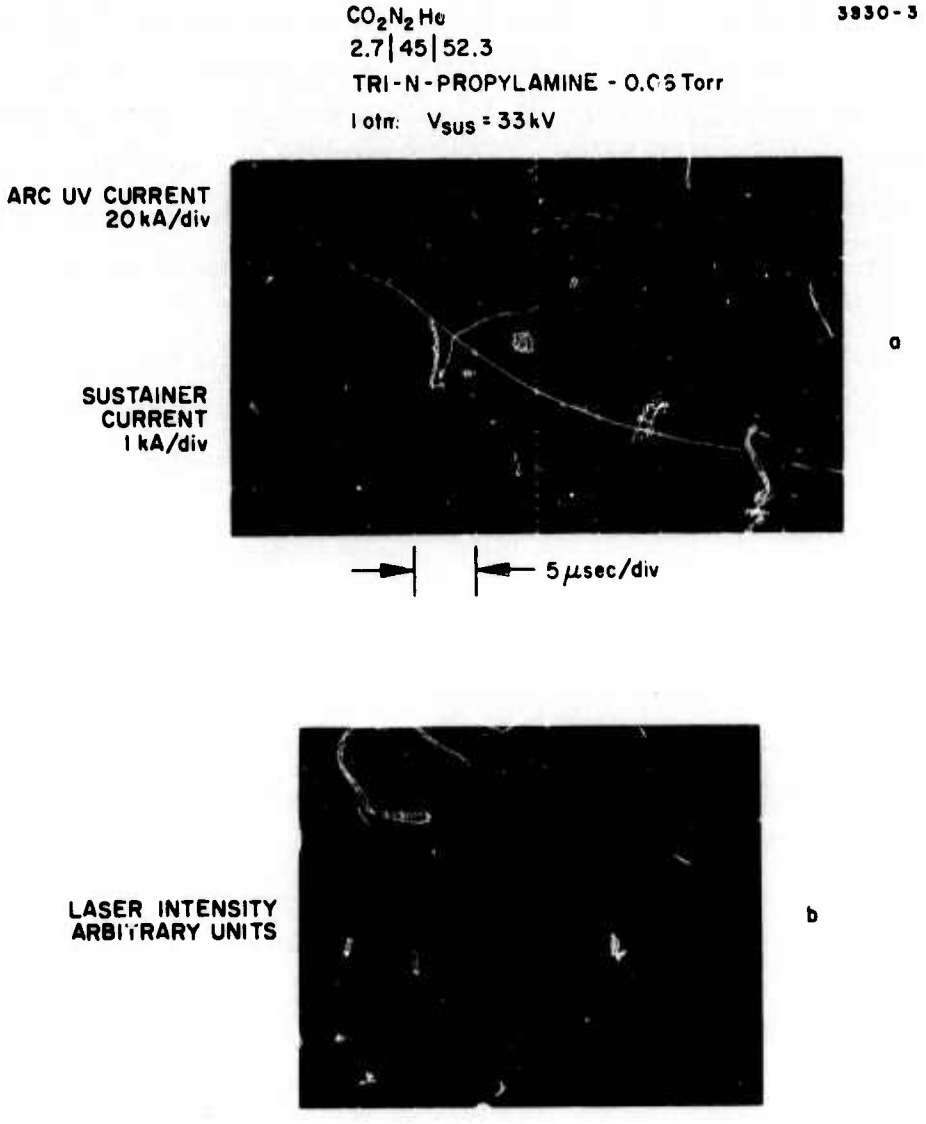

Fig. B-11. (a) Sustainer and uv arc current waveforms.
(b) Laser pulse shape.

laser output amplitude remains nearly constant in time for a period longer than the sustainer current. This is due to the large concentration of N_2 in the mixture which is transferring its stored energy to the CO_2 during the pulse duration. Calculation of the laser pulse shape was made using the kinetic code. The results of such a calculation, for a sustainer voltage of 28.5 kV, is given, together with that obtained experimentally, in Fig. B-12. We see that the agreement is very good, particularly in determining the turn-on time, turn-off time, and peak power density.

Having established the mode volume based on the burn pattern obtained, the output energy density can be determined. Using the best experimental results, the output energy density as a function of sustainer voltage, is given in Fig. B-13. We see that the maximum achieved is 28 J/l-atm. Using the input energy density for this case the laser efficiency is 15%. This result is below that achieved previously on the medium size device (see Fig. A-15). We believe the high loss in the hole coupled output mirror due to scattering from the holes is the major cause for these lower results. This question will be resolved when the unstable resonator is tested (see below). In lieu of such results, it is of interest to determine what level of loss is predicted for the system by the kinetic code which has now been established to be consistent with the measurements. In Fig. B-13 the calculated energy density for various losses of 2, 4, 6, and 8% per mirror is given. We see that the curve for the high loss case of 8% per mirror is in close agreement with that obtained experimentally. A further substantiation for this high loss comes from calculations of the laser turn-on time as a function of sustainer voltage. Such results are given in Fig. B-14 for a loss of 2% and 8% per mirror. It is clear that the experimental results, shown as the solid error bars, follow the 8% results closely and are distinctly different from the 2% case. One further comparison was the laser pulse shape already discussed in Fig. B-12. Here the peak power density is a strong function of the losses. For the comparison given, the 8% per mirror value was used in the calculations. It must be emphasized that for the computed

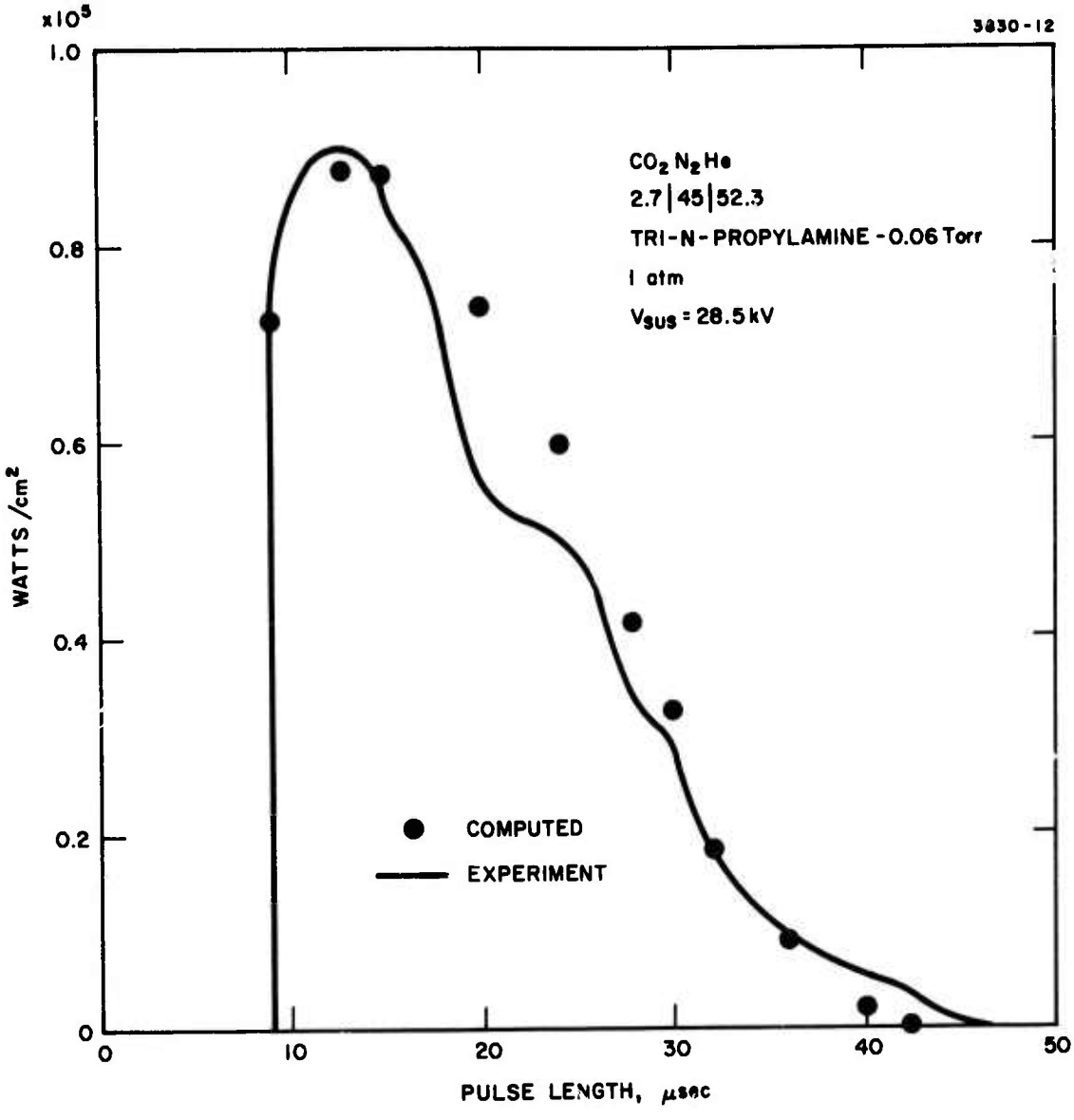

Fig. B-12. Laser pulse shape, comparison of theory and experiment.

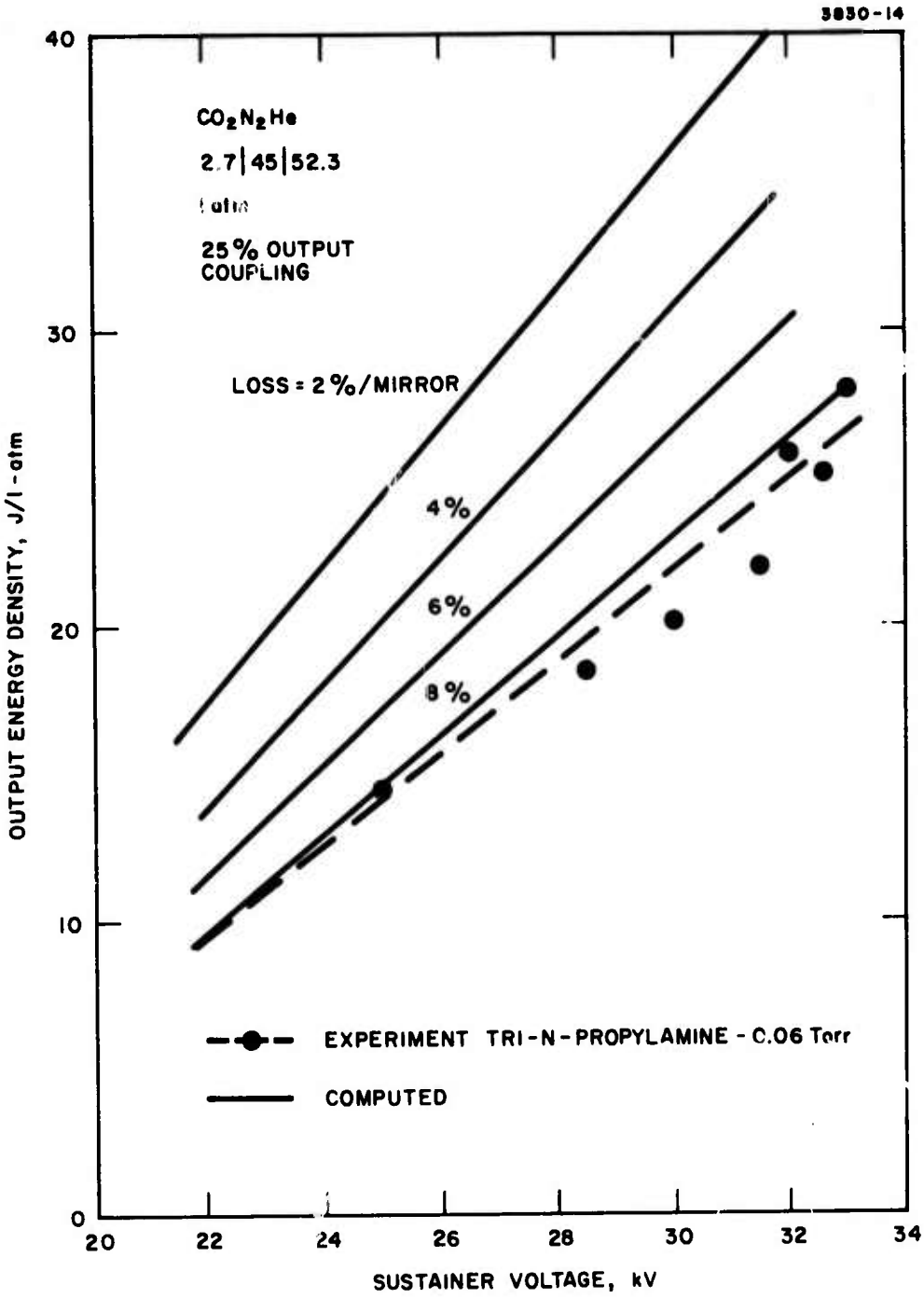

Fig. B-13. Output energy density as a function of sustainer voltage.

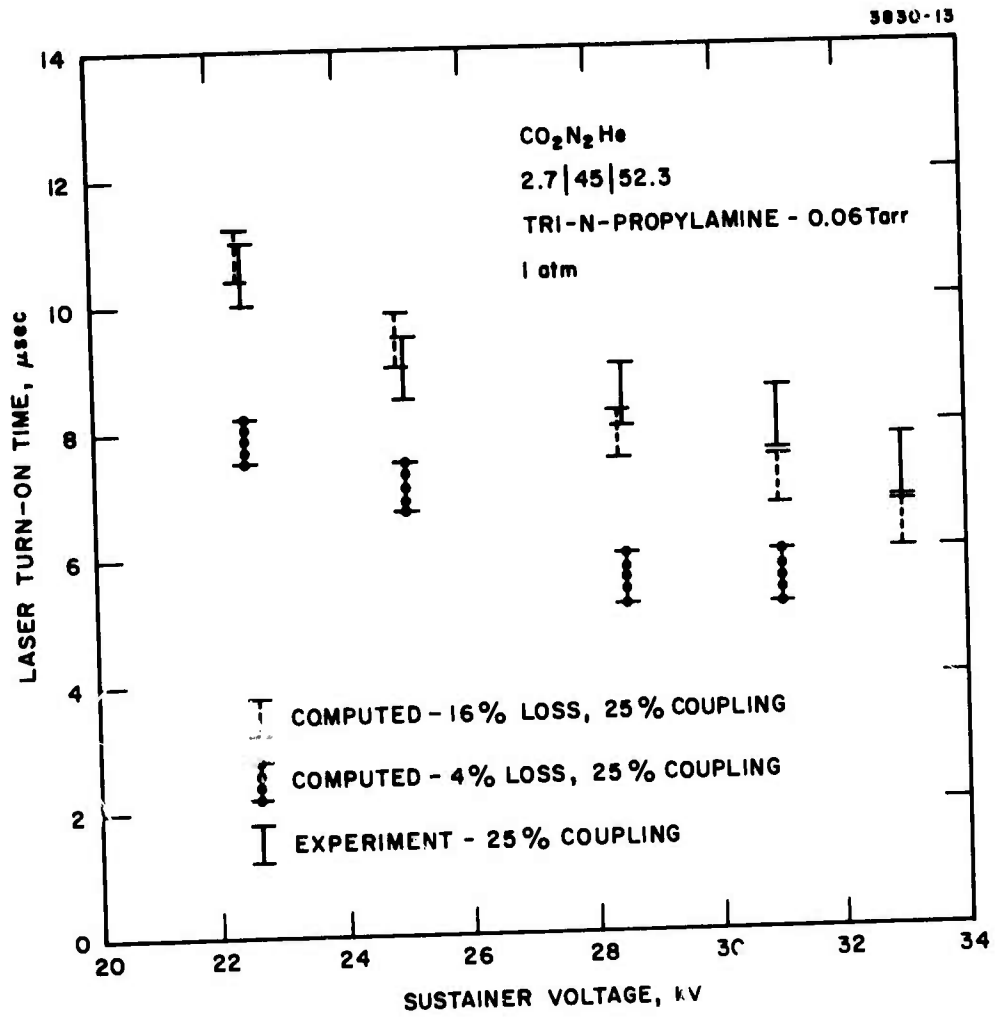

Fig. B-14. Laser turn-on time as a function of sustainer voltage for 4 and 16% loss.

results the gas mixture, pressures, discharge length, sustainer voltage, sustainer current density, and pulse shape are input to the program for each case with the only adjustable parameters being the output coupling and mirror loss. As a final calculation Fig. B-15 gives the potential output expected for lower loss systems as a function of the output coupling (for the maximum input loading case). We see that in excess of 40 J/l-atm outputs can be expected and, in fact, have been achieved in the medium scale device where a dielectric mirror was used as the output coupler (see Fig. A-15).

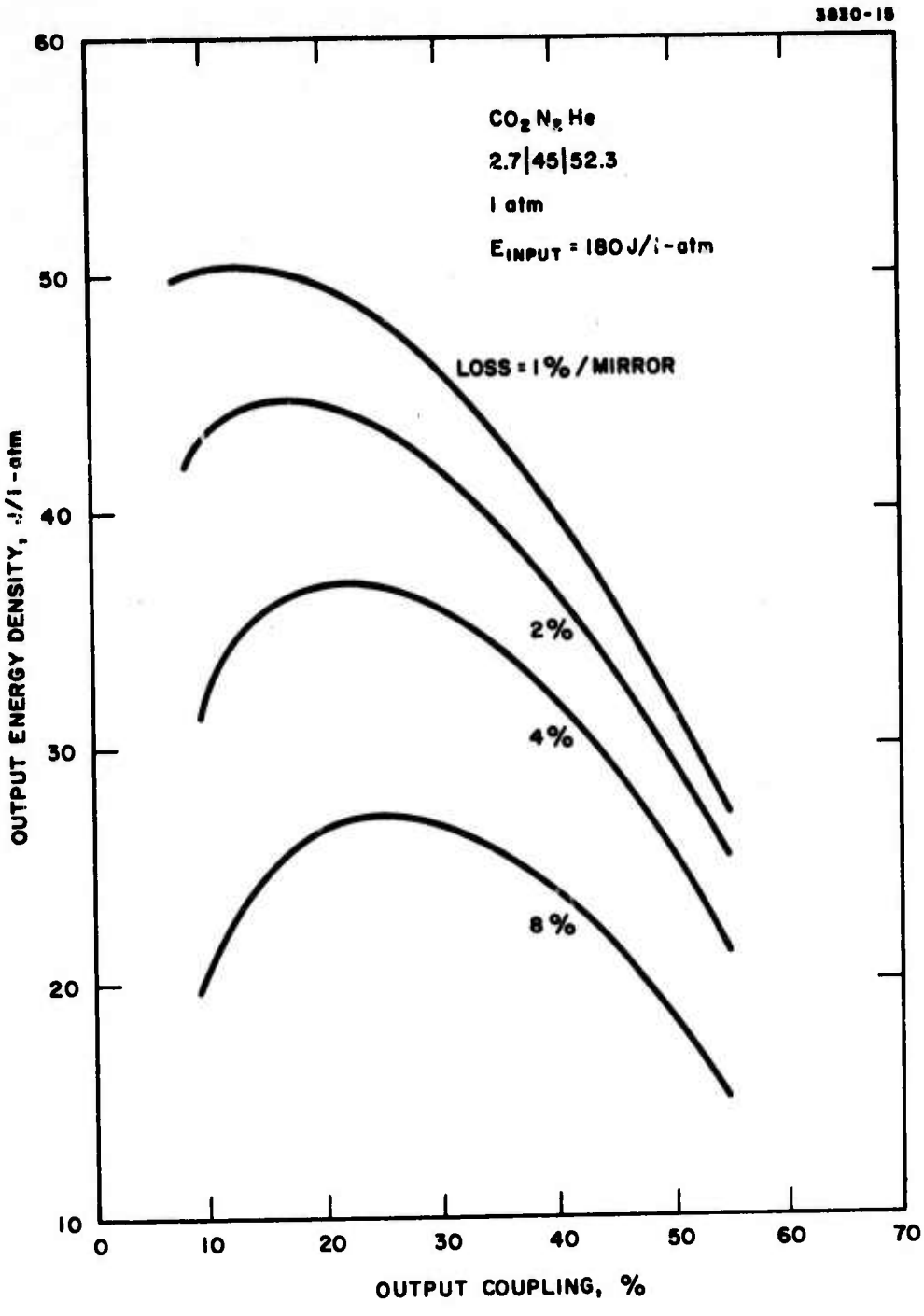

Fig. B-15. Calculated output energy density as a function of output coupling.

4. Energy Extraction Results — Unstable Resonator

The unstable resonator employed is of rectangular dimensions. The electrode gap, fixed at 6 cm, forms one aperture with the nominal discharge width of 20 cm forming the other. An output coupling of 30% is used. This coupling represented a reasonable compromise between having as low a coupling as possible for complete saturation of the medium (see Fig. B-14) and having a larger coupling for ease of alignment.

The demonstrated energy extraction is shown in Fig. B-16. A typical near burn field pattern is shown in Fig. B-17. The output energy is plotted as a function of sustainer voltage for the unstable resonator case (the previously obtained stable cavity results are also shown). It can be seen that approximately 270 J has been achieved at 30 kV. Tests at the higher voltage of 34 kV, where maximum power extraction with the stable cavity was achieved, were postponed due to a system problem currently being corrected.

It is plausible to assume that the increase in energy achieved with the unstable cavity is a consequence of the increased active volume size of the resonator. That is, the nominal discharge width is 20 cm but previously (stable cavity, see Fig. B-8) the optics limited the region of power extraction to 13 of the 20 cm. With the unstable resonator the full 20 cm is used to extract power. The energy density therefore remains constant at a value of approximately 25 J/l-atm. This gives a laser efficiency of 13.0% and an overall efficiency, including uv source of 7% (overall efficiency will be higher for fully saturated medium and for larger gap height which more optimally utilized available uv photons, see Appendix C. The laser efficiency achieved is below that previously obtained on the medium size device (see Fig. A-15 in Appendix A) as were the stable cavity

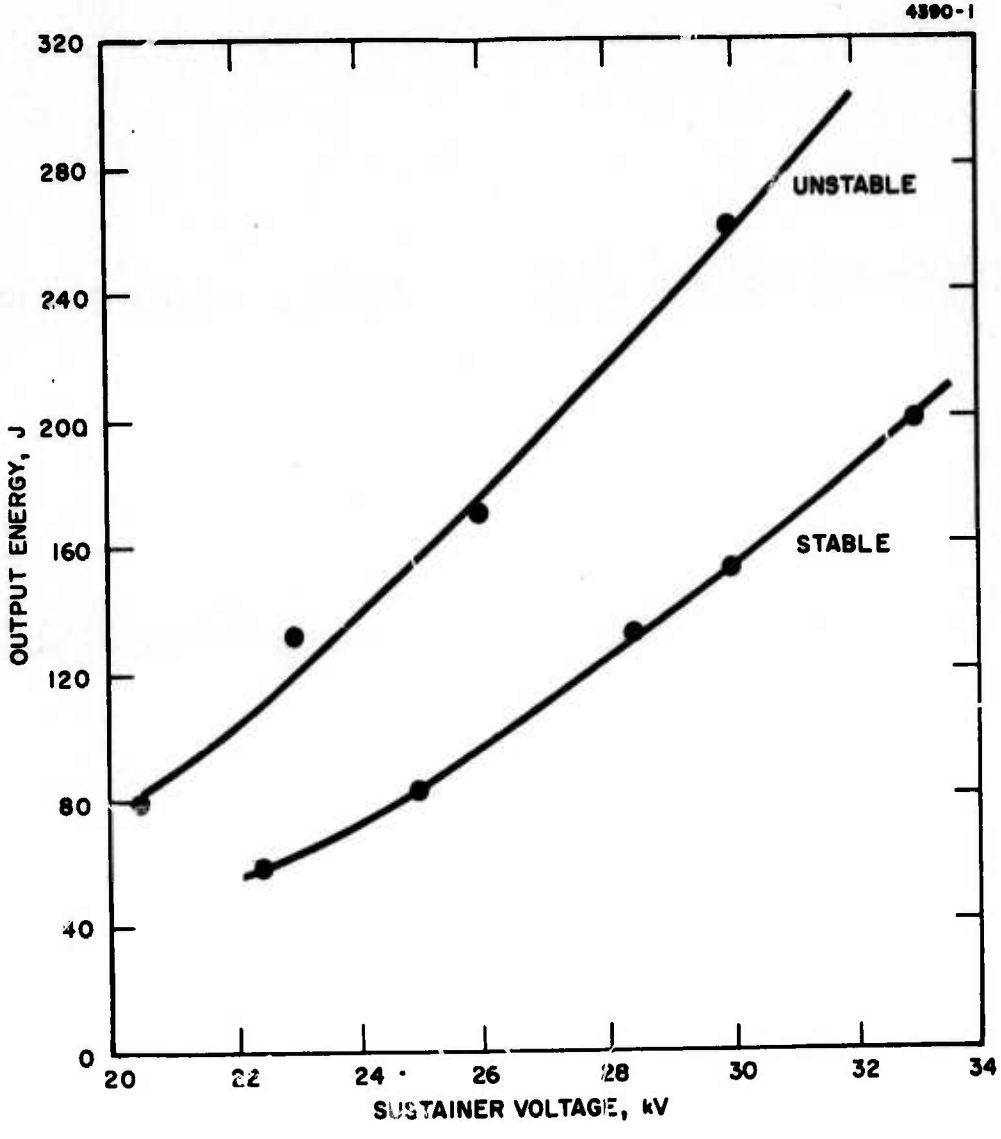

Fig. B-16. Laser output as a function of sustainer voltage.

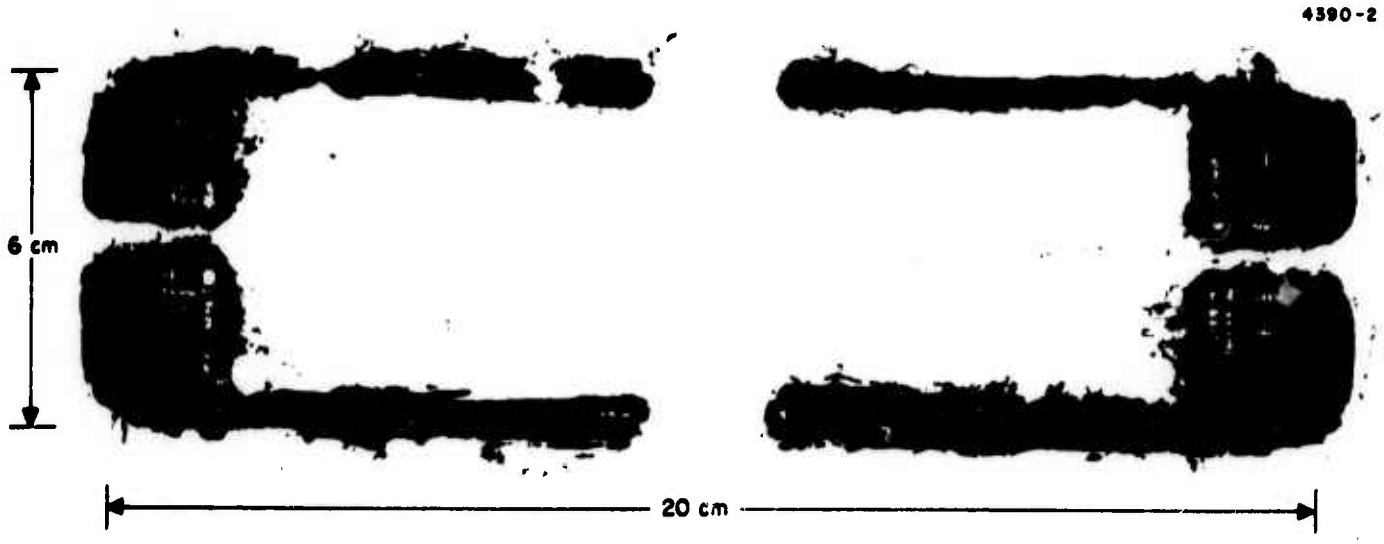

Fig. B-17. Near-field burn pattern.

results (see discussion following Fig. B-11 in Appendix B). For the previous stable cavity measurements it was speculated that the lower output energy was due to a high loss in the cavity. The high loss was believed to be due to scattering from the holes of the hole-coupled output mirror. Apparently this is not the explanation. Alternative explanations and possible corrective actions are currently being pursued.

5. Medium Quality Studies

Extensive medium homogeneity measurements were made using double-exposure pulsed holographic interferograms. For this technique, one of the exposures of the hologram (in our case it was always the second one) was taken with no discharge firing, and the other exposure at some specific time during the laser pulse. The double exposed film, after being properly developed, was then illuminated by a cw He-Ne laser and the resulting fringes recorded on polaroid film.

Figure B-18 shows schematically the experimental arrangement used. The ruby laser was Q-switched by means of a Pockels cell and produced 25 nsec output pulses with a peak power of 1 MW. The output beam was made to operate on a single transverse mode by using a 2 mm diameter aperature located inside the optical cavity, and an etalon was used for single longitudinal mode selection.

A reference hologram, made with no discharge firing, but with a 1 atm laser mixture in the uv-sustained laser device is shown in Fig. B-19.

Complete sets of holograms were taken at two transverse locations in the discharge; one in the central 13 cm of the discharge and one in which the discharge edge was included (the beam expander optics limited the field of view to 13 cm). Holograms were taken for various sustainer voltages, uv energy levels, and times after the start of the uv pulse. Typical holograms obtained are shown in Fig. B-20. These

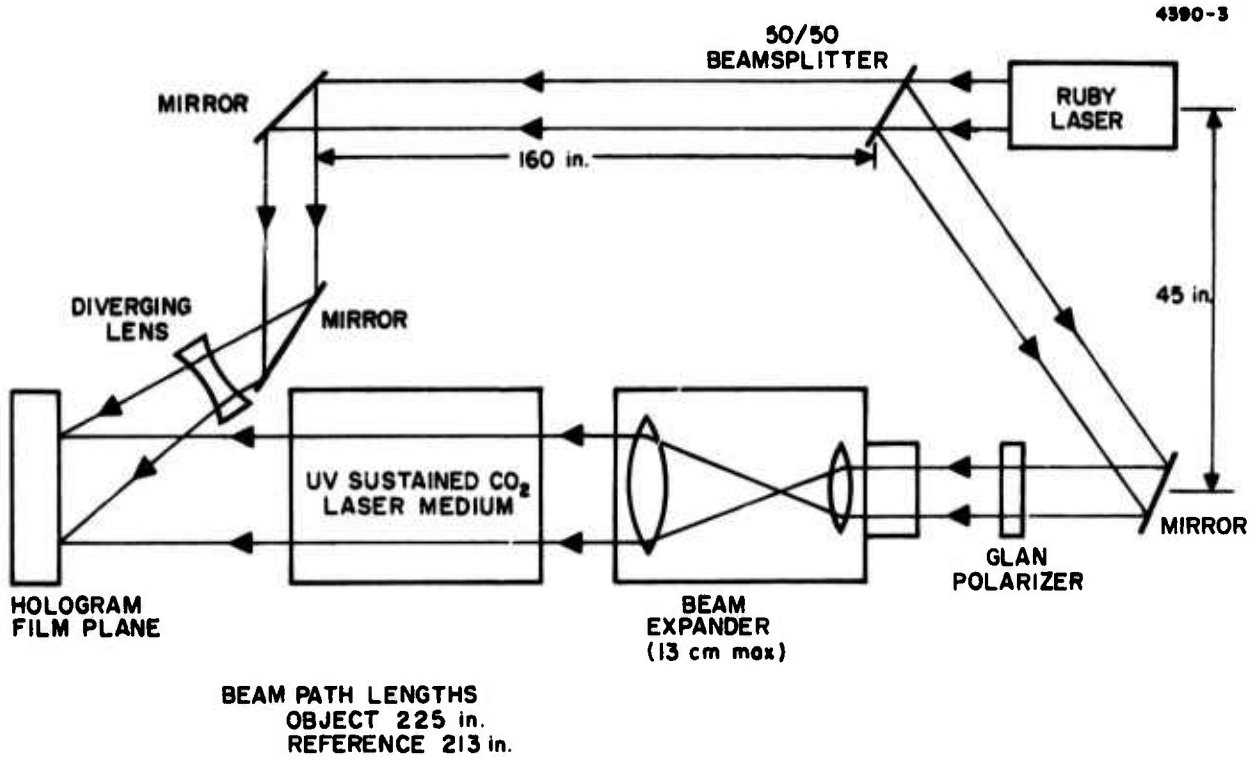

Fig. B-18. Holographic experimental setup.

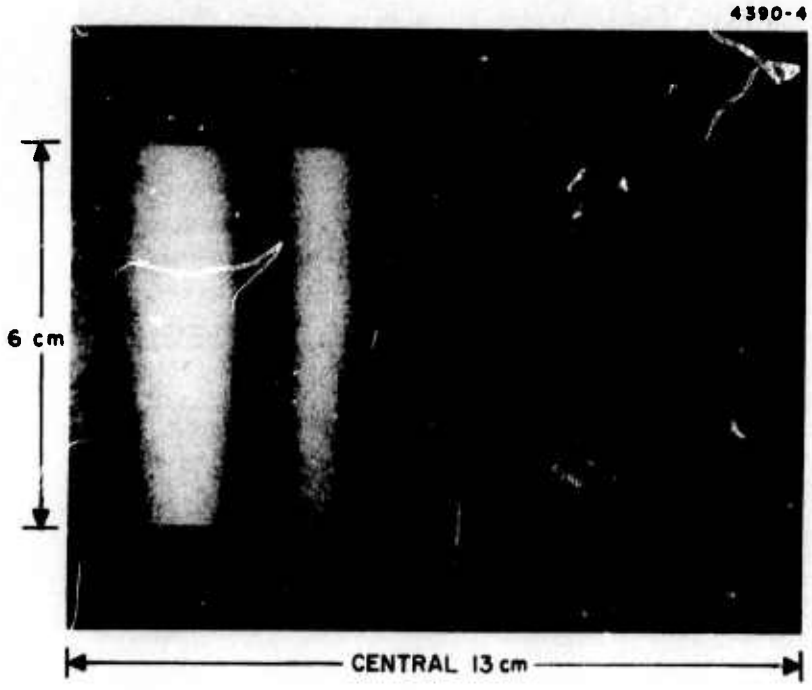

Fig. B-19. Reference hologram.

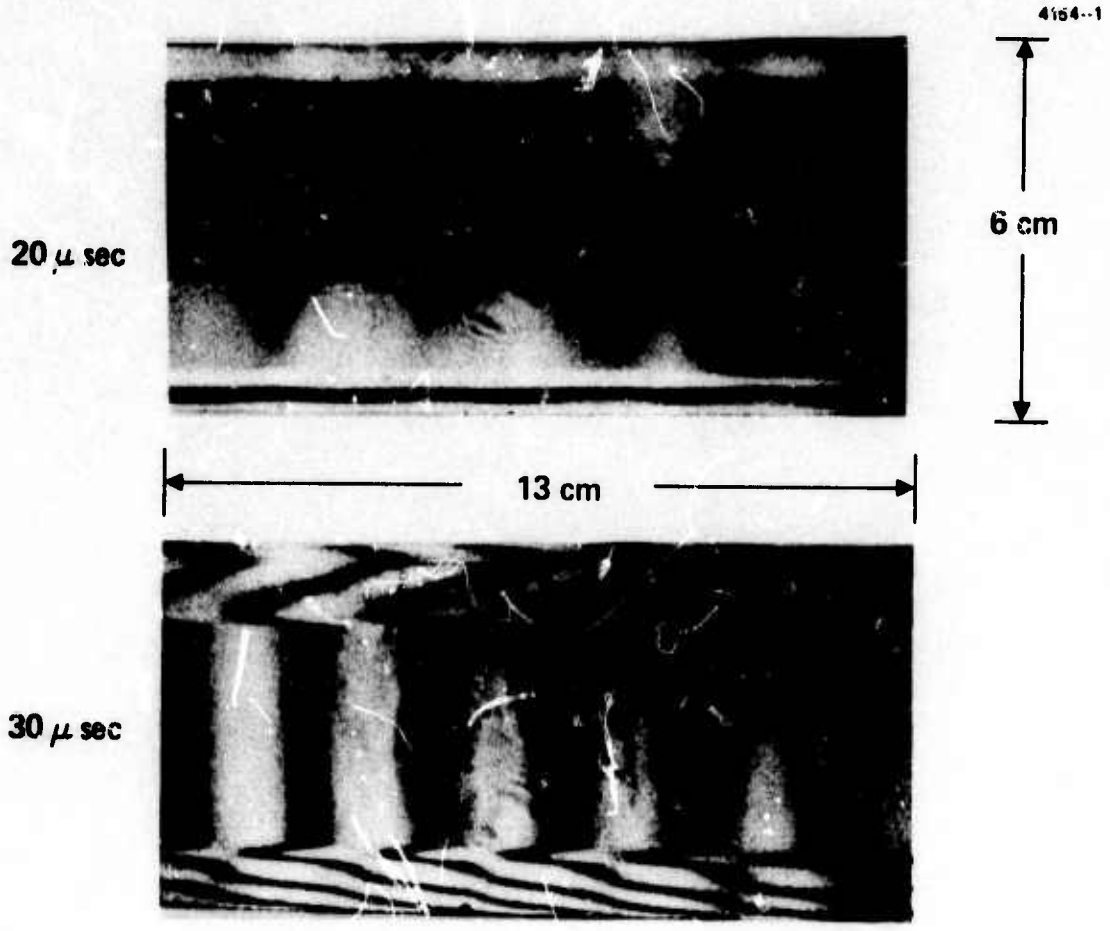

Fig. B-20. Media holograms. (a) 20 μsec after start of uv pulse, (b) 30 μsec after start of uv pulse.

holograms represent all of the essential features that occur with discharge firing. They were taken over the central 13 cm of the discharge with a sustainer voltage of 30 kV at 20 and 30 μsec after the start of the uv pulse. The cathode is at the bottom in both photographs and the uv sources are located behind each electrode.

From these photographs the acoustic disturbances produced by the upper uv source and by the combined cathode and lower uv source are clearly shown. The distance traveled by the wave fronts in the time frame given in the photographs is consistent with the speed of sound in the mixture ($\sim 4.5 \times 10^4$ cm/sec). It is clear from the holograms that the medium does not suffer inhomogeneities in the region between the uv and cathode waves. This implies a medium quality of better than $\lambda/30$ at 10.6 μm. The fringe shifts obtained in the disturbed region show an initially compressed and heated regime followed by the expansion of this hot gas back through the mesh screens into the region occupied by the UV source. Accounting for all the fringe shifts in traversing the 6 cm gap we find that the medium quality is good to $\lambda/8$ at 10.6 μm. Figure B-21 gives a hologram taken at the edge of the discharge for conditions identical to Fig. B-20(b). The essential features remain the same with the media quality unaffected by the edge waves. The results from these holograms imply that the far-field beam quality of a high energy uv-sustained laser should be near diffraction limited.

As an interesting sidelight, an additional hologram taken (Fig. B-22) shows a strong localized energy deposition in the upper uv source region. This implies that one or more of the rows of arcs traveling down the board did not traverse the complete board length (discharge width). Thus the remaining stored energy in those rows of capacitors was discharged in a small region (the circuit being completed through an arc to the mesh screen at the local ground potential). The energy deposition in the laser mixture was essentially unaffected by this but a post arc did occur. That is, about 1 msec after the pulse an arc occurred (the sustainer voltage is applied dc to the electrodes).

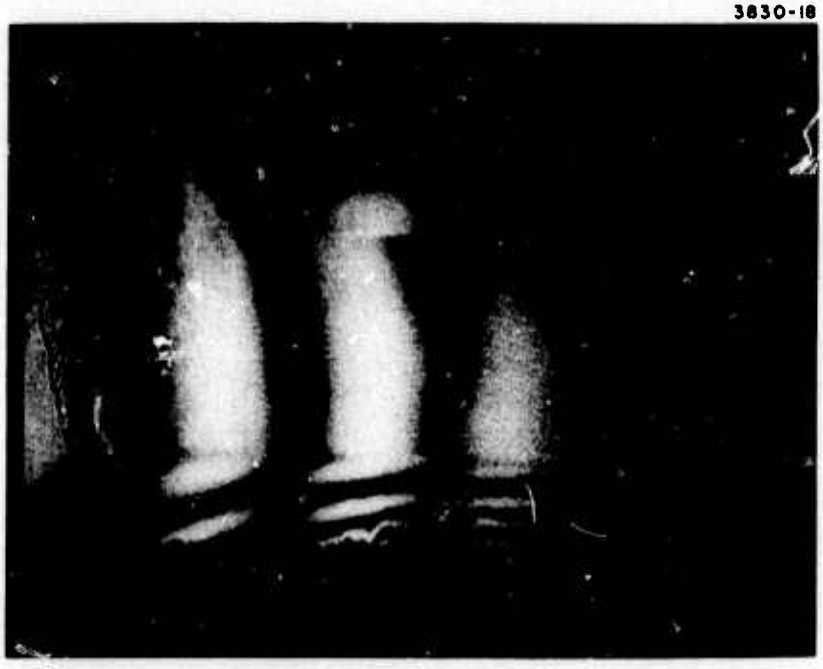

Fig. B-21. Media hologram; edge of discharge at 30 μsec.

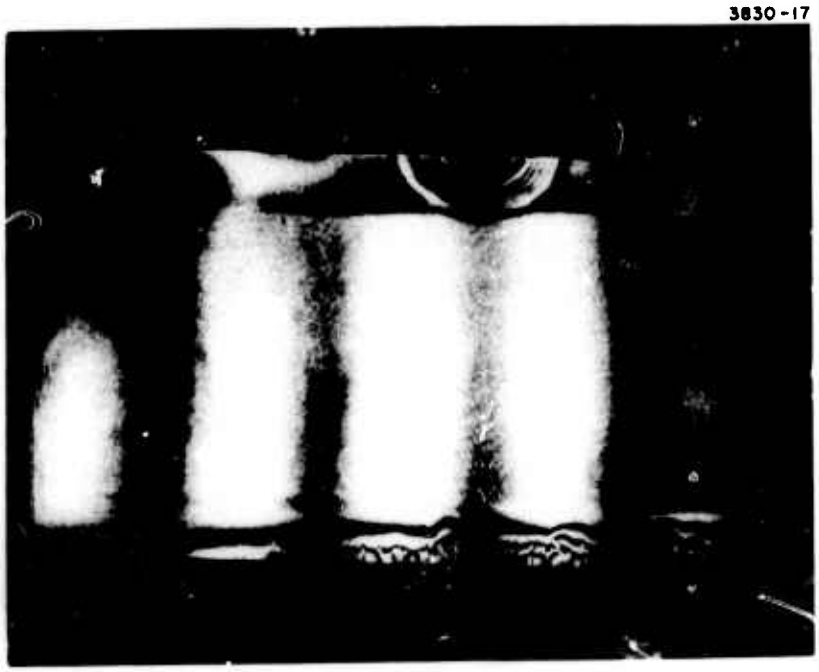

Fig. B-22. Media hologram; center of discharge at 20 μsec.

It is possible that the post arc may have been triggered by this localized high electron density region in the discharge. While such an arc does not degrade the performance of the laser (it occurs after the pulse is over) it discharges the large (50 kJ) sustainer bank into the screen causing permanent damage requiring screen replacement.

APPENDIX C

ULTRAVIOLET SUSTAINED LASER SCALABILITY

The purpose of this section is to present scaling relations for a uv-sustained CO_2 laser. These relations are determined from a scaling model that incorporates the important optical, electrical, and laser processes as understood at this time. Based on these relations, the conceptual design of a high power uv-sustained laser is presented. In addition, the scalability projections of power extraction and overall efficiency are presented for the large scale device (LSD) experiments discussed in Appendix B.

A. Scaling Model

For a nonavalanche discharge, the magnitude and spatial variation of the electron density is determined primarily by the source function. In the present case, the source function is the uv radiant intensity in the 1200 to 1700 Å region produced by a large number of arc discharges located behind each sustainer electrode (see Fig. C-1 for geometry). Because of the geometry and the finite absorption of the uv by the medium, the electron density will be a minimum at the center of the electrode gap. It is this spatial variation in electron density that leads to the fundamental scaling limitations of the uv-sustained technique.

To determine the important scaling parameters, a model has been developed. This model is described briefly below (see Appendix D for a description of the equations used).

The source function is first calculated as a function of gap height and uv absorption length. The electron density is then calculated assuming a recombination dominated plasma. Since the current density across the gap must be a constant, the electric field will vary in inverse proportion to the electron density. This electric field variation is then calculated, including the dependence of recombination on

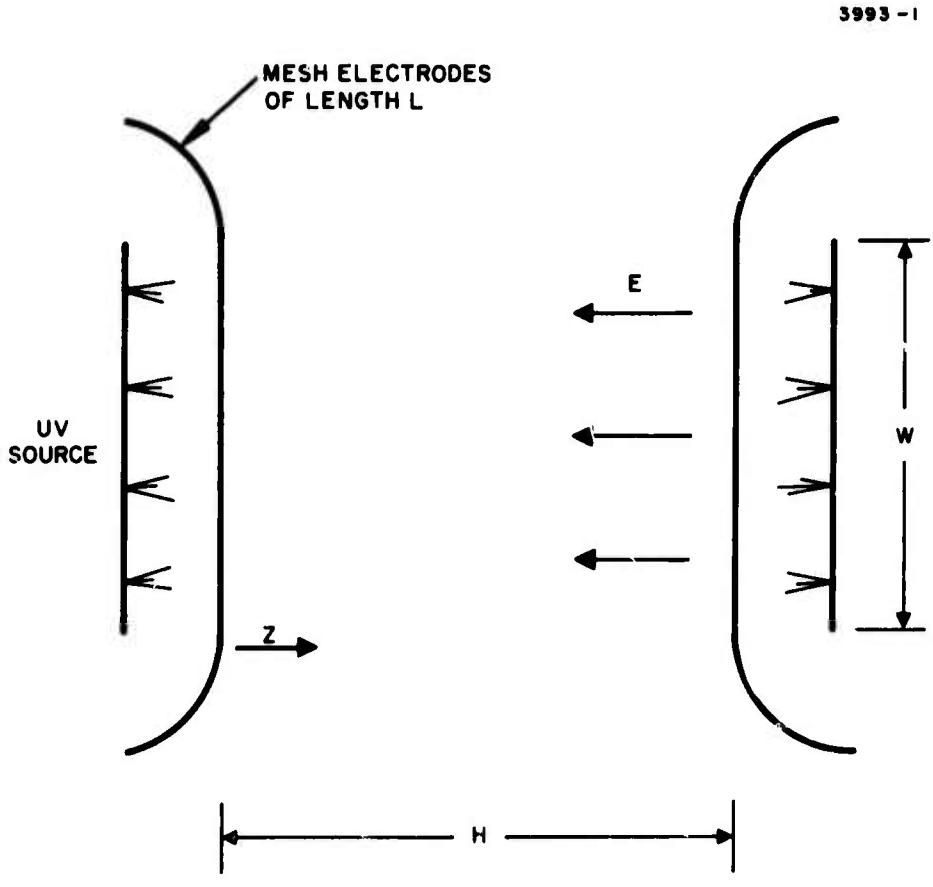

Fig. C-1. Model geometry.

electric field. In principle, this adjustment by the electric field could compensate for the spatial nonuniformity in the electron density and scalability would be unlimited. However, as the electrode gap is increased the electric field in the center, where the electron density is a minimum, will eventually increase to a value at which avalanching begins and ultimately lead to an arc. Consequently, the maximum electric field must be limited so that the mean electric field across the gap will permit arc-free operation. The limiting electric field has been determined from experiments on the LSD ($E_{max} \approx 5.5$ kV/cm-atm) and incorporated into the model. This limitation results in both a lowering of the current density and applied field as the gap spacing is increased. Figure C-2 shows the calculated uv intensity distribution as a function of position in the gap (z) for two gap heights of 6 and 20 cm and a uv mean-free path of 7.7 cm. (The uv source is located 2 cm behind each electrode.) The 7.7 cm mean-free path was established by fitting theoretical energy input calculation to the input energy measurements on the LSD. This procedure is discussed in Appendix D. In Fig. C-3 the resulting electric field and current density variation is given as a function of gap height. Since the input energy is a product of the electric field and current density, the input loading is reduced as the gap height is increased. This leads to decreased optical output and efficiency. While this limitation will always exist, it will be shown in the next section that by improving the uv source function, scaling can be extended to dimensions compatible with high energy requirements.

1. Scaling Calculations

The fundamental result of the physical processes discussed above is that the input energy loading will decrease as the gap height is increased. This result is shown in Fig. C-4. (Refer to curve titled – "uv Source Not Scaled"). The input energy density scale shown is normalized to the measured input energy density from the LSD experiments (measurements made with a gap height H of 6 cm). This normalization is necessary because the absolute magnitude of the uv intensity, in the photoionization wavelength range, is a quantity not

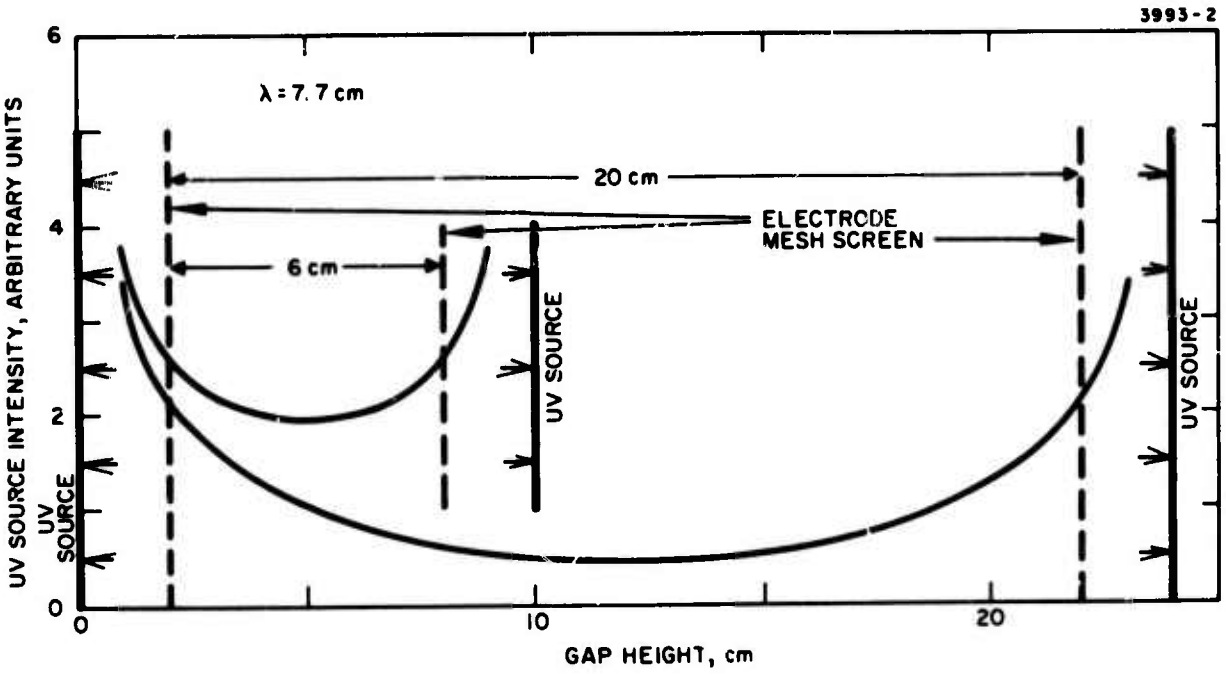

Fig. C-2. Ultraviolet intensity as a function of position (z).

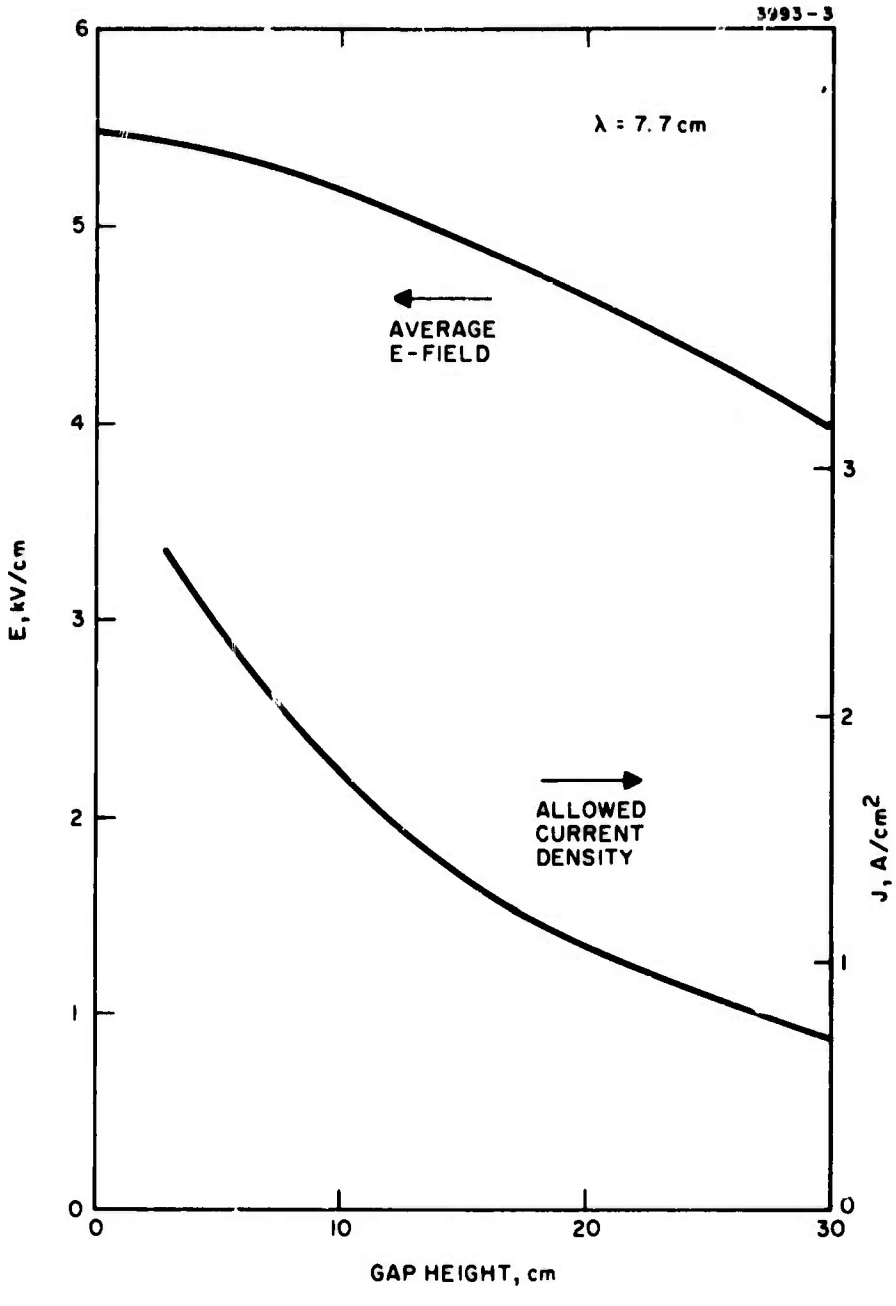

Fig. C-3. Electric field and current density as a function of gap height.

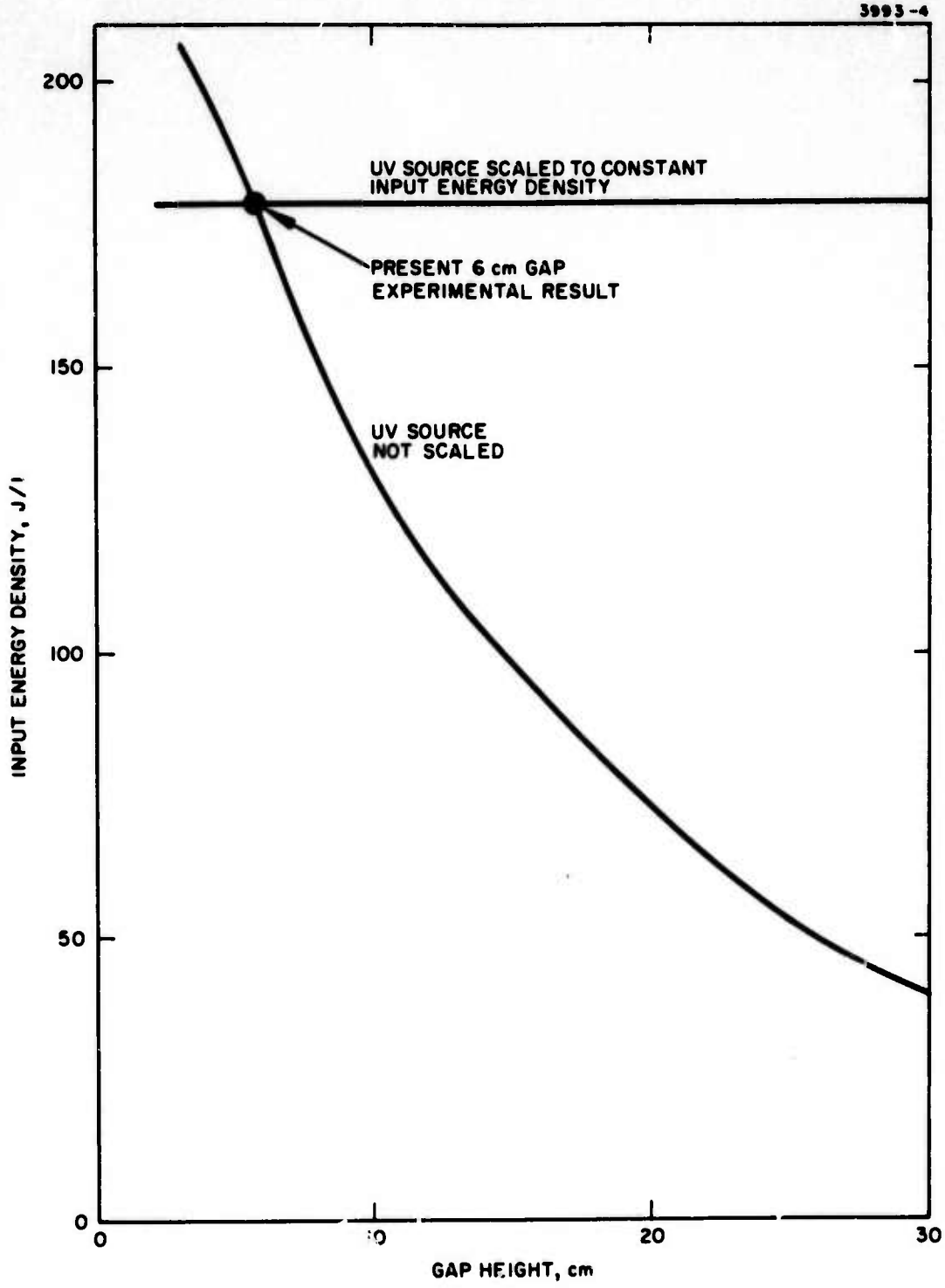

Fig. C-4. Input energy density as a function of gap height.

amenable to calculation or direct measurement, and represents an adjustable parameter in the model. More explicitly, write the useful uv energy (that which contributes to photoionization) as a product of two efficiencies as follows

$$E_{\substack{useful \\ UV}} = \epsilon_{el} \cdot \epsilon_{uv} \cdot E_{stored}$$

where ϵ_{el} is the conversion efficiency of stored electrical to total radiated energy, ϵ_{uv} is the fraction of total radiated energy that is effective in photoionizing the seed gas, and E_{stored} is the electrical energy stored in the capacitors. The efficiency ϵ_{el} can be measured but ϵ_{uv} is more difficult to determine. This quantity is adjusted when normalizing the scaling model results to the LSD experiments. For the calculations shown in Fig. C-4, the uv source intensity is that derived from the 6-cm gap height data and is fixed at this value for all gap height calculations presented. The calculated laser output energy density (averaged over the discharge volume) as a function of gap height is shown in Fig. C-5 (see curve labeled "uv source not scaled"). This output energy was calculated using the HRL CO_2 kinetic code with the electron-vibrational pumping rates obtained from the HRL electron Boltzmann equation code. The vertical scale is in units of kilojoules per centimeter of discharge width. These results were obtained for the particular length of 5 m, a value that is optimum for the uv-sustained laser (to be discussed later). We see from this curve that the output energy peaks at a gap height of about 10 cm. This gap height represents the scaling limit for the present uv source.

Competitive laser energy and efficiency for electrode gaps greater than 10 cm can only be achieved by increasing the uv source intensity. The exact increase required can be calculated from our scaling model by adjusting the source intensity to obtain some fixed performance goal (i.e., output joules/liter, input joules/liter, or

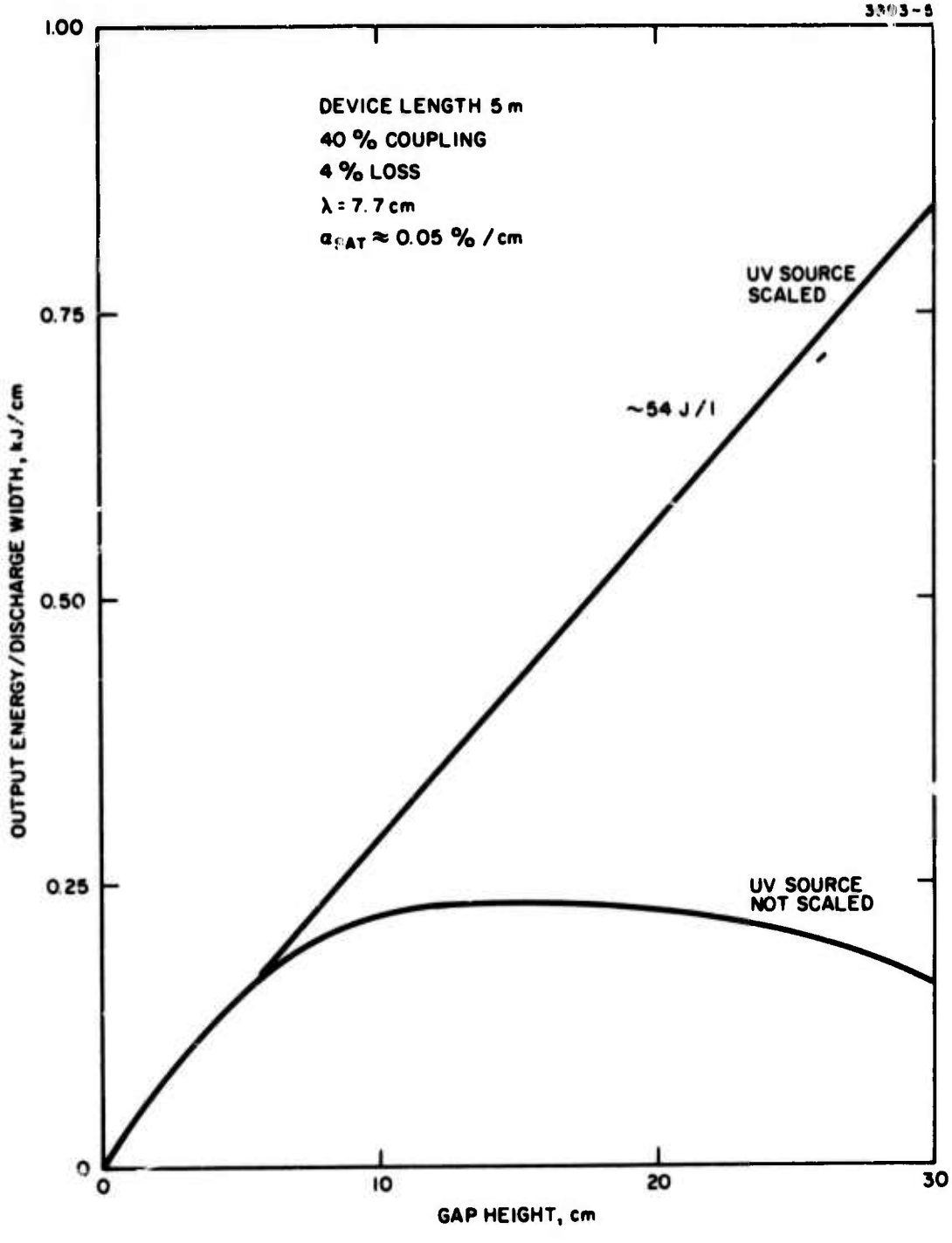

Fig. C-5. Output energy as a function of gap height.

efficiency). Figure C-6 is the result of such a calculation in which the uv source intensity has been adjusted at each gap height to produce a constant electrical input energy of 180 J/l (see Fig. C-4). The vertical scale shows the uv source intensity required relative to that obtained with the present LSD source.

Assuming that the uv source can be scaled in the manner shown in Fig. C-6, we can repeat the earlier calculation of expected output energy versus gap height. This result is shown in Fig. C-5 by the curve labeled uv source scaled. The predicted output energy no longer reaches a maximum but continues to increase with gap height at a constant energy density of ~54 J/l (this is not surprising since the input energy density is being held constant).

The remainder of this section will consider the impact of the uv source improvements on laser performance, particularly on the overall electrical efficiency of the laser.

Qualitatively, it is obvious that improving the source efficiency will increase the overall laser efficiency, while increasing the source input energy will decrease the efficiency or at best leave it unchanged. To put this on a more quantitative basis, calculations of laser efficiency have been made for a hypothetical 5 m long device assuming 40% output coupling and an internal loss of 2% per mirror. The results are presented in Fig. C-7. The upper curve labeled "limiting laser efficiency" represents the efficiency that would be achieved if the uv source required no energy. This efficiency is somewhat higher than is predicted for conventional CO_2-N_2 laser due to the very low CO_2 concentration. The lower curve shows what happens when the uv source input energy is included in the efficiency calculation.

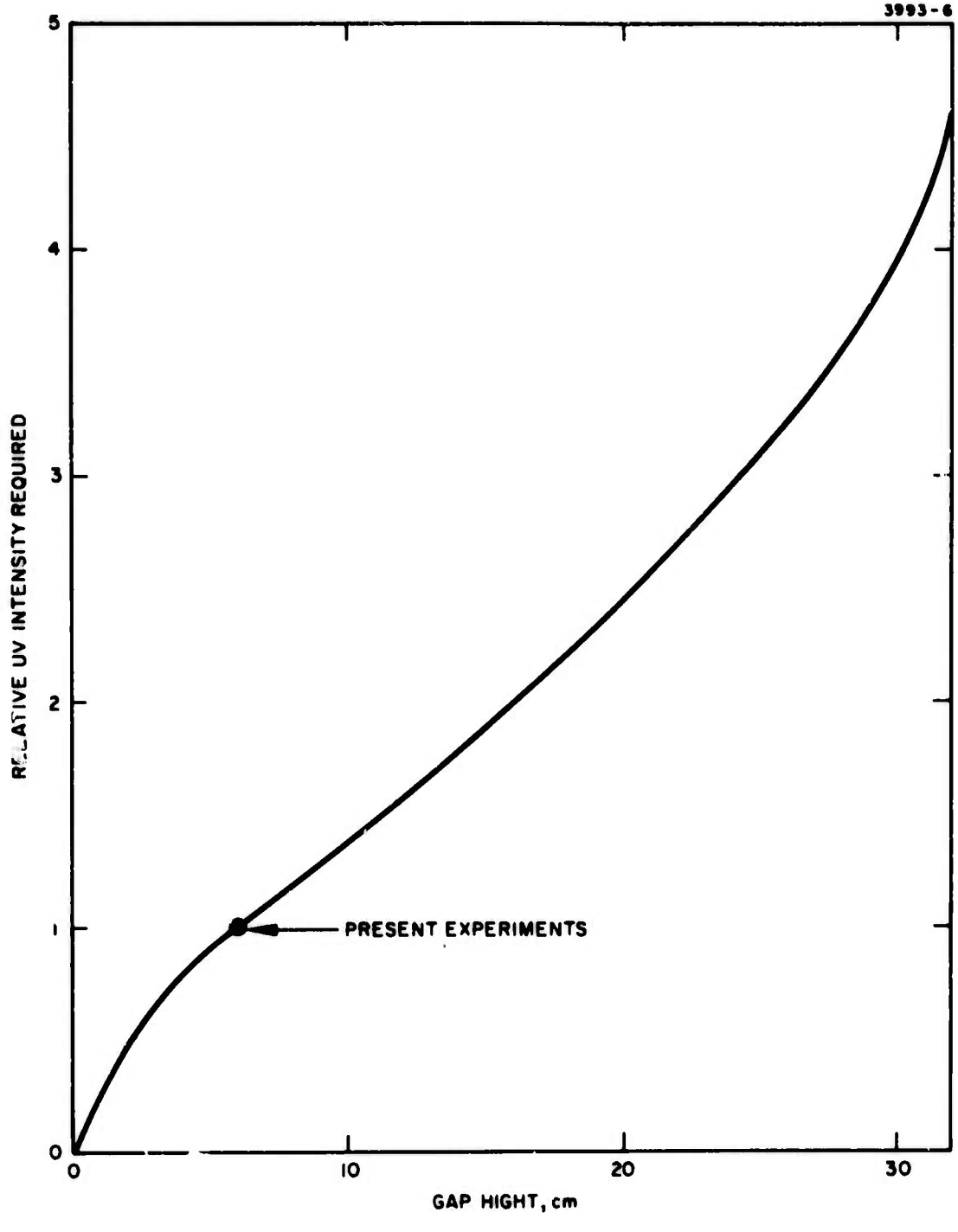

Fig. C-6. Relative uv intensity required as a function of gap height.

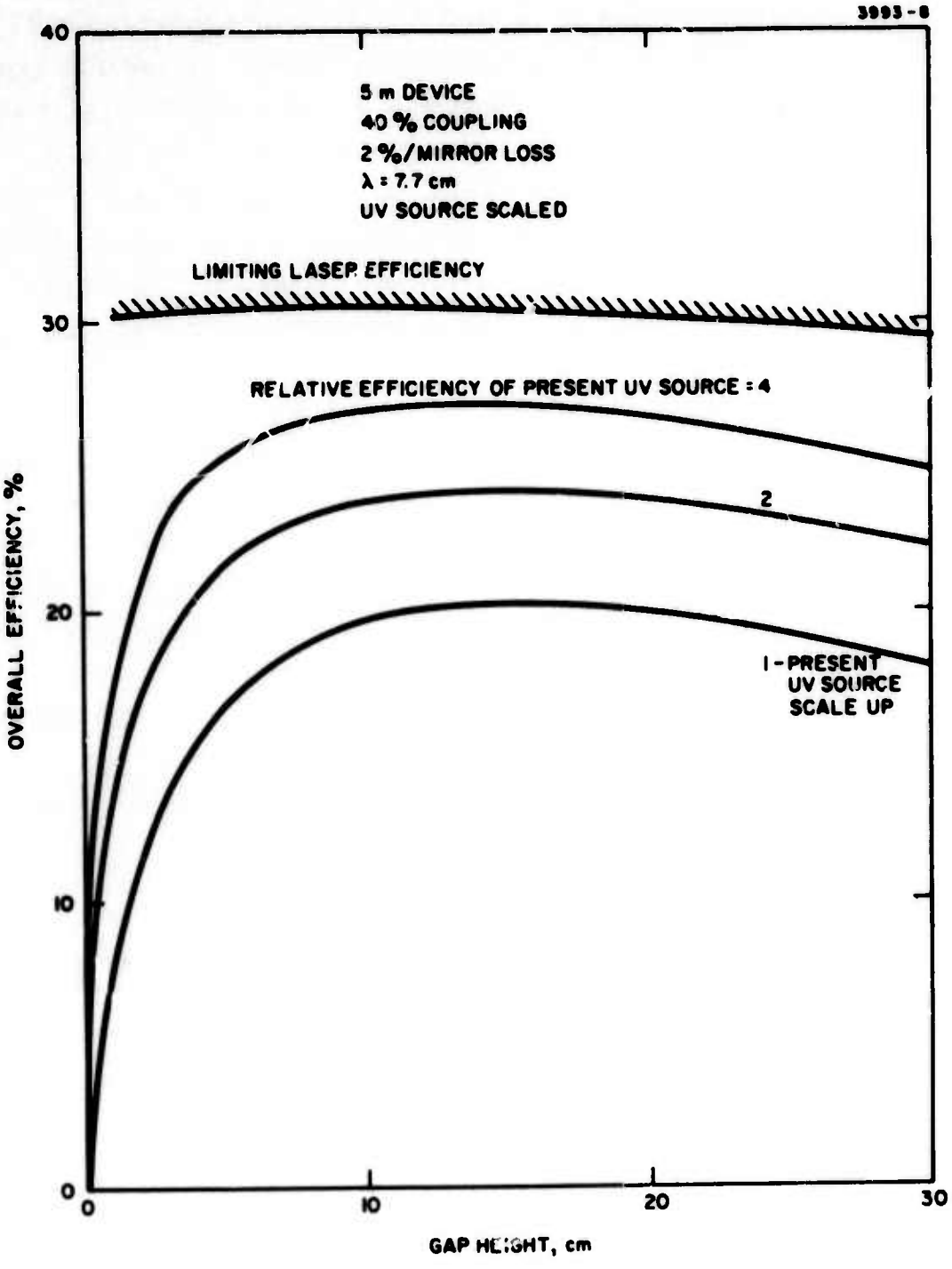

Fig. C-7. Overall efficiency as a function of gap height.

Each curve gives the calculated overall laser efficiency for a fixed uv source efficiency and with the source strength scaled with gap height as shown in Fig. C-6. As expected, the efficiency decreases at large gap heights, but not rapidly. In fact, the efficiency is almost constant out to 20 cm gap height. In this interval, the increased source energy required is offset by the increased energy output. Only for gap heights >25 cm does the exponentially increasing source input begin to dominate the linearly increasing laser output and cause the efficiency to decrease.

The curve labeled "1" shows the efficiency predicted for a source with the conversion efficiency of the present LSD source. The curve labeled "2" assumes the same source energy input increase given by Fig. C-6 and a two-fold increase in the electrical to uv conversion efficiency. Curve "4" is a four-fold increase. As expected, increasing the conversion efficiency causes a direct increase in the laser efficiency. With a uv source of the present type operating at 2.4 times the LSD input energy, a laser with a 20 cm high x 500 cm long cavity can be operated at 20% overall efficiency. At the same uv source input energy and a two times increase in conversion efficiency, the overall laser efficiency increases to ~24%.

2. Summary of Scaling Results

Based on the above calculations, the following general points can be made:

a. To maintain a reasonable device efficiency, the gap height should lie in the range $6 < H < 20$ cm.

b. It is feasible to achieve efficiencies of up to 20%.

c. A specific energy of 55 J/l is possible for large scale devices.

However, these results depend on having a uv source with performance superior to that presently demonstrated.

B. Implications for Scaled uv Sustained Laser

Assuming successful development of improved uv sources, we can establish, based on the above results, guidelines for the construction of a scaled uv-sustained laser.

To begin, an optimum length dimension must be determined. For the uv-sustained laser with its inherent low gain (~0.8%/cm), scaling in the length direction is important for fully saturating the medium. This can be seen in Fig. C-8, where output energy density as a function of output coupling for various lengths and losses is given. Choosing a 4% loss (2%/mirror) as representative of average laser mirrors, scaling from 1 m to 5 m increases the specific energy from 44 to 54 J/l at optimum output coupling. In addition, if operation with high output couplings is desired (for good mode discrimination), the 5 m output drops to only 50 J/l at 70% coupling. Clearly, lengths greater than 5 m would be even better, but we have taken 5 m as a limit based on considerations of overall system size and stability. We conclude from these arguments that

- The length should be as great as possible and at least 5 meters
- The optimum output coupling is 40 to 50% but can be as high as 70 to 80% with a small sacrifice in specific energy
- Output energies of 50 J/l can be achieved.

The minimum electrode gap separation (H) and resulting efficiencies have been established previously and we find that

- For optimum efficiencies, H should be greater than 6 cm
- The overall efficiency is 20 to 24%.

To estimate the maximum gap separation we make an estimate of a factor of two expected improvement in uv source performance.

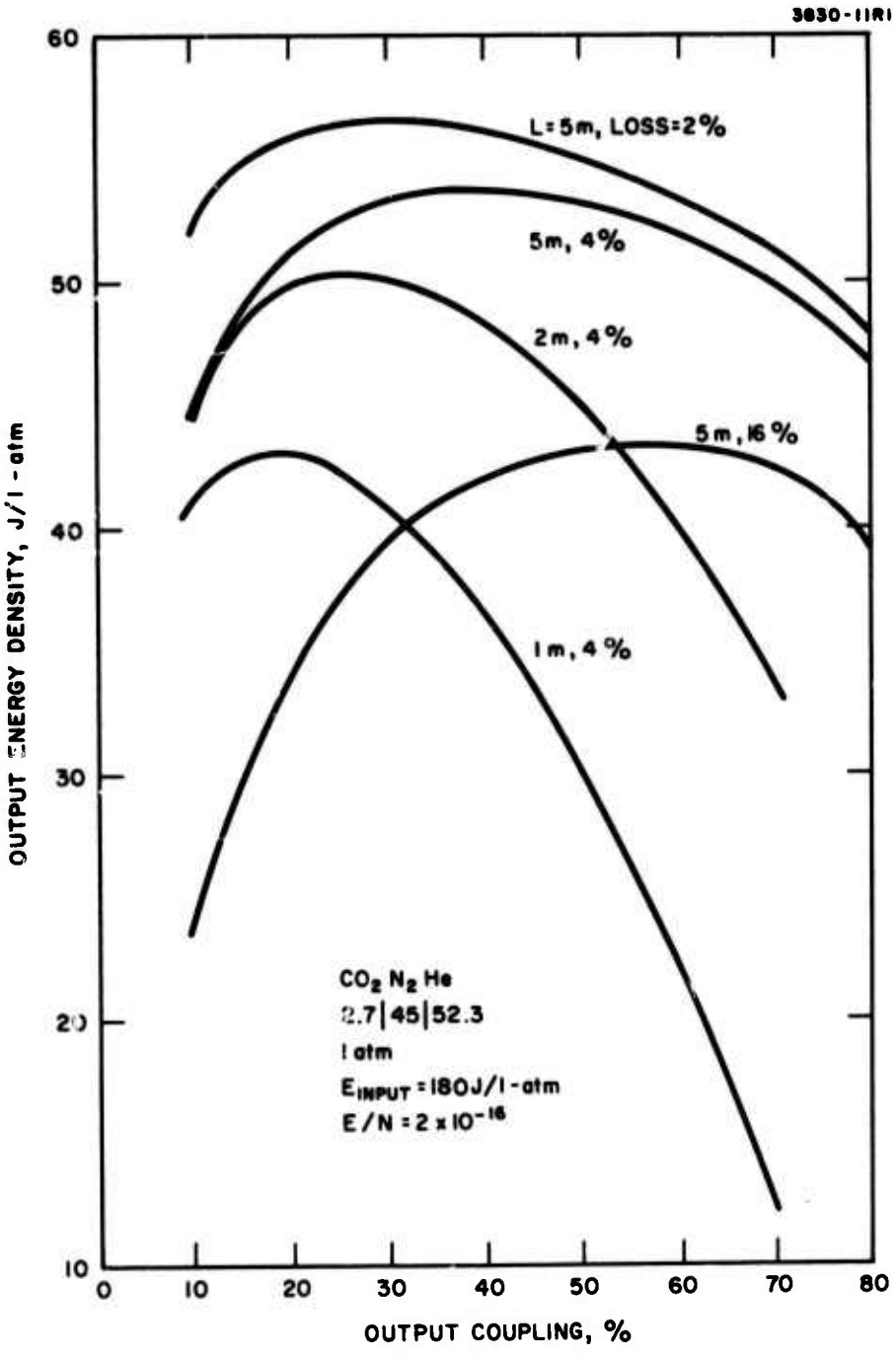

Fig. C-8. Output energy density as a function of output coupling.

Further increases in uv intensity are of marginal utility since gaps greater than 20 to 25 cm require undesirably high sustainer voltages. Based on these considerations the height H should be

$$H \approx 20 \text{ cm} \quad .$$

In the width (W) direction, the uv source scaling sets no limit in contrast to the situation with e-beam ionization where annular geometries are required. The width W is not limited by uv source considerations. However, for a single pass oscillator device, in order to maintain efficient operation of an unstable resonator used to extract the laser output, the W/H ratio should not be excessive. A reasonable limit is probably W/H = 3.

C. Large Scale Device Scalability Projections

The model discussed above was used to calculate the expected scaling of the LSD experiments. Figure C-9 shows the predicted output energy and overall efficiency for the 1 m device. As before, the results are presented for two cases: uv source scaled and uv source not scaled. The curves labeled "uv source scaled" show that the output energy increases linearly with gap height, and a value of 1 kJ at an overall efficiency of 13% is reached at a gap height of 13 cm. It is important to realize that the 13% efficiency number is below the 20 to 24% discussed previously, because the medium is not fully saturated in a 1 m device such as the LSD. However, a demonstration of 13% efficiency projects to 20% efficiency with a device built 5 m in length. This follows because the efficiency increase is a direct result of increased laser power extraction due to increased gain at fixed input energy. This laser output energy calculation is a result of a well established CO_2 kinetic code.

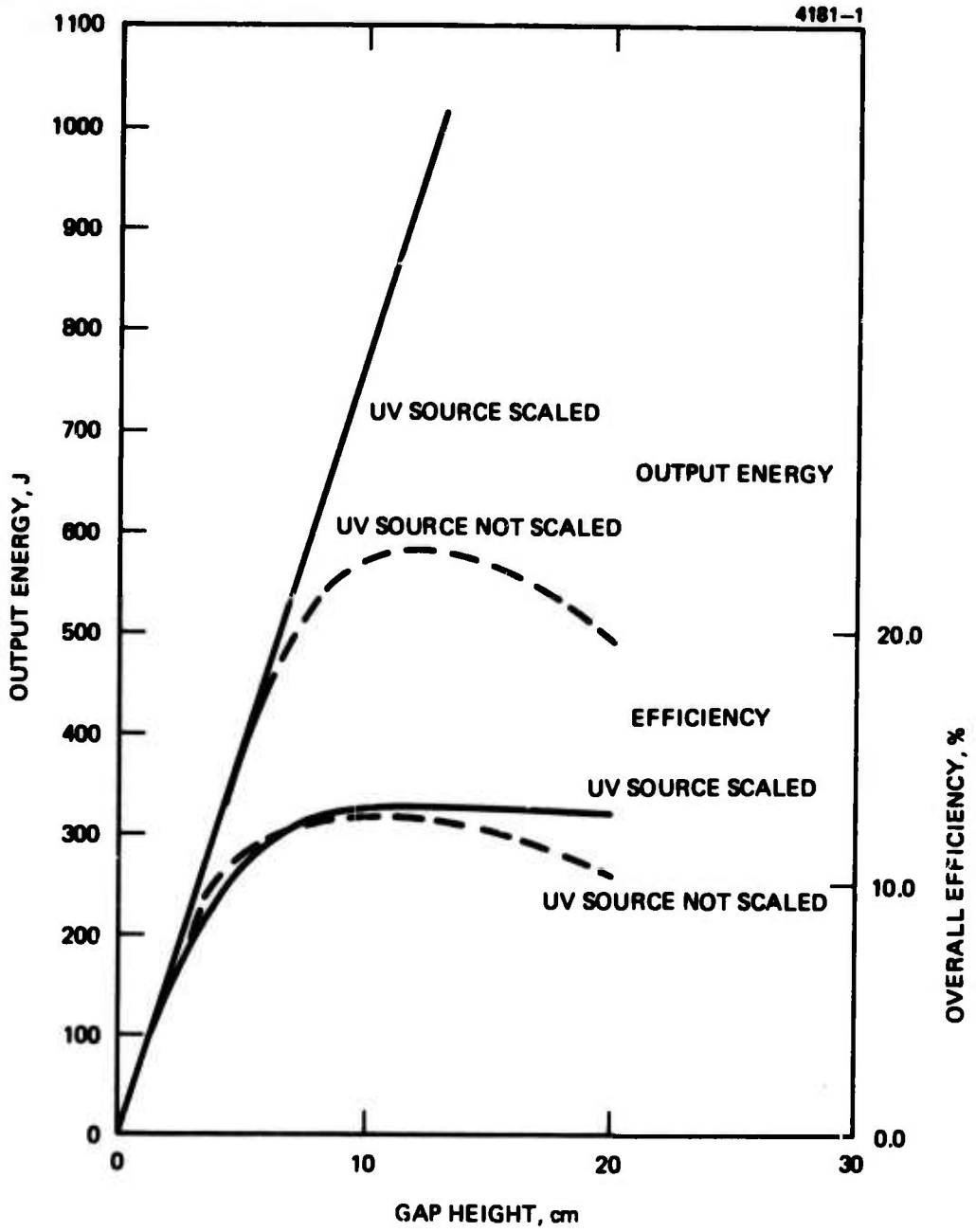

Fig. C-9. LSD scalability model projections.

Referring to Fig. C-9 and the curve labeled "uv source not scaled," we see that at approximately a 12-cm gap height the output power reaches a peak value of 575 J. For the peak to occur at 12 cm is not surprising. This distance represents twice the projected 8 cm mean-free path (6 cm plus 2 cm source – electrode separation) consistent with symmetric source operation as employed on the LSD. More importantly we see that for a 6 cm gap height approximately a 400 J output is expected. As previously discussed we have to date at 6 cm gap height, demonstrated about 300 J output.

APPENDIX D

SCALING MODEL

This appendix contains the basic equations employed in the scaling model.

To begin, the radiative intensity from the UV source configuration is determined. The model used here is discussed in the second semi-annual report. Only the final equation is given here. For the specific intensity at any point x_o, y_o, z_o in the discharge region we have

$$I_{nm} = K\left(\frac{z_o e^{-R_o/\lambda}}{R_o^3} + \frac{(H - z_o)\, e^{-R_H/\lambda}}{R_H^3}\right) \qquad (1)$$

where

$$R_o^2 = (x_n - x_o)^2 + (y_m - y_o)^2 + z_o^2$$

$$R_H^2 = (x_n - x_o)^2 + (y_m - y_o)^2 + (z_o - H)^2$$

H is the electrode separation

λ is the mean free path of the radiation

K is a constant relating to the magnitude of the intensity from the emitters and

I is the specific intensity.

This expression is written for an nxm two-dimensional array of UV emitters. It must then be summed over all emitters to give

$$I = \sum_{n,\,m} I_{nm} \quad . \tag{2}$$

The source function appropriate to the case of single-step photoionization of an added seed gas is given by

$$S = \frac{1}{\lambda} \frac{1}{h\nu_{UV}} \tag{3}$$

where S is the source function, $h\nu_{uv}$ is the energy of the emitter UV radiation.

The electron density is determined from a solution of the electron rate equation, and for a recombination dominated plasma at steady state we have

$$n_e = \sqrt{S/\alpha(E)} \tag{4}$$

where $\alpha(E)$ is the field dependent recombination coefficient. We take the field dependence to be

$$\alpha = KE^{-P} \tag{5}$$

and assume that $P \simeq 2$. When these expressions are combined we obtain an equation relating n_e, E and I

$$n_e = f(E, I) \tag{6}$$

From conservation of charge across the gap we must have

$$J = en_e V_d = \text{const} \tag{7}$$

where V_d is the electron drift velocity in the laser mixture and is determined from the electron Boltzmann code to be

$$V_d = a + bE \tag{8}$$

in the operating E range of the UV sustained laser experiments. When this expression is substituted into (7) and then using (6) we have

$$J = g(E, I) = \text{const.} \tag{9}$$

To determine the value of the constant we require that the maximum value of E, which occurs in the center of the discharge, be of such a magnitude that the mean value of E defined as

$$E_{mean} = \frac{1}{H}\int_{gap} Edz \tag{10}$$

is below the avalanche value for arc-free operation. This value of E_{mean} has been determined to have a value of ~5.5 kV/cm from the LSD experiments. Since the intensity is known in the middle, we can determine the constant in eq. 9. That is, we first assume a value for J, solve eq. (9) for E and then determine E_{mean} from (10). If E_{mean} satisfies the arc-free criteria, we have determined the correct value of the constant J. If not, we iterate until satisfied. This constant is, of course, the current density. Since the value of I in the center decreases as the gap spacing is made larger (see Fig. 9) since E is fixed in the middle, the value of J decreases. This decrease in J is the primary reason for the drop in input energy as discussed in the text.

With the value of J known and E_{mean} calculated, we then determine the input energy from

$$E_{input} = \int_{pulse} E_{mean} \cdot J \cdot dt \quad . \tag{11}$$

The laser output is determined from the CO_2 kinetic code using the input energy value determined above.

Finally, the overall efficiency is calculated from

$$\epsilon = \frac{E_{laser}}{E_{input} + E_{uv}} \quad . \tag{12}$$

As seen from equation(1) the mean free path of the radiation in the CO_2 laser mixture must be known. For use in the model, it was determined by comparing the model predictions of input energy with experimentally determined values from the LSD experiments. In particular, experiments were run at two different CO_2 concentrations, yielding two values for the input energy. The mean free path was then adjusted in the model until agreement with these two measured values was obtained. Such a procedure yielded a mean free path of 7.7 cm, a value in close agreement with that derived in previous work (see 1st semiannual report).